The Philosophical Magazine

UNIVERSITY OF HAWAI
LIBRARY
AUG 61

FIRST PUBLISHED IN 1798

A Journal of Theoretical Experimental and Applied Physics

Vol. 6 May 1961 No. 65
Eighth Series

25s. 0d., plus postage
Annual Subscription £13 10s. 0d., payable in advance

ALERE FLAMMAM

Printed and Published by
TAYLOR & FRANCIS LTD
RED LION COURT, FLEET STREET, LONDON, E.C.4

THE PHILOSOPHICAL MAGAZINE

Editor

Professor N. F. Mott, M.A., D.Sc., F.R.S.

Editorial Board

Sir Lawrence Bragg, O.B.E., M.C., M.A., D.Sc., F.R.S.
Sir George Thomson, M.A., D.Sc., F.R.S.
Professor A. M. Tyndall, C.B.E., D.Sc., F.R.S.

Authors wishing to submit papers for publication in the Journal should send manuscripts directly to the Publishers.

Manuscripts should be typed in *double* spacing on one side of quarto (8 × 10 in.) paper, and authors are urged to aim at absolute clarity of meaning and an attractive presentation of their texts.

References should be listed at the end in alphabetical order of authors and should be cited in the text in terms of author's name and date. Diagrams should normally be in Indian ink on white card, with lettering in soft pencil, the captions being typed on a separate sheet.

A leaflet giving detailed instructions to authors on the preparation of papers is available on request from the Publishers.

Authors are entitled to receive 25 offprints of a paper in the Journal free of charge, and additional offprints can be obtained from the Publishers.

The *Philosophical Magazine* and its companion journal, *Advances in Physics*, will accept papers for publication in experimental and theoretical physics. The *Philosophical Magazine* publishes contributions describing new results, letters to the editor and book reviews. *Advances in Physics* publishes articles surveying the present state of knowledge in any branch of the science in which recent progress has been made. The editors welcome contributions from overseas as well as from the United Kingdom, and papers may be published in English, French and German.

Numerical Methods of Curve Fitting

P. G. GUEST

A comprehensive account of methods for reducing sets of observations and for fitting curves to numerical data. It brings together many treatments hitherto published only in original papers and makes them readily accessible to research workers and students. Each method is illustrated by a numerical example, complete with a full calculating scheme. Full derivations are given of the formulae used. 80*s. net*

CAMBRIDGE UNIVERSITY PRESS

UNIVERSITY OF QUEENSLAND

READER, SENIOR LECTURER AND LECTURER IN MATHEMATICS

The University invites applications for three new posts in the Department of Mathematics. Applicants' special fields of interest may lie in Pure Mathematics, Applied Mathematics or Mathematical Statistics. The positions and salary ranges are:—

Reader	£A2960–60–£A3200
Senior Lecturer	£A2520–70–£A2870
Lecturer	£A1830–70–£A2330

The qualifications for Lecturer are an Honours Degree in Mathematics and preferably some postgraduate study; for Senior Lecturers, experience in research; and for Reader, publication of significant contributions to Mathematics.

The University has recently planned a Computer Centre and a G E 225 computer is expected to be in operation within one year.

The successful applicants will be entitled to participate in the benefits available to the academic staff which include F.S.S.U. type Superannuation, Housing Assistance, Study Leave and Travel Grants.

Additional information about the positions and the staffing and activities of the Department together with application forms will be supplied upon request to the Secretary, Association of Universities of the British Commonwealth, 36 Gordon Square, London, W.C.1.

Applications close, in Australia and London, on 31*st July*, 1961.

REVISED CHEAPER EDITION FOR LIBRARIES AND SCHOOLS

A History of Mathematics

From antiquity to the early nineteenth century

By J. F. SCOTT, B.A., D.Sc., Ph.D.

Vice-Principal of St. Mary's College, Strawberry Hill, Twickenham, Middlesex

Author of *The Scientific Work of René Descartes* (1596–1650),
Mathematical Work of John Wallis, D.D., F.R.S. (1616–1703), and other works

CONTENTS: Mathematics in Antiquity—Greek Mathematics—The Invention of Trigonometry—Decline of Alexandrian Science and the Revival in Europe—Mathematics in the Orient—Progress of Mathematics during the Renaissance—New Methods in Geometry—The Rise of Mechanics—The Invention of Decimal Fractions and of Logarithms—Newton and the Calculus—Taylor and Maclaurin, the Bernoullis and Euler, Related Advances—The Calculus of Variations, Probability, Projective Geometry, Non-Euclidean Geometry—Theory of Numbers—Lagrange, Legendre, Laplace, Gauss. This volume is intended primarily to help students who desire to have a knowledge of the development of the subject but who have too little leisure to consult works and documents. The author has availed himself of the facilities afforded by the Royal Society and other learned Societies to reproduce extracts from manuscripts and many scarce works.

Size $9\frac{3}{4}'' \times 6\frac{3}{4}''$. 266 pp. **Price 27s. 6d.** plus postage and packing 2*s.* 0*d.*

Some Reviews of the First Edition

" The invention of trigonometry, decimal fractions, logarithms and the calculus are each discussed clearly and concisely. The book is easy to read for anybody who knows the elements of mathematics and, although not free from minor errors, can be strongly recommended."—*British Book News*, April 1958.

" Physicists will find that the development in applied mathematics are clearly set out, from ancient times, through that of Archimedes, to the mechanics of the sixteenth century when interest was revived. Significant advances made by Stevin, Galileo, Descartes, Huygens and others are stressed, and help the reader to appreciate what Newton achieved. There are useful appendices giving brief biographical notes on mathematical topics and terminology, followed by a bibliography."—*Proceedings of The Physical Society*, September 1958.

" . . . it has been written with clarity and balance, and the excellent printing helps to make it a pleasure to read."—*The Times Educational Supplement*, 21 March 1958.

" . . . his (Dr. Scott's) wide knowledge of the material, his careful description of methods combine to provide an account which at times gives a sense of the excitement of discovery."—*Nature*, 26 July 1958.

" The printers and publishers are to be congratulated upon having produced such an attractive volume, ... We feel sure the book will be received with delight by all those interested in mathematical histories."—*BEAMA Journal*, August 1958.

" The work comes to life mainly because of his admirable use of the writings of mathematicians themselves, which vividly illustrates the great difficulties under which many of them laboured. This is not a book for the layman but both the student and anyone to whom figures are a fascination, will find the subject clearly and pleasantly presented."—*Technical Bookguide*, March 1958.

Printed and Published by

TAYLOR & FRANCIS LTD

RED LION COURT, FLEET STREET, LONDON, E.C.4

Large Dislocation Loops in Antimony Telluride†

By P. Delavignette and S. Amelinckx
Centre d'Etude de l'Energie Nucleaire, MOL, Belgium

[Received November 17, 1960]

Abstract

When slowly grown from the melt, antimony telluride contains large hexagonal loops. The observations suggest that these are prismatic loops resulting from deviations of the stoichiometric composition. In particular it is proposed that tellurium vacancies precipitate in prismatic loops, from which the 'geometrical' stacking fault is eliminated, by glide of a partial. An explanation is given for the occurrence of pairs of concentric loops elongated in direction differing by 60°. The equilibrium shape as calculated on the basis of the model agrees reasonably well with the observed shape.

§ 1. Introduction

In the course of a study of dislocation in Sb_2Te_3 an interesting precipitation phenomenon was found. A brief description was already presented at the Delft Meeting on Electron Microscopy. The phenomenon is as yet not completely understood but we believe it worth while to present the experimental facts and suggest a possible explanation. These observations may possibly provide some insight in the question how stoichiometric deviations are accommodated in a crystal.

§ 2. Experimental

Crystals of antimony telluride were prepared by melting together the elements in the stoichiometric proportion in evacuated and sealed quartz capsules. The melt was cooled very slowly in order to obtain large grains. Specimens for electron microscopic observation were prepared in the way described earlier, i.e. by cleavage (Delavignette and Amelinckx 1960). It was found that the specimens contained invariably large elongated hexagonal loops of the kind shown in fig. 1(*c*)‡. The lines exhibit diffraction contrast. We will further present evidence that they are prismatic dislocation loops.

In more rapidly cooled specimens smaller rounded loops were found (fig. 1 (*a*, *b*)); in quenched specimens no loops at all were observed suggesting that they are *not* due to thermally generated frozen-in point defects. In other words the loops presented here are not quench loops. Qualitative experiments seem to indicate that the number and total area covered by loops depend on the composition of the melt, from which the crystal grew.

---

† Communicated by Dr. J. Goens.
‡ Figures 1 and 2 are shown as plates.

In specimens which were very slowly cooled very often concentric pairs of large loops are found. The two loops are then systematically elongated in directions which differ by 60°, as shown in fig. 2. The sides of the hexagons are in all cases parallel to the close-packed directions of the lattice. Other dislocations interact visibly with the hexagons, especially with the small ones (fig. 1 (*b*)). The loops are sessile; whereas other dislocations frequently move, no such movement was ever noticed for the loops. Bismuth telluride specimens treated in a similar way did *not* show analogous features.

§ 3. NATURE OF THE LOOPS

From most of the photographs it is evident that the loops show an inhomogeneous contrast; certain segments give practically no contrast. If the set of planes that gives rise to the contrast is perpendicular to the short segment, no contrast is observed for that segment, the others show some. This is represented schematically in fig. 3 (*a*, *b*). If the set of diffracting planes is perpendicular to one of the larger segments all segments give contrast. These observations are in accord with the theory of Howie and Whelan (1961) on the contrast from prismatic dislocation loops. The observations further suggest that the Burgers vector should be inclined with respect to the plane of the loop, in the direction perpendicular to the short segment.

No stacking fault contrast is found in the loops.

Fig. 3

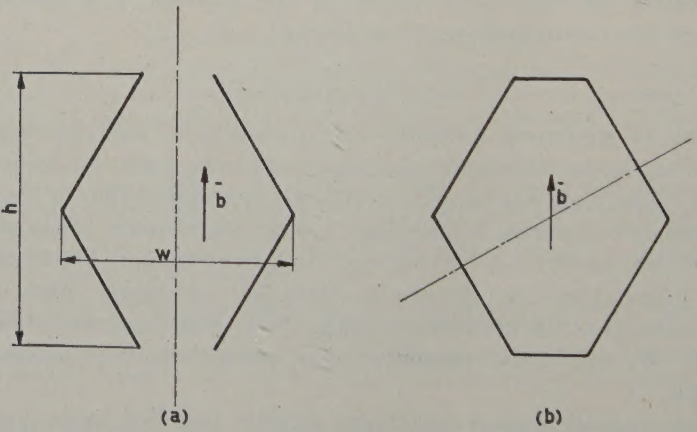

Schematic representation of the contrast effects observed at loops. The bar-dot line represents the trace of the reflecting planes.

§ 4. DISCUSSION

4.1. *The Crystal Structure of* Sb_2Te_3

The crystal structure of Sb_2Te_3 is isomorphous with that of Bi_2Te_3. It consists of a cubic stacking of close-packed layers of antimony and tellurium.

If greek letters represent antimony and latin letters tellurium the stacking sequence in one unit cell can be symbolized as:

$$a\beta c\alpha b, c\alpha b\gamma a, b\gamma a\beta c, \ldots$$

where a, (or α), b (or β) and c (or γ) stand for the three possible positions. It is clear that tellurium occurs in two different positions, we call $\mathrm{Te_I}$ the atom sites limiting the five-layered lamellae, $\mathrm{Te_{II}}$ the sites in the centre of these lamellae. The bonds between the two $\mathrm{Te_I}$ layers are the weakest and the glide plane is therefore very probably located there.

Antimony telluride prepared from the melt seems to be invariably non-stoichiometric, in particular containing an excess of antimony (Offergeld and Van Caekenberghe 1959). It is further generally thought that the disorder in this compound is of the anti structure type, i.e. antimony occupying tellurium sites and vice versa (Kroger and Vink 1956).

4.2. *Generation Mechanism of the Loops*

Although the origin of the loops is not completely understood it is fairly clear that the reason for their occurrence has to be sought in the deviations from stoichiometry. This point of view is based on the fact that similar features do not occur in bismuth telluride (which is nearer to stoichiometry when grown from the melt) and also because the number and size of the loops were found to be sensitive to deviations from stoichiometry. It should be mentioned that these deviations were in all cases smaller than those needed to give rise to a second phase.

It is now clear that the crystal should contain a number of point defects which make up for the non-stoichiometry. In view of the type of disorder, one would expect at high temperatures more antimony atoms on tellurium sites than vice versa. The vacancies cannot be given a name as a consequence of the disorder, since they may occupy both types of sites. By cooling slowly the atoms will tend to occupy their proper sites and this will result in a preferential occupation of the Te layers by vacancies. Since bonds are weakest and diffusion easiest between two $\mathrm{Te_I}$-layers, vacancy loops will preferentially nucleate in one of these. There is a further reason why this type of layer is preferred, but this will only become apparent *a posterio.*

The type of loops that would result is shown in fig. 4 (a). It contains a 'chemical' and a 'geometrical' fault. Since the basal dislocations in these crystals are *not* dissociated the stacking-fault energy is relatively large and the geometrical stacking fault will therefore be eliminated out of the loop by the nucleation of a partial, as in aluminium (Hirsch *et al.* 1958). Since the plane of the loop is a glide-plane this should be not too difficult; it would be difficult if the loop were to nucleate in another layer than a $\mathrm{Te_I}$-layer. The final result is then as shown in fig. 4 (b). The Burgers vector is now inclined with respect to the c-plane in agreement with the observed contrast effect. The two pure edge segments presumably climb somewhat more rapidly than the four segments of mixed character. In this way a natural explanation for the elongated shape is found. We show further that the equilibrium shape is such that the edge segments should be shorter.

Fig. 4

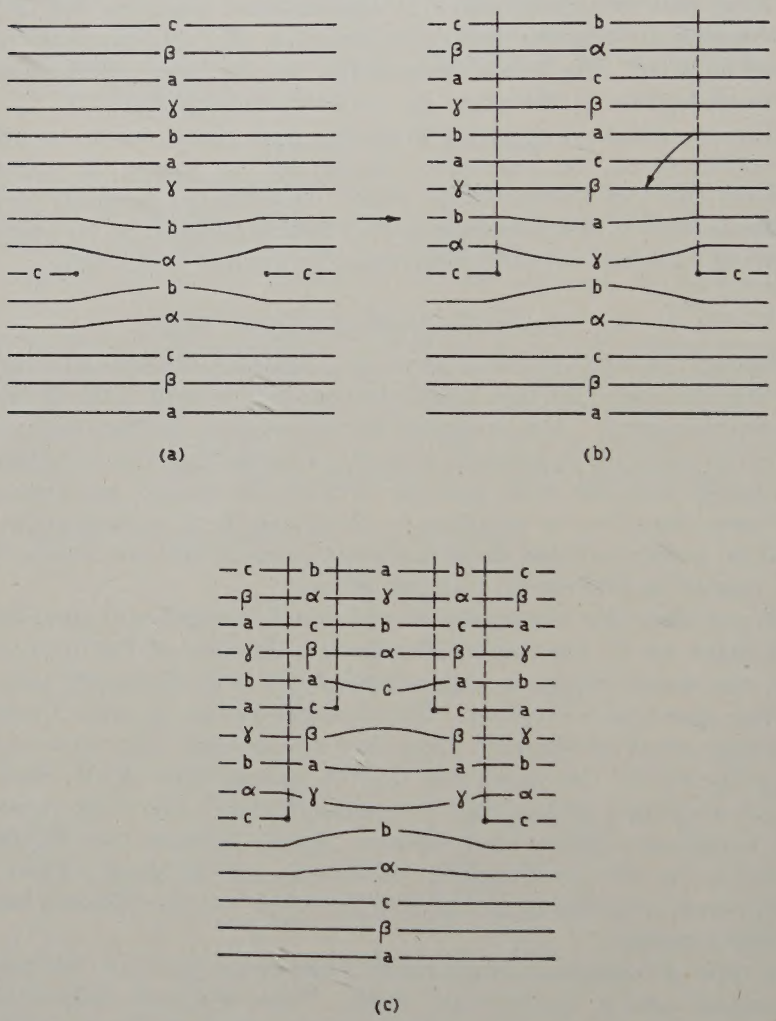

Arrangement of layers in the prismatic loops. (*a*) Loop without shift; (*b*) loop after elimination of geometrical stacking fault; (*c*) two concentric loops.

The loops do not contain a geometrical stacking fault, i.e. the stacking is again close-packed cubic. They still contain the 'chemical' stacking fault. This is however difficult to detect since the scattering factor for electrons of Sb and Te is very nearly equal, in other words electrons do not distinguish between Sb and Te.

On the same basis a plausible explanation for the particular geometry of the pairs of loops can be provided. As a consequence of the elastic interaction between vacancies and dislocations the centre of a prismatic loop is the preferred site for nucleation of a new prismatic loop (Frank 1956).

It is reasonable to assume that the nucleation will take place in the $\mathrm{Te_I}$ layer which is nearest to the first loop plane, i.e. in the plane indicated by the arrow in fig. 4 (*b*). This loop will evidently have the same character as the first. The question now arises: which will be the Burgers vector of the partial nucleated to remove the stacking fault? As in the first loop, the partial has to transform an *a*-layer into a *c*-layer and it has therefore the choice between three possible vectors, one of which is the same as in the first loop. A dislocation with this vector will however not be favoured as compared to the others because it would be repelled by the segments of the existing loop. Choice of the other vectors will on the other hand lead to an attracting partial dislocation. The direction of elongation of the second loop will thus differ from the one of the first by the observed angle (fig. 5).

Fig. 5

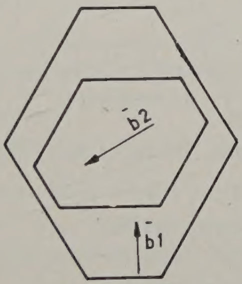

The projection of the Burgers vectors for the two concentric loops.

It is clear that the deviations from stoichiometry might also be accommodated by the introduction of antimony interstitial loops. It is however well known that the geometrical stacking fault resulting from the introduction of a layer of interstitials in a cubic stacking, cannot be removed by glide along the plane of the loop. We should therefore find a 'geometrical' as well as a 'chemical' fault; and this should give rise to stacking-fault contrast, which is *not* observed. We can therefore exclude this possibility.

A number of interactions between the loops has been observed. Such interactions have been analysed in detail in the case of zinc (Fourdeux *et al.* 1960, Fourdeaux *et al.*, to be published) where the loops were however due to the condensation of point defects created during cold work.

In fig. 1 (*b*) (in the points marked A) interactions between the sessile loops and glissile dislocations, leading to pinning of the latter are clearly visible. The basal component of the Burgers vector of the loops may react with the complete glissile dislocation and produce a different partial dislocation. Using the notation introduced previously (Delavignette and

Amelinckx 1960) and ignoring the vertical component ($c/15$) of the Burgers vector of the loop, we can represent the reaction as shown in fig. 6 (*a*). Along the segments XZY the reaction

$$\gamma\mathrm{C}+\mathrm{CB}\rightarrow\gamma\mathrm{B}$$

takes place.

Repulsion between the glissile dislocations and the loop may also occur (fig. 6 (*b*)) in fig. 2, e.g. the dislocation UVW is clearly repelled by the large loop, whilst other dislocations are attracted.

Fig. 6

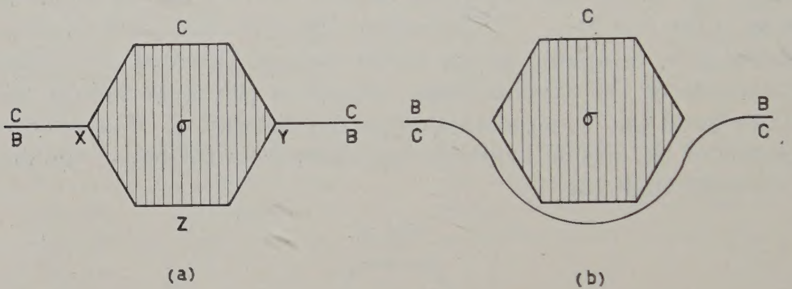

Interaction between a sessile loop and a glissile basal dislocation. (*a*) Attraction; (*b*) repulsion.

4.3. *Equilibrium Shape of the Dislocation Loops*

The isolated large loops that result after slow cooling may be assumed to have adopted an equilibrium shape.

We will now calculate this equilibrium shape for a loop of the kind considered in the previous paragraphs.

Its shape will be described by the two parameters x and h (fig. 7). The total area of the loop is then

$$S=(x+z)h. \qquad (1)$$

We assume that the equilibrium shape is such that for constant area S, the total energy E is a minimum.

We call the magnitude of the Burgers vector b; AB and ED are pure edges with b as a vector. The edge components of the mixed segments are given by

$$b_{\mathrm{e}}^2=(\tfrac{1}{4})b^2(\sin^2\alpha+4\cos^2\alpha) \qquad (2)$$

where α is the angle between the normal to the loop plane and the Burgers vector. The screw component of the mixed segment is

$$b_{\mathrm{s}}^2=(\tfrac{3}{4})b^2\sin^2\alpha. \qquad (3)$$

The line energy per unit length of the edge segments AB and ED is

$$E_{\mathrm{e}}=[\mu b^2/4\pi(1-\nu)]\ln(r_1/r_0), \qquad (4)$$

whilst the corresponding quantity for the mixed sections is:

$$E_{\mathrm{m}}=(\mu/4\pi)\ln(r_1/r_0)[b_{\mathrm{e}}^2/(1-\nu)+b_{\mathrm{s}}^2]. \qquad (5)$$

Neglecting the interaction energy between different segments of the loop the total energy associated with the loop is given by

$$E = 2 \times E_{\mathrm{e}} + 4yE_{\mathrm{m}}. \qquad (6)$$

If we assume the stacking to be perfectly close-packed cubic we have $\sin^2\alpha = \frac{2}{3}$ and $\cos^2\alpha = \frac{1}{3}$; if we further accept $\nu = \frac{1}{3}$ one finds

$$E = 2\left[\mu b^2 \ln\left(\frac{r_1}{r_0}\right) \Big/ 4\pi(1-\nu)\right][x + (\tfrac{5}{3})y]. \qquad (7)$$

Since $x = (S/h) - (\sqrt{3}/6)h$ and $y = (\frac{1}{3})h\sqrt{3}$, one can easily minimize E with respect to h, and subject to the condition $S =$ constant, this leads to

$$h^2 = 18S/7\sqrt{3}. \qquad (8)$$

The quantity w/h, which is more easily compared with the observations, is then given by

$$w/h = (x + 2z)/h \simeq 0{\cdot}96. \qquad (9)$$

Fig. 7

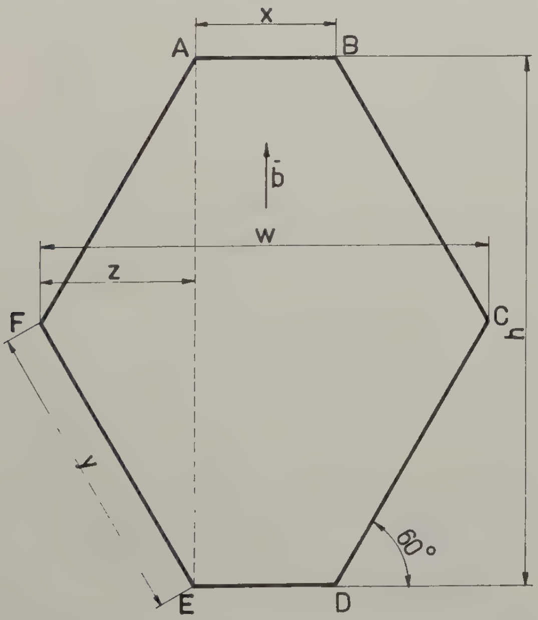

To illustrate the notation used in calculating the equilibrium shape of the loops.

A number of well-formed loops were measured. From the deviations of the angles from 60°, the inclination of the plane of the foil with respect to the lectron beam can be calculated and hence taken into account in the measurments of h and w.

The results are given in the table. The agreement is not too bad especially since we neglected the interaction energy; it should be best for large loops.

These observations lend further support to the model adopted for the loops; no conclusion concerning the generation mechanism can of course be drawn from these considerations.

w†	h(†)	w/h‡	
22	27	0·81	fig. 1 (*c*)
27	35	0·77	
21	25	0·84	
22	27	0·81	
18	23	0·78	
42	52	0·81	

† In arbitrary units, made on an enlarged photograph.
‡ In the regular hexagon $w/h = 1{\cdot}16$.

§ 5. Conclusions

It is clear that the explanation offered here is somewhat speculative in its details. The important point which we hope to have made plausible is that the deviations from stoichiometry can be accommodated in a crystal, at least partly, by the precipitation of a number of vacancies in certain lattice planes into dislocation loops. Especially in layer structures this should be a probable feature. This picture may account for the large influence of small changes in stoichiometric composition on the mechanical properties of some of these compounds. The sessile loops should indeed very much hamper the movement of dislocation on the basal plane.

Acknowledgments

We are indebted to Mr. Goens, Director of the C.E.N., Mol, for permission to publish this paper. We also wish to thank Mr. Nicasy for his skilful preparation of specimens and Mr. Beyens for careful photographic work.

References

Delavignette, P., and Amelinckx, S., 1960, *Phil. Mag.*, **5,** 533.

Frank, F. C., 1956, *Deformation and Flow of Solids* (Berlin: Springer Verlag), p. 73

Fourdeux, A., Berghezan, A., and Webb, W. W., 1960, *J. appl. Phys.*, **31,** 918.

Fourdeux, A., Berghezan, A., and Amelinckx, S., 1961, *Acta Met.* (to be published).

Hirsch, P. B., Silcox, J., Smallman, R. E., and Westmacott, K. H., 1958, *Phil. Mag.*, **3,** 897.

Howie, A., and Whelan, M. J., 1961, *Proceedings of the Delft Conference on Electron Microscopy* 1960 (to be published).

Kroger, S., and Vink, H., 1956, *Solid State Physics*, Vol. 3 (New York: Academic Press), p. 310.

Offergeld, G., and van Caeckenberghe, J., 1959, *J. Phys. Chem. Solids*, **11,** 310.

The Scattering of Phonons by Bound Electrons in a Semiconductor†

By I. C. Pyle
Cavendish Laboratory, University of Cambridge‡

[Received November 28, 1960]

Abstract

In a fairly pure semiconductor at low temperatures, the carriers are in states bound to impurity atoms. In compensated material, there will be some bound states which are not occupied.

A carrier can jump from one impurity state to an unoccupied neighbour, and thereby interact with lattice waves, setting up a thermal resistance. We calculate the effective mean free path of phonons affected by this mechanism. This mean free path varies inversely as the number of carriers and the number of vacancies, and as a function of temperature has a minimum, at about 0·2°K for 'light' holes in germanium. Some phenomena in the thermal conductivity of germanium are thought to be due to this effect.

The thermal conductivity of germanium has been measured at low temperatures by Carruthers *et al.* (1957), and Carruthers (private communication, 1958). The measurements were made at temperatures between 0·2 and 90°K, on a number of specimens of different purities, which contained from 10^{13} to 10^{19} p-type carriers at room temperature.

Under these conditions, the heat is carried almost entirely by lattice waves (Rosenberg 1954), and in order to explain the results we must consider the various mechanisms by which phonons may be scattered. Point defects in the lattice (isotopes and chemical impurities) cause Rayleigh scattering, which can be estimated by extrapolation from the high-temperature results. The effect of boundary scattering can also be calculated (Casimir 1938), and approximately allowed for. The residual thermal resistance must be due to the scattering of phonons by some other mechanism. This resistance was found to depend strongly on the impurity content of the specimen, and is given in fig. 1 expressed as an effective mean free path for phonons.

In the purest specimens (Ge 2, 3, 4, 5 and 10, containing up to 10^{15} impurity atoms per cm^3), phonons have relatively long mean free paths, which indicate that the thermal resistance is fairly well explained by boundary and isotope scattering. But for the less pure specimens there is a significant amount of scattering of phonons, which indicates the presence of a new mechanism.

---

† Communicated by Dr. J. M. Ziman.

‡ Present address: Theoretical Physics Division, A.E.R.E., Harwell.

The behaviour of the most impure specimens (Ge 11 and 12, which contained more than 10^{18} impurity atoms per cm^3) has been explained by Ziman (1956 b). The additional thermal resistance is attributed to the absorption and emission of phonons by 'free' electrons which behave like a degenerate Fermi gas because of the strong overlap between centres.

One specimen, of intermediate purity (Ge 7, with $2{\cdot}3 \times 10^{16}$ impurity atoms per cm^3), behaved in a very surprising manner, quite different from either of the extreme types. The distinctive feature of the results for this specimen is that the effective mean free path decreases as the temperature falls, from about 5°K down to the lowest temperatures at which observations were made (0·2°K). This contrasts markedly with the 'normal' increase, which would be caused by Rayleigh scattering, and also with the type of curve predicted for the impure specimens, which has a minimum mean free path at about 5°K.

Fig. 1

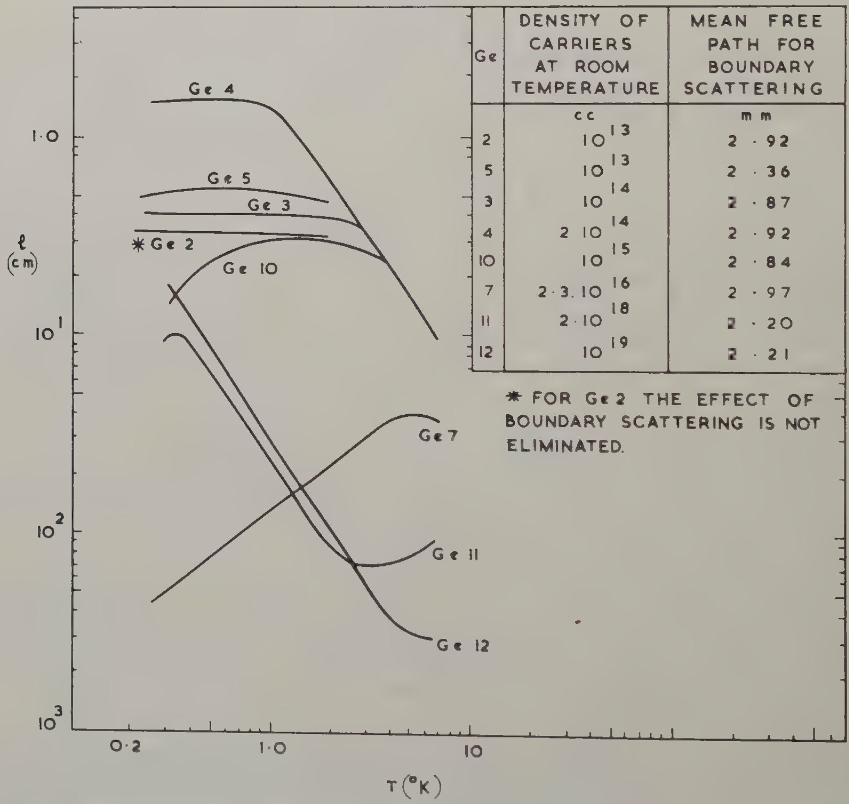

Ge	DENSITY OF CARRIERS AT ROOM TEMPERATURE	MEAN FREE PATH FOR BOUNDARY SCATTERING
	cc	mm
2	10^{13}	2·92
5	10^{13}	2·36
3	10^{14}	2·87
4	$2\ 10^{14}$	2·92
10	10^{15}	2·84
7	$2{\cdot}3.10^{16}$	2·97
11	$2{\cdot}10^{18}$	2·20
12	10^{19}	2·21

* FOR Ge 2 THE EFFECT OF BOUNDARY SCATTERING IS NOT ELIMINATED.

The positive value of $\partial\lambda/\partial T$ implies that the interaction increases as the phonon wavelength increases, i.e. as the local distortion of the lattice becomes smaller. It seems unlikely that there will be a continuing increase for even longer wavelength phonons, and we therefore presume that a minimum exists in the curve, at or below 0·2°K; the scatter of the experimental points is very large at the lowest temperatures, and it is extremely difficult to detect a minimum.

In the present paper a calculation is made to try to explain this anomaly. The additional thermal resistance is still assumed to be due to interaction with electrons introduced into the semiconductor by impurities, but because of the smaller concentration of impurities, one no longer has a degenerate gas, but electrons are able to tunnel from one centre to another. This is only possible if the semiconductor is compensated (Conwell 1956) so that there are vacant centres for the electron to tunnel into. As pointed out by Mott (1956) the charged minority carries introduce a considerable random field, so that the potential energy of some centres is lower than others. An activation energy is thus necessary to allow the electrons to move, and this accounts for the temperature-dependence of the resistivity. We shall, nonetheless, assume that there is a large number of pairs of centres which have nearly the same energy, and which share a single electron, so that resonance between them is possible. This may be possible, even at quite low temperatures ($< 1\,^{\circ}\mathrm{K}$) if the degree of compensation is high. We do not know that what degree of compensation was in the experiments quoted; further experimental work in this would be of interest. We shall assume that acceptors and donors are present in comparable concentration.

Our model is thus that of a number of pairs of centres distant R apart, each pair sharing an electron. The energy separation of the two lowest states, similar to the bonding and anti-bonding states of H_2^+, depends sensitively on R. The phonon is scattered due to a process in which the electron jumps from one of these states to the other. We calculate the probability of this process; the actual distribution of ions in the crystal is taken into account by averaging this result over all values of R.

In order to obtain this average, we need to know the distribution of separations between pairs of ions. The most probable separation R_0 in material containing N impurity atoms per cm^3 is given by

$$2\pi N(R_0)^3 = 1. \qquad (1)$$

We define the relative separation $r = R/R_0$, the probability distribution for which is

$$P(r)\,dr = 2r^2\,dr. \qquad (2)$$

The wave functions for the simple system of two ions and one electron are analogous to these of a hydrogen molecule ion H_2^+ (Pauling and Wilson 1935). If we assume that the basic lattice is a continuum with dielectric constant ϵ (of value 16 for germanium), and that the electrons have effective mass m^*, then the units of length and energy corresponding to the Bohr radius a_0 and energy W_0 are

$$a = a_0 \,.\, \epsilon m/m^*, \qquad (3)$$

$$W = W_0 \,.\, m^*/m\epsilon^2. \qquad (4)$$

Since the temperature is low, we consider only the two lowest eigenstates of the system. These are the symmetrical and antisymmetrical combinations $w_{\pm}(\mathbf{r})$ of the hydrogen-like wave functions $u(\mathbf{r} \pm \mathbf{R}/2)$ for the ground states of the individual ions. These eigenstates have energies $E_{\pm}$, given by

$$E_{\pm} = -\tfrac{1}{2} + \frac{1}{R}\left\{1 - \frac{J \pm K\,.\,R}{1 \pm \Delta}\right\}, \qquad . \quad . \quad . \quad . \quad . \quad . \quad (5)$$

where

$$J = 1 - (1+R)\exp(-2R),$$
$$K = (1+R)\exp(-R),$$
$$\Delta = (1+R+R^2/3)\exp(-R),$$

the units for R and E being a and W respectively. The difference between the energies of the two states is

$$E(R) = \frac{2}{R} \cdot \frac{K\,.\,R - J\,.\,\Delta}{1-\Delta^2}. \qquad . \quad . \quad . \quad . \quad . \quad . \quad . \quad (6)$$

We write

$$E_{\pm} = E_{\text{mean}} \mp \tfrac{1}{2}E(R).$$

The wave function for the unperturbed system consists of a linear combination of the eigenfunctions $w_{\pm}$ with their respective energies $E_{\pm}$:

$$[g_+ w_+ \exp\{iE(R)t/2\hbar\} + g_- w_- \exp\{-iE(R)t/2\hbar\}]$$
$$\times \exp\{-iE_{\text{mean}}t/\hbar\}.$$

This represents the quantum mechanical resonance of the electron between the two impurity atoms, with angular frequency $E(R)/2\hbar$. The probability that an electron is in one of the states $w_{\pm}$ depends on its energy, and is given by the Fermi–Dirac distribution:

$$|g_{\pm}|^2 = f_{\pm} = [1 + \exp(E_{\pm}/kT)]^{-1}.$$

The effect of lattice waves on the system is to cause transitions between the two eigenstates, with the simultaneous absorption and emission of phonons. The present situtation is rather unusual, because two eigenstates have non-zero initial probability amplitudes:

$$a_+(t=0)g_+\exp(i\phi), \qquad a_-(t=0)g_-\exp(-i\phi)$$

where ϕ is an arbitrary phase. Conventional perturabtion theory results are based on the assumption that the system is initially completely in a definite eigenstate. The modification to cover the present case needs a little care, but is not difficult. It will be noted that since the squares of the probability amplitudes are involved, the arbitrary phase ϕ in the initial probability amplitude cancels out.

Using first-order perturbation theory, and the deformation potential method, with coupling constant $G = 2{\cdot}3$ ev (Shockley 1950), we obtain expressions for the probability amplitudes $a_{\pm}(t)$ of the eigenstates at time t, from which are derived the transition probabilities. The result of this calculation is that the process of emission of a phonon $\underset{\approx}{\mathbf{p}}$, together with an electronic transition from the antisymmetric to the symmetric state occurs at the rate

$$W(+\mathbf{p};\ -) = \frac{2\pi}{\hbar} f_-(1-f_+)\frac{G^2p^2\hbar(n_{\mathrm{p}}+1)}{2MN\omega_{\mathrm{p}}}|\langle+\mathbf{p}-\rangle|^2\delta(E(R)-\hbar\omega_{\mathrm{p}}), \quad . \quad (7)$$

where n_{p} and ω_{p} are the number and frequency of phonons in mode $\underset{\approx}{\mathbf{p}}$. The crystal, of volume V, is assumed to contain N atoms of mass M:

thus its density is $\rho = MN/V$. The matrix element $\langle + \mathbf{p} - \rangle$ depends on the wave functions of the electronic states:

$$\langle + \mathbf{p} - \rangle = \int w^*_+(\mathbf{r}) \exp(-i\mathbf{p}\,.\,\mathbf{r}) w_-(\mathbf{r})\, d\mathbf{r}$$
$$= i[1 + (\tfrac{1}{2}ap)^2]^{-2} \sin \mathbf{p}\,.\,\mathbf{R}. \qquad (8)$$

This result for the interaction at a single pair of impurity atoms is now averaged over all values of the inter-ion separation R. Since each value of R corresponds to a particular value of $E(R)$, the delta function is removed, and instead we have a relation between R and p which gives the energy conservation condition for the interaction:

$$E(R) = \hbar\omega_{\mathrm{p}}. \qquad (9)$$

Thus pairs of ions which are distant from each other are responsible for scattering low-energy phonons, and close pairs of ions scatter high-energy phonons.

The total effective mean free path l is determined by the method of Ziman (1956 a), which is based on the assumption that N-processes are dominant in determining the phonon distribution. We write

$$l = l_{01}\,.\,\lambda_1(T),$$

where

$$l_{01} = \frac{1}{n(N-n)} \cdot \frac{W\rho \boldsymbol{v}^2}{4\pi^2 G^2 a^2}, \qquad (10)$$

and

$$\frac{1}{\lambda_1} = \frac{15}{16\pi^4} \int_0^\infty \frac{x^4 e^x}{e^x - 1} \, \frac{e^{\frac{1}{2}x} - 1}{e^{\frac{1}{2}x} + 1} \cdot \frac{\frac{1}{2}ap}{[1 + (\frac{1}{2}ap)^2] E'(R)}$$
$$\times \left\{ 1 - \frac{\sin pR}{pR} \right\} R_0{}^2 P(R/R_0)\, dx, \qquad (11)$$

in which $x = \hbar\omega_{\mathrm{p}}/kT$, $E(R) = \hbar\omega_{\mathrm{p}} = \hbar vp$, $E'(R) = dE/dR$.

A graph of the function $\lambda_1(T)$ (obtained by numerical integration) is given in fig. 2 (curve 1). The essential form of the curve is due to the differing interactions of the dominant phonons at different temperatures. At high temperatures, the phonon wavelength is short compared with the size of the wave function for a bound electron on a single impurity, and adjacent half-wavelengths of the phonon give contributions which cancel in the matrix element (8). On the other hand, at low temperatures the dominant phonon wavelength is long; thus the basic lattice is only slightly distorted, causing a relatively small deformation potential, and little interaction with the electron. The interaction is greatest when the dominant phonon wavelength is somewhat greater than the extent of the electronic wave function for a single ion.

The density of impurity ions does not strongly affect this result, because the distribution (2) of inter-ion distances does not change with impurity density. Of course, the actual magnitude of the interaction does depend on the impurity density.

We now consider how well the above calculation agrees with the observed results for specimen Ge 7. This involves putting numerical values for the various quantities into the expression (10) and finding whether the results are consistent with a mean free path of the observed magnitude decreasing as the temperature falls to 0·2°K.

Fig. 2

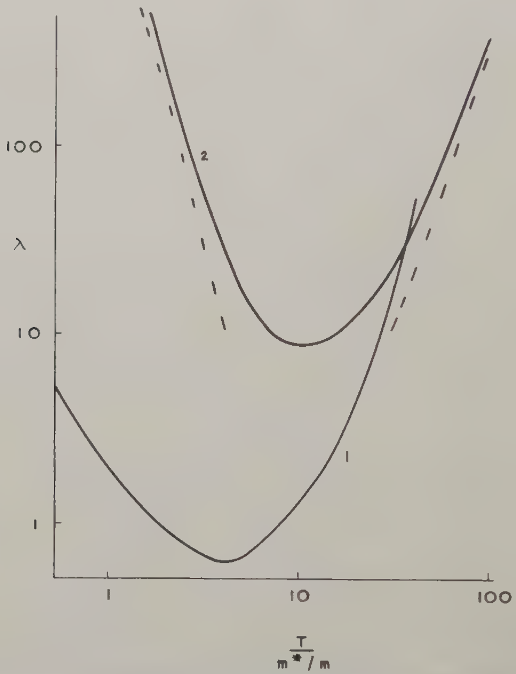

The temperature at which the minimum mean free path is predicted depends on the effective mass parameter m^*/m, and not on the density of impurities N. But the actual situation in germanium is not as simple as has been assumed for this calculation. The effective mass of holes in germanium is not a definite, well defined quantity, but has a more complicated structure than the simple scalar here assumed. Due to degeneracy, there are two types of holes in germanium: 'heavy' holes, with effective mass $0{\cdot}3\,m$, and 'light' holes, for which $m^* = 0{\cdot}04m$ (Dresselhaus *et al.* 1953). If we assume that heavy and light holes interact independently with the phonons, there should be minima in the mean free path curve at temperatures of 1·5 and 0·2°K.

Both these values are lower than the temperature of the minimum calculated by Ziman (1956 b), for the impurity band model. The value for light holes is consistent with the observed results.

The magnitude of the minimum mean free path depends on the quantity l_{01} which involves both the effective mass and the impurity density. Substituting numerical values for the other quantities, we obtain

$$l_{01} = \frac{1}{n(N-n)}\left(\frac{m^*}{m}\right)^3 . \, 1{\cdot}36 \times 10^{36}\ \text{cm.} \quad . \quad . \quad . \quad . \quad (12)$$

The density of impurity atoms N, is not known accurately, because the only measurements on the specimens indicating their purity was their room temperature electrical conductivity, which gives the number of holes which are not trapped by acceptor ions. However, these quantities are of the same order of magnitude, and we obtain an estimate of the required result by assuming that there are as many vacant impurity states as there are occupied ones. This assumption leads to the following calculated values for the minimum mean free path in a sample having the composition of specimen Ge 7:

for heavy holes	10 cm,
for light holes	0·08 cm.

Thus this mechanism alone would produce a phonon mean free path with two minima, a low one at a mean free path of 0·08 cm, and a temperature of 1·5°K. Since the mechanism does not act in isolation, the separation of the mean free path curve into components for different mechanisms is only approximate, and not reliable for large mean free paths, it is to be expected that only the lower minimum should be observable, and that the other should be masked by the general background of interactions.

We now have an explanation of the continued fall of the mean free path curve down to 0·2°K, but the calculated mean free path is about ten times larger than was the observed. Further, the gradients of the curves are not the same: the observed gradient is appreciably smaller in magnitude than the theoretical value for temperatures about one decade above the minimum.

We therefore consider whether further terms in the perturbation expansion lead to a larger result. Using second-order perturbation theory, we calculate the mean free path for phonons which are scattered at an impurity centre of the type described. In this case, a phonon is virtually absorbed by an electron, and then re-emitted in another direction. Since energy need not be conserved in virtual transitions, there is no condition corresponding to (9) for this interaction: all phonons may be scattered at any impurity centre, instead of only those which have the right energy.

The calculation is very similar to that described above, with the same matrix elements, now taken in pairs, for the two virtual transitions involved in the scattering. The evaluation of the integrals is straightforward, without the rather awkward relation (9) between variables. The result can be written

$$l = l_{02} \,.\, \lambda_2(T)$$

where

$$l_{02} = \frac{1}{n(N-n)} \cdot \frac{h^2 \rho^2 v^6}{8\pi G^4 a} \qquad . \; . \; . \; . \; . \; . \; . \quad (13)$$

and $\lambda_2(T)$ is a complicated function, the graph of which is given in fig. 2 (curve 2). This function is very similar to that obtained by first-order perturbation theory, and consequently only the magnitude of the effect may be modified, without any serious change in its essential nature.

To determine whether this second-order effect is appreciable, we must calculate the numerical value of l_{02}. We find

$$l_{02} = \frac{1}{n(N-n)} \,.\, (m^*/m)^{-1} \,.\, 1{\cdot}68 \times 10^{33}\ \text{cm} \qquad . \; . \; . \quad (14)$$

which leads to the conclusion that for effective masses of order unity ($m^*/m > 0{\cdot}2$), the second-order interaction is stronger, but for the low effective masses with which we are here concerned, the first-order interaction is dominant (by a factor of 5^4 for $m^*/m = 0{\cdot}04$): the real absorption and emission of phonons constitutes a much stronger mechanism than virtual transitions leading to scattering.

The dependence of these results on the impurity concentration in the specimen is seen from the eqns. (12) and (14) which define l_0. For small concentrations of impurities, there is little interaction and a large mean free path. The mean free path falls as the concentration increases, as long as the model is valid. But of course, for concentrations over a certain value, the electronic wave functions are no longer localized, and the electrons form a degenerate gas. This model suggests that the greatest thermal resistance of the described type will be shown by the specimens whose impurity content is just insufficient for this to occur.

The conclusion we reach is that the model described goes some way towards explaining the apparent anomaly in the residual thermal resistances in germanium, but fails to produce detailed agreement.

Although the present work was carried out with a particular physical system in mind (impurity atoms in a crystal of germanium), the same model would apply to any crystal containing charged impurities. Whether electrons or holes are bound to impurity centres, the carriers diffuse through the crystal by the method described, and similarly interact with lattice waves in the crystal.

Pohl (1960) has shown that the thermal resistance of crystals of lithium fluoride containing F-centres (halogen vacancies to which electrons are bound) is not completely explained by theories which do not take into account the motion of electrons between centres. Since frozen-in vacancies will here always lead to compensation, the present model may help in explaining the discrepancy.

ACKNOWLEDGMENTS

I should like to acknowledge the constant help and encouragement which I received from Dr. J. M. Ziman during the course of this work. I am also indebted to the Department of Scientific and Industrial Research for a maintenance allowance.

REFERENCES

CARRUTHERS, J. A., GEBALLE, T. H., ROSENBERG, H. M., and ZIMAN, J. M., 1957, *Proc. roy. Soc.* A, **238,** 502.

CASIMIR, H. B. G., 1938, *Physica*, **5,** 495

CONWELL, E. M., 1956, *Phys. Rev.*, **103,** 51.

DRESSELHAUS, G., KIP, A., and KITTELL, C., 1953, *Phys. Rev.*, **92,** 827.

MOTT, N. F., 1956, *Canad. J. Phys.*, **34,** 1356.

PAULING, L. A., and WILSON, E. B., 1935, *Introduction to Quantum Mechanics* (New York: McGraw-Hill), p. 327.

POHL, R. O., 1960, *Phys. Rev.*, **118,** 1499.

ROSENBERG, H. M., 1954, *Proc. phys. Soc. Lond.* A, **67,** 837.

SHOCKLEY, W., 1950, *Electrons and Holes in Semiconductors* (New York: Van Nostrand), pp. 335, 520.

ZIMAN, J. M., 1956 a, *Canad. J. Phys.*, **34,** 1256; 1956 b, *Phil. Mag.*, **1,** 191.

The Electronic Structure of Disordered Systems†

By S. F. Edwards
Theoretical Physics Department, The University, Manchester

[Received October 28, 1960]

Abstract

The problem of the states of electrons moving under the influence of disordered scattering centres is discussed in the simplest case of one dimension and weak interaction. It is shown how to define a density of levels $n(E)$ and an energy and momentum density $\rho(k, E)$ and the variation of those functions from the case of completely disordered scattering centres to the completely ordered case is discussed. In the weak interaction case it is long-range order which dominates the problem and the effect of even slight disorder results in the appearance of states inside the energy gap of the ordered system.

§ 1. Introduction

In order to initiate a discussion of the electronic structure of disordered systems it is natural to consider firstly the simplest model which retains the essentials of the disordered state. So this paper will consider the electrons non-interacting with themselves except inasmuch as the Pauli principle applies, and interacting weakly with atoms which are represented by fixed predefined potential wells. The final simplification is to consider only a one-dimensional system, a restriction which is removed in a second paper.

There are two limiting cases which exist when discussing order, those of complete order and complete disorder. In the case of complete order the periodicity of the atom lattice implies the periodicity of the wave functions and this theorem leads, irrespective of detailed calculation, to the existence of gaps in the energy spectrum. The other extreme is the state of complete disorder in which it is purposeless to discuss any particular wave function corresponding to any particular configuration and instead one must discuss the probability of an electron having a certain momentum and a certain energy. It will be shown that a mathematical formalism can be set up which, within the limitation of the model, will describe both of the limits and which can then be applied with confidence to the state of disorder. Before presenting this formalism it is worth discussing qualitatively the kinds of situation that could occur. Consider then a perfect lattice and a wave function with the periodicity of the lattice. Any such wave can be split into two components, one of which has its nodes at the atoms and the other its antinodes. The energy associated with these two waves will be separated by the gap energy. It is not possible to have a wave of this frequency which has sometimes nodes and sometimes antinodes, it is a case of all or nothing. Now consider the completely disordered case. A wave function now will not be periodic, so for comparison consider one which has the same number of nodes. Then sometimes such a wave function will, relative to the atoms, locally resemble the wave functions whose nodes were at the atoms, sometimes the wave function whose antinodes were at the atoms, and sometimes it will be a rapidly varying mixture. Now as one moves away from the state of complete order to the state of complete disorder one must eventually reach the chaotic wave function described above.

---

† Communicated by the Author.

Fig. 1

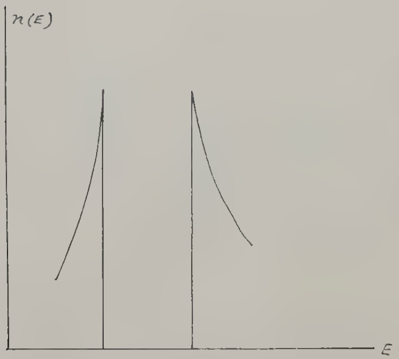

Fig. 2

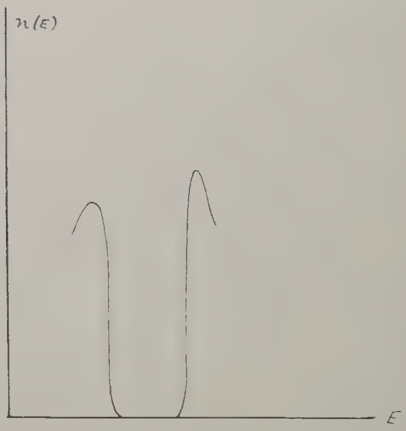

Fig. 3

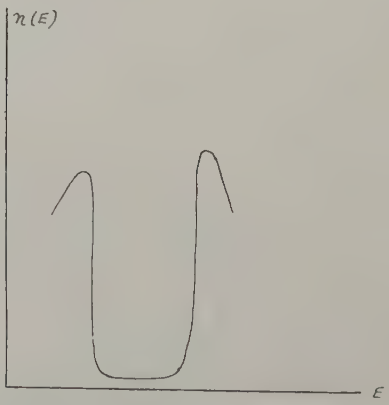

Working back to order, two kinds of situation can be envisaged. One can think of a wave function which is slightly disordered in a way that follows the lattice. But one can also consider that this 'following the lattice' will not last throughout the lattice but owing to the disorder it is possible to have functions which change over from being the kind with nodes at atoms to the kind with antinodes at atoms and thus having an intermediate energy. The ability of the slightly disordered system to sustain states of this latter type has to be investigated in the detailed calculations but it is clear that there are two ways in which an energy gap in the density of states can be filled upon the onset of disorder, for of course ultimately it must be filled when the system is highly disordered. The two ways are exemplified by figs. 2 and 3 which can be considered as derived from fig. 1, which shows the distribution of states in a one-dimensional perfect lattice, by the imposition of disorder. In fig. 2 the walls of the gap soften whilst still leaving a gap in between them, and it will be shown below that such a figure results from a state which has short range disorder whilst retaining long-range order. This is the state of affairs to be expected when the disorder merely distorts the wave functions of the electron. In fig. 3 the floor of the gap rises immediately giving a non-zero density of states right across the gap. This state of affairs will be shown to arise with the failure of long-range order and hence the possibility of getting more radically different wave functions.

Thus the calculations below will suggest that in the free electron model a liquid metal, inasmuch as its properties may be suggested by the one-dimensional model, will have a density of states like fig. 3, since the failure of long-range order is the characteristic of the liquid state.

§ 2. THE BASIC FORMULATION

The Schrödinger equation for an electron moving in the presence of fixed centres R_α which give rise to electron-centre potentials $U(r-R_\alpha)$ is

$$\left(\frac{\hbar}{i}\frac{\partial}{\partial t}-\frac{\hbar^2}{2m}\nabla^2+\sum_\alpha U(r-R_\alpha)\right)\psi=0. \quad . \quad . \quad . \quad . \quad (2.1)$$

In order to be able to discuss average properties however the solution G of the inhomogeneous equation, will be required,

$$\left(\frac{\hbar}{i}\frac{\partial}{\partial t}-\frac{\hbar^2}{2m}\nabla^2+\sum_\alpha U(r-R_\alpha)\right)G(r,r';\,t,t')$$
$$=\delta(r-r')\delta(t-t') \quad . \quad . \quad . \quad . \quad . \quad . \quad . \quad (2.2)$$

A solution G_+ to this equation is given in terms of the eigenfunction of the Schrödinger equation

$$G_+(r,r';\,t,t')=\frac{i}{\hbar}\sum_n\psi_n(r)\psi_n{}^*(r')\exp\left[-\frac{i}{\hbar}E_n(t-t')\right]\Theta(t-t') \quad (2.3)$$

where
$$\Theta=1 \quad t>t'$$
$$=0 \quad t<t'.$$

In terms of energy by Fourier transforming G one has

$$G_+(r,r';\,E)=\sum\psi_n(r)\psi_n{}^*(r')(E-E_n+i\epsilon)^{-1}. \quad . \quad . \quad . \quad (2.4)$$

The $i\epsilon$ in the denominator is needed to define the sense in which the pole

2 R 2

at $E-E_n$ is to be taken, since there are two basic solutions of (2.2) corresponding to outgoing waves, i.e. to (2.3), and also to ingoing waves which use $-i\epsilon$ in the denominator. Now since the functions ψ_n are normalized

$$\int G_+(r, r;\ E)\, dr = \sum_n (E-E_n+i\epsilon)^{-1}, \quad . \quad . \quad . \quad . \quad (2.5)$$

so that since

$$(E-E_n-i\epsilon)^{-1}-(E-E_n+i\epsilon)^{-1}=2\pi i\delta(E-E_n), \quad . \quad . \quad (2.6)$$

$$\int [G_+(r, r;\ E)-G_-(r, r;\ E)]\, dr = -2\pi i\delta(E-E_n) \quad . \quad . \quad (2.7)$$

$$= -2\pi i n(E) \quad . \quad . \quad . \quad (2.8)$$

where $n(E)$ is the density of levels. The average density of levels is obtained by averaging $n(E)$ over the configurations of centres in the probability with which the various configurations occur. Denoting this averaging process by brackets one therefore has

$$-2\pi i\langle n(E)\rangle = \int [\langle G_+\rangle - \langle G_-\rangle]\, dr. \quad . \quad . \quad . \quad (2.9)$$

Now if, as will be the case, the averaging is such as to destroy all inhomogeneity in the problem the averaged Green functions G_+ and G_- will be functions of $r-r'$ alone

$$\langle G_+(r, r';\ E)\rangle - \langle G_-(r, r';\ E)\rangle$$
$$= -2\pi i\rho(r-r';\ E). \quad . \quad . \quad . \quad . \quad . \quad (2.10)$$

In terms of the Fourier transform of ρ:

$$\langle n(E)\rangle = \int_{-\infty}^{\infty} \rho\,(k, E)\, dk. \quad . \quad . \quad . \quad . \quad . \quad (2.11)$$

To interpret this result physically return to (2.4) and write every $\psi_n(r)$ in terms of its Fourier decomposition:

$$\psi_n(r) = \int \alpha^{(n)}(k) \exp\,(ikr)\, dk. \quad . \quad . \quad . \quad . \quad (2.12)$$

Then

$$\langle G_+(r, r';\ E)\rangle = -\sum \langle \alpha^{(n)}(k)\alpha^{*(n)}(j)\rangle \exp\,(ikr-ijr')$$
$$\times (E-E_n+i\epsilon)^{-1}. \quad . \quad . \quad . \quad . \quad . \quad (2.13)$$

But this average must be a function of $r-r'$, thus the average of the α's must vanish unless $k=j$. This means that one can write

$$\rho(k, E) = 2\pi \sum_n \langle \alpha^{(n)}(k)\alpha^{*(n)}(k)\rangle \delta(E-E_n). \quad . \quad . \quad . \quad (2.14)$$

Physically therefore $\rho(k, E)$ corresponds to the 'mean square' probability of finding an electron having energy E and momentum k. Even though the main objective is to calculate $n(E)$, to do so via $\rho(k, E)$ will greatly clarify the situation. Mathematical manipulations are however much easier to perform on the $\langle G\rangle$ rather than on ρ since the $\langle G\rangle$'s satisfy inhomogeneous equations and so allow simple expansions as will appear in detail below. The analysis now to be given follows closely that given by

Edwards (1958) (hereafter referred to as I). Similar treatments are given by Abrams and Weiss (1958), Abrikosov *et al.* (1959) and Langer (1960). Another approach is due to Chester and Thelling (1959). The basic idea is that G can be averaged by considering its expansion in terms of the deviation of the potential $\left(V=\sum_{\alpha}U(x-R_{\alpha})\right)$ from its mean and this series can be averaged without difficulty. After averaging the series may be justifiably summed up again.

Write symbolically

$$G_{+}=G_0-\int G_0(V-\langle V\rangle)G_0 \\ +\int G_0(V-\langle V\rangle)G_0(V-\langle V\rangle)G_0-\dots \quad . \quad . \quad . \quad (2.15)$$

where G_0 satisfies, in one dimension explicitly,

$$\left(\frac{\hbar}{i}\frac{\partial}{\partial t}-\frac{\hbar^2}{2m}\frac{\partial^2}{\partial x^2}+\langle V\rangle+i\epsilon\right)G_0(x,x';\ t,t') \\ =\delta(x-x')\delta(t-t'); \quad . \quad . \quad . \quad . \quad . \quad (2.16)$$

i.e.

$$G_0=(2\pi i\hbar/m(t-t'))^{1/2}\Theta(t-t') \\ +\exp\left[\frac{im}{2\hbar}(x-x')^2(t-t')^{-1}-\frac{i}{\hbar}\langle V\rangle(t-t')\right] \quad . \quad . \quad (2.17)$$

or in Fourier transform upon t and x (the same symbol G_0 will be used), using units which absorb the constants

$$G_0=(E-k^2+i\epsilon+\langle V\rangle)^{-1}. \quad . \quad . \quad . \quad . \quad . \quad (2.18)$$

In (2.15) $\int G_0VG_0$ means, for example,

$$\int G_0(x,y;\ t,t'')V(y)G_0(y,x';\ t'',t')\,dy\,dt''.$$

The series can now be averaged. Use brackets to denote the average value

$$\langle G_{+}\rangle=G_0-\int G_0\langle V-\langle V\rangle\rangle G_0 \\ +\int G_0\langle V-\langle V\rangle\rangle G_0\langle V-\langle V\rangle\rangle G_0-\dots . \quad (2.19)$$

Resuming the series one has

$$\left(E-k^2+i\epsilon+\langle V\rangle-\int\langle VG_0V\rangle+\int\langle V\rangle G_0\langle V\rangle+\dots\right)\langle G_{+}\rangle=1. \quad (2.20)$$

Now it has been shown, for example in I, that when V is weak all the odd averages (except $\langle V\rangle$) are small compared with the even averages which precede them. Thus the validity of the summation above depends on the smallness of

$$\langle VG_0VG_0VG_0V\rangle-\langle VG_0V\rangle G_0\langle VG_0V\rangle \quad . \quad . \quad . \quad (2.21)$$

and similar higher combinations. That this is so was explicitly shown in I for the case of a random distribution of weak interactions, and as will appear below it gives the standard results in the completely ordered case. A full discussion of this point in the one-dimensional case is given in a recent paper by Eisenschitz and Sah (1960). However, it is not so easily justified in three dimensions as in one. Since it is therefore discussed in detail in a following paper, which deals with the three-dimensional case, it will not be discussed further here. Henceforward, then, (2.20) will be adopted as the basis of this paper.

§ 3. The Description of Disorder

The average $\langle U(x-R_\alpha)U(y-R_\beta)\rangle$ must be a function of $x-y$ from the spatial homogeneity of the problem. This can be expressed in terms of the correlation function $c(k)$ defined by

$$c(k)=\sum_{\alpha,\,\beta}\langle \exp ik(R_\alpha-R_\beta)\rangle, \quad . \quad . \quad . \quad . \quad . \quad . \quad . \quad (3.1)$$

so that if $V(k)$ is the Fourier transform of $V(x)$

$$\sum_{\alpha,\,\beta}\langle U(x-R_\alpha)U(y-R_\beta)\rangle=\int \exp\,[ik(x-y)]V(k)V^*(k)c(k)\,dk.$$

If E is redefined by displacing it to $E+\langle V\rangle$, to avoid the repeated appearance of $\langle V\rangle$, then (2.20) written out in full is

$$\Big[(E-k^2+i\epsilon)-\int(E-(j-k)^2+i\epsilon)^{-1}V(j)V^*(j)c(j)\,dj$$
$$+\int(E-(j-k)^2+i)^{-1}\epsilon\delta(j)V(0)V^*(0)\Big]\langle G_+(k,\,E)\rangle=1. \qquad (3.2)$$

Since V is assumed weak and there is no question of discussing bound states, V can be considered a δ function in space, so that $V(k)$ is a constant v. As a convenient measure of the strength of the potential we shall take

$$\lambda=v(NL^{-1})^{1/2} \quad . \quad . \quad . \quad . \quad . \quad . \quad . \quad . \quad (3.3)$$

where N is the number of scattering centres and L the total volume. Then (3.1) becomes

$$\Big[E-k^2+i\epsilon-\lambda^2N^{-1}\int c(j)(E-(k-j)^2+i\epsilon)^{-1}\,dj$$
$$+\lambda^2(E-k^2)^{-1}\Big]\langle G_+\rangle=1. \quad . \quad . \quad . \quad . \quad . \quad . \quad . \quad (3.4)$$

Now consider the structure of $c(k)$. For a completely disordered system for all $k\neq 0$, only the terms with $\alpha=\beta$ survive the averaging

$$\sum_{\alpha,\,\beta}\langle \exp ik(R_\alpha-R_\beta)\rangle=\frac{1}{L^2}\sum_{\alpha\neq\beta}\int\!\!\int \exp\,(ik(R_\alpha-R_\beta))\,dR_\alpha\,dR_\beta \qquad (3.5)$$
$$+\sum_\alpha\frac{1}{L}\int dR_\alpha$$
$$=N \quad (k\neq 0). \quad . \quad . \quad . \quad . \quad . \quad . \quad . \quad . \quad (3.6)$$

When $k=0$ one gets N^2 instead, and this is clearly always the value irrespective of ordering. In passing to a large number of particles in a large volume, $c(k)$ behaves like $\delta(k)$ at $k=0$, and this behaviour exactly cancels the terms in (3.1) coming from $\langle V\rangle G_0\langle V\rangle$. In future this term and the $\delta(k)$ function in $c(k)$ will not be considered further since they always cancel, and the random case will be taken to be simply $c(k)=N$.

For a completely ordered system $R_\alpha - R_\beta = (L/N)(\alpha-\beta)$, where L is the length of the system, taken to have cyclic boundary conditions. Taking R_α as the origin, since k has to take the values m/L where m is an integer

$$\sum_0^{N-1} \exp(ikL\beta/N) = \{1-\exp(ikL)\}/\{1-\exp(ikL/N)\} \quad . \quad . \quad (3.7)$$

$$= 0 \quad \text{if} \quad k \neq nk \quad . \quad . \quad . \quad . \quad . \quad . \quad . \quad . \quad (3.8)$$

$$= N \quad \text{if} \quad k = nk \quad . \quad . \quad . \quad . \quad . \quad . \quad . \quad . \quad (3.9)$$

where $2\pi N = LK$, K being the reciprocal lattice vector. In the limit of L and N being large so that one can treat k as a continuous variable, eqn. (3.7) becomes

$$c(k) = \sum_{n=-\infty}^{\infty} \delta(k-nk). \quad . \quad . \quad . \quad . \quad . \quad . \quad (3.10)$$

These two limits are of course both standard results. Now consider a disordered system. Firstly consider each atom distributed by a function $f(R_\alpha - R_\alpha^{(0)})$ about its lattice point $R_\alpha^{(0)}$ which is fixed in space. Then

$$\begin{aligned}
&\sum_{\alpha\beta} \langle \exp ik(R_\alpha - R_\beta)\rangle \\
&\quad = L^{-2} \sum_{\alpha\neq\beta} \int f(R_\alpha - R_\alpha^{(0)}) f(R_\beta - R_\beta^{(0)}) \exp[ik(R_\alpha - R_\beta)]\, dR_\alpha\, dR_\beta \\
&\qquad\qquad + L^{-1} \sum_\alpha \int f(R_\alpha - R_\alpha^{(0)})\, dR_\alpha \\
&\quad = L^{-2} \sum_{\alpha\neq\beta} \int f(R_\alpha{}') f(R_\beta{}') \exp[ik(R_\alpha{}' - R_\beta{}')] \exp[ik(R_\alpha^{(0)} - R_\beta^{(0)})]\, dR_\alpha\, dR_\beta \\
&\qquad\qquad + L^{-1} \sum_\alpha \int f(R_\alpha{}')\, dR_\alpha \\
&\quad = N[1 - f(k) f^*(k)] + \sum_{n=-\infty}^{\infty} f(k) f^*(k) \delta(k-nk). \quad . \quad . \quad . \quad . \quad . \quad . \quad (3.11)
\end{aligned}$$

The effect of this kind of disordering is to alter the strength of the δ functions in $c(k)$ and to add to it a continuous function, but it does not alter the δ function nature. Consider next a disordering in which each atom has a distribution function relative to its nearest neighbour, for the sake of definiteness on the left say. Then

$$R_{\alpha+1} = R_\alpha + \epsilon_\alpha \quad . \quad . \quad . \quad . \quad . \quad . \quad . \quad . \quad (3.12)$$

and ϵ_α is distributed via some $f(\epsilon_\alpha)$. This gives

$$\begin{aligned}
&\Big\langle \sum_{\alpha,\beta} \exp ik(R_\alpha - R_\beta)\Big\rangle \\
&\quad = \int \sum_{\alpha\beta} \exp\left[ikLN^{-1}(\alpha-\beta) - ik\sum_{\gamma=\alpha}^{\beta} \epsilon_\gamma\right] \prod_i f(\epsilon_i)\, d\epsilon_i. \qquad (3.13)
\end{aligned}$$

Taking R_α as origin as before, and using $\mathscr{R}$ for 'real part of':

$$
\begin{aligned}
c(k) &= \mathscr{R}\sum_{0}^{N-1}\exp\,[(ikLN^{-1}+\log f(k))\beta] \\
&= \mathscr{R}\{1-\exp\,[(ikLN^{-1}+\log f(k))N]\} \\
&\quad \times\{1-\exp\,[(ikLN^{-1}+\log f(k))]\}^{-1} \\
&= \mathscr{R}\{1-f^{N}(k)\}\{1-f(k)\exp\,(iLkN^{-1})\}^{-1}. \qquad (3.14)
\end{aligned}
$$

Fig. 4

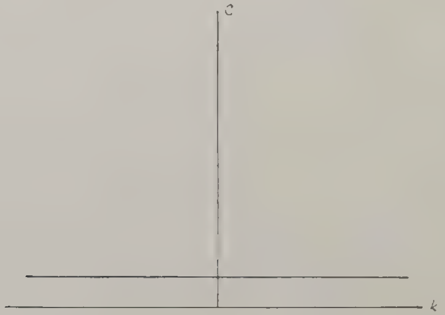

Fig. 5

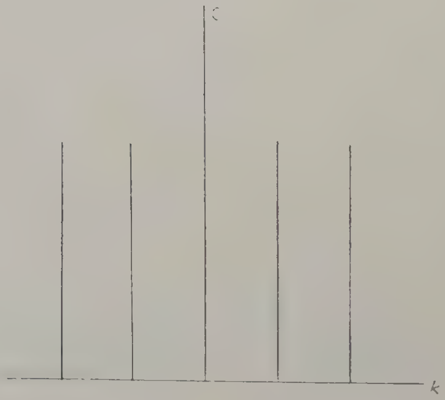

Apart from the δ function behaviour at $k=0$, which as has been noted above is unaltered and irrelevant, the δ functions of the ordered state are in this case smudged out in a way depending upon $f(k)$, for example if

$$f(\epsilon)=(2\pi)^{-1/2}\exp\,(-\tfrac{1}{2}\epsilon^{2}\mu^{-2}),$$

then

$$f(k)=(2\pi)^{-1/2}\exp\,(-\tfrac{1}{2}k^{2}\mu^{-2}).$$

A graphical representation of $c(k)$ for these cases is given below using the height given to the δ functions as a measure of their strength and omitting the δ function at the origin.

Fig. 6

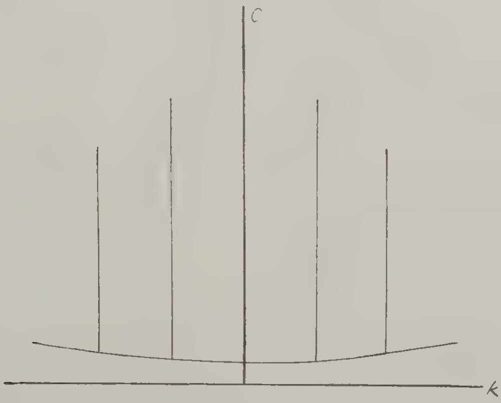

Fig. 7

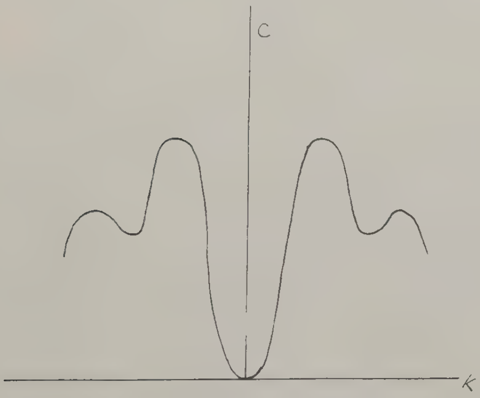

Since

$$\begin{aligned}\int c(j)\,dj &= N\delta(0)\\ &= NL\end{aligned}$$

the area under each of these curves is the same and one can consider fig. 5 for the perfectly ordered case becoming partly disordered into fig. 7 then being finally flattened into the complete disorder fig. 4. Comparison of fig. 6 with fig. 7 is of interest since the effect of the disorder in fig. 6 upon the δ function is to alter their strength but not their widths, which are altered in fig. 7. The width of the 'δ' function is thus a measure of the long-range disorder present in fig. 7 but not in fig. 6, whilst the background is a measure of the short-range disorder present in both. Since the case of a liquid is more reasonably described by fig. 7 than fig. 6, it will be case fig. 7 which is discussed in detail below, i.e. the consequences of the failure of long-range order. It must be emphasized however that in the tight-binding approximation the effects of figs. 6 and 7 are not very different, so that at present the analysis below only applies in the weak interaction case.

§ 4. THE EVALUATION OF $\rho(k, E)$

The kernel in eqn. (3.1) can be split into its real and imaginary parts by the identity

$$(E-j^2+i\epsilon)^{-1}=P(E-j^2)^{-1}-i\pi\delta(E-j^2) \quad . \quad . \quad . \quad (4.1)$$

where P indicates that the singularity is understood as a Cauchy principal part. Then

$$\begin{aligned}\lambda^2 &\int c(k-j)(E-j^2+i\epsilon)^{-1}\\ &=\lambda P\int c(k-j)(E-j^2)^{-1}-i\pi\lambda^2 c(k-\sqrt{E})/2\sqrt{E} \quad . \quad . \quad (4.2)\\ &=Q-i\Gamma \text{ say.} \quad . \quad . \quad . \quad . \quad . \quad . \quad . \quad . \quad . \quad . \quad . \quad (4.3)\end{aligned}$$

In the completely disordered case c is a constant and the principal part (for this case of δ function potentials) vanishes and the kernel is pure imaginary

$$\Gamma=\pi N\lambda^2/2L\sqrt{E}. \quad . \quad . \quad . \quad . \quad . \quad . \quad . \quad . \quad (4.4)$$

Thus $$\langle G_+\rangle=(E-k^2+i\Gamma)^{-1} \quad . \quad . \quad . \quad . \quad . \quad . \quad . \quad . \quad (4.5)$$

and $$\rho(k, E)=\Gamma[(E-k^2)^2+\Gamma^2]^{-1}, \quad . \quad . \quad . \quad . \quad . \quad . \quad (4.6)$$

a Poisson distribution about the original parabola $E=k^2$ which tends back to $\delta(E-k^2)$ as Γ tends to zero.

In the completely ordered system it is only the principal part which matters since the imaginary part is a δ function which vanishes where $\rho(k, E)$ is non-vanishing. The value of $\rho(k, E)$ is itself a δ function

$$\begin{aligned}\pi\rho(k, E)&=\mathscr{I}\left(E-k^2+i\epsilon-\lambda^2\sum_n(E-(k-nk)^2)^{-1}\right)^{-1}\\ &=\pi\delta\left(E-k^2-\lambda^2\sum_n(E-(k-nk)^2)^{-1}\right). \quad . \quad . \quad . \quad . \quad (4.7)\end{aligned}$$

Since λ is small one may consider the region where only one of the denominators in the sum matters, $n=1$, giving in this neighbourhood

$$\rho(k, E)=\delta([(E-k^2)(E-(k-K)^2)-\lambda^2][E-(k-K)^2]^{-1}). \qquad (4.8)$$

If

$$\left.\begin{aligned}E_1&=(k-K)^2\\ E_2&=\tfrac{1}{2}[k^2+(k-K)^2+\sqrt{\{[k^2-(K-k)^2]^2+4\lambda^2\}}]\\ E_3&=\tfrac{1}{2}[k^2+(k-K)^2-\sqrt{\{[k^2-(K-k)^2]^2+4\lambda^2\}}]\end{aligned}\right\} \qquad (4.9)$$

this can be written

$$\begin{aligned}\rho(k, E)&=\delta([E-E_2][E-E_3][E-E_1]^{-1})\\ &=(E-E_1)(E-E_2)^{-1}\delta(E-E_3)\\ &\quad+(E-E_1)(E-E_3)^{-1}\delta(E-E_2). \quad . \quad . \quad . \quad (4.10)\end{aligned}$$

So the k, E diagram consists of the curve $E=E_3$ and $E=E_2$ and the work above is reproducing the usual weak interaction theory as for example given by Peierls (1955). If one plots $E=k^2$ ($=E_0$ say), $E=E_1$ $E=E_2$, $E=E_3$ as on fig. 8, one finds $E=E_2$ and $E=E_3$ tend to $E=E_0$, $E=E_1$ at their extremities and have the usual energy gap of λ, as shown in fig. 8.

Fig. 8

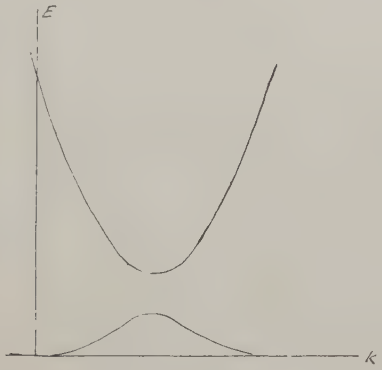

The probability function $\rho(k, E)$ (which in this case, since it is entirely made up of δ functions, is really a 'certainty' function) tells one more than just the k, E relation, for the factors $(E-E_1)$ $(E-E_2)^{-1}$ and $(E-E_1)$ $(E-E_3)^{-1}$ give the density of states along the curves $E=E_3$ and $E=E_2$. By adding in all the other values of n in the sum in (4.7) one obtains further energy gaps where the other parabolae $E=(k-nK)^2$ meet the principal parabola $E=E_0$, and by going to approximations higher than (3.2), also the energy gaps where these parabolae meet one another until the complete set of Bloch curves is developed. The additional information in $\rho(k, E)$ is the amount of each wave present, i.e. the magnitude of the fourier coefficients when a Bloch wave is analysed into plane waves whose frequencies of course differ by multiples of K. It is useful to visualize this additional information by considering the three-dimensional surface $\rho=\rho(k, E)$, fig. 8 being the projection of this surface onto the E, k plane. The extra information contained in the values of ρ, e.g. in the perfectly ordered case the strength of the δ function, is lost if one considers only a basic cell. In addition one does not wish to invoke the Bloch periodicity theorem since this only holds in the case of a perfectly periodic system. The $\rho(k, E)$ diagram for the completely disordered system consists of a Poisson distribution based upon the original parabola $E=E_0$. According to the formula (4.4), Γ is infinite at $E=0$ but the approximation (3.1) is not valid here since the scattering by a single potential well cannot be treated by Born approximation near $E=0$. A more accurate treatment using the exact scattering modifies $E^{-1/2}$ to $E^{-1/2}(1+\frac{1}{2}i\lambda E^{-1/2})^{-1}$ (as will be discussed in a subsequent paper on the tight binding approximation) so in drawing the projection of $\rho(k, E)$ on the E, k plane the width will be left finite; this point has no bearing on the rest of the paper. The diagram is given in fig. 9.

Fig. 9

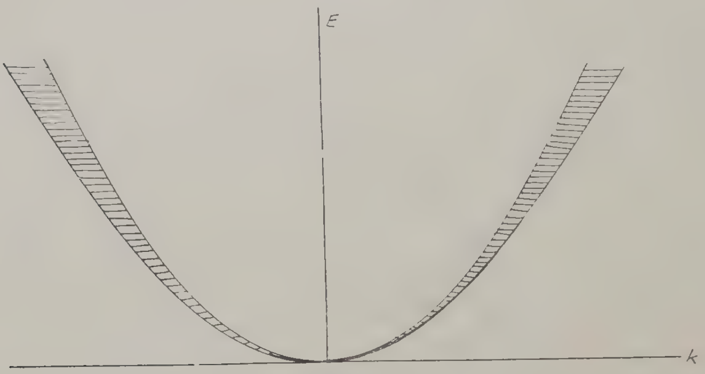

Fig. 10

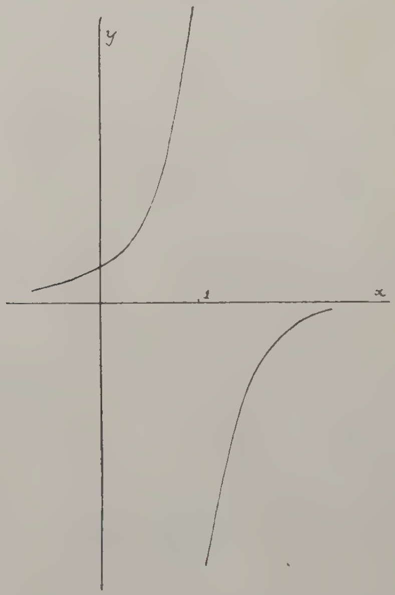

This diagram does not of course have a sharp edge to its width but it is difficult to draw otherwise. Since the decrease in order from fig. 5 to fig. 4 goes via fig. 7 there must be a $\rho(k, E)$ diagram corresponding to fig. 7 which lies between figs. 5 and 4. The key to understanding the situation can be obtained by looking at the simple function

$$y = \frac{1}{1-x}$$

which is shown in fig. 10.

Now consider y averaged by the definition

$$\langle y\rangle = P\int \frac{f(\epsilon)\,d\epsilon}{1-x+\epsilon},$$

in particular consider the two examples

$$\langle y\rangle = \frac{P}{2\alpha}\int_{-\alpha}^{\alpha}\frac{d\epsilon}{1-x+\epsilon}$$
$$= \frac{1}{2\alpha}\log\left|(1-x-\alpha)/(1-x+\alpha)\right|,$$

which is given in fig. 11 and

$$\langle y\rangle = \frac{\alpha}{2\pi}P\int_{-\infty}^{\infty}\frac{d\epsilon}{(\epsilon^2+\alpha^2)}\,\frac{1}{(1-x+\epsilon)}$$
$$= (1-x)[(1-x)^2+\alpha^2]^{-1}$$

which is given in fig. 12.

Fig. 11

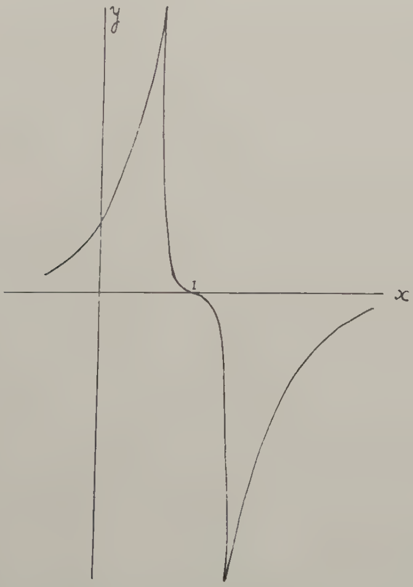

As α tends to zero, these diagrams tend back to $y=(1-x)^{-1}$ and at $\alpha=0$ that part of the curve which links the peaks on the left and on the right of the singularity at $x=1$ vanishes, so the diagrams can be described as being very similar to the $y=(1-x)^{-1}$ curve but with a *linking curve* which joins the two peaks. These results can immediately be translated into the $\rho(k, E)$ diagram, for

$$\rho = \Gamma[(E-k^2+Q)^2+\Gamma^2]^{-1}, \quad . \quad . \quad . \quad . \quad . \quad (4.11)$$

so the projection of ρ onto the k, E plane will have its maximum intensity near $E-k^2+Q=0$. The integral (4.2) for Q has the form of the model (fig. 12) above, for one can write

$$(E-(K-k)^2)=\tfrac{1}{2}E^{-1/2}[(\sqrt{E}-(K-k))^{-1}+(\sqrt{E}+(K-k))^{-1}] \qquad (4.12)$$

and, if for the moment only the neighbourhood of the first gap $k=K/2$ is considered (so that the second term corresponding to the gap at $k=-K/2$ can be ignored), the models (figs. 11 and 12) above correspond to

$$\begin{aligned} c(k)&=0, \quad |k-K|<2\alpha \\ &=(2\alpha)^{-1}, \quad |k-K|<2\alpha \end{aligned} \qquad (4.13)$$

and

$$c(k)=\pi\alpha[(k-K)^2+\alpha^2]^{-1} \qquad (4.14)$$

respectively

Fig. 12

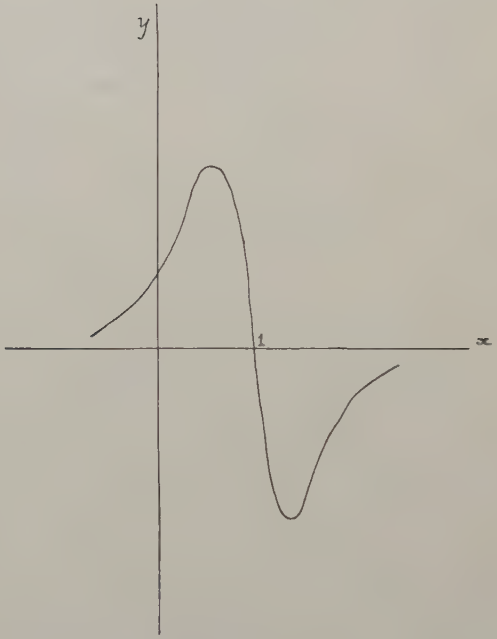

The diagrams of $E-k^2+Q=0$ for these two models of $c(k)$ are respectively figs. 14 and 15. The projection of $\rho(k, E)$ upon the (k, E) plane is sketched, as was fig. 9, in fig. 15. Again of course there are not really sharp boundaries to the distribution of states but the intensity dies away in a Poisson distribution manner. For model (4.13) the width exists only within the two parabolae $E=(k-K+\alpha)^2$ and $E=(k-K-\alpha)^2$ which are dotted in, and thus only the linking branch has a width as shown in fig. 16. One can visualize the development of fig. 8, from the parabola $E=E_0$ by thinking of the parabola as being made of rubber, clasped at the two points at which it is cut by the curves $E=(K-k+\alpha)^2$ and $E=(K-k-\alpha)^2$ and pulled out along these two parabolae in opposite directions. As α tends to zero the amount of the curve $E = E_0$ which is to be sketched out into the linking curve tends to zero and the number of states in the gap vanishes. The number of states available at say $E = k^2/4$, the middle of the gap, can be estimated when α is small by integrating (2.11) and if N_0 is the density of states at this point on the unperturbed parabola $E = E_0$, i.e. $N_0 = (2\sqrt{E})^{-1}$, E_g is the energy gap, and E_α is the energy associated with the momentum spread α, i.e. α^2, then

Fig. 13

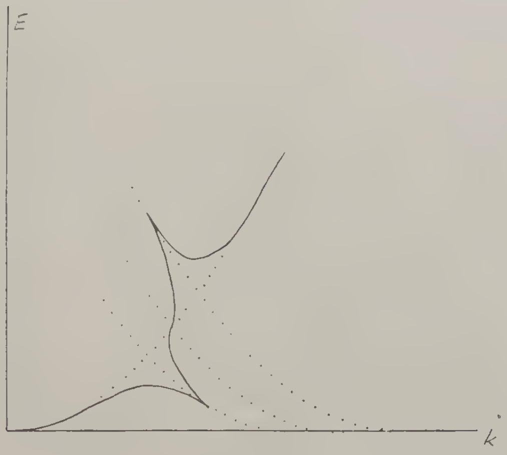

Fig. 14

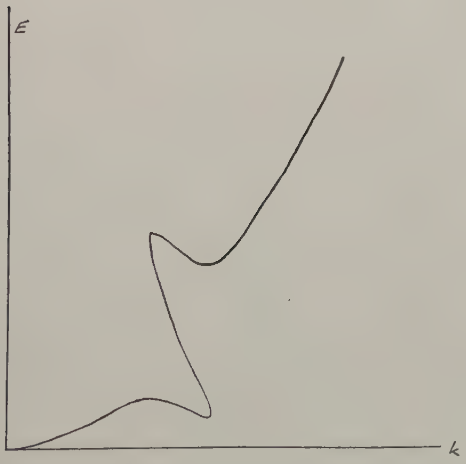

$$n_{\text{gap}} \cong n_0 E_\alpha / E_g \quad (E_\alpha \ll E_g).$$

Diagrams for $n(E)$ will be discussed in the next section. As α becomes large the curve (fig. 15) straightens out, the linking curve becoming parallel to the E axis at $\lambda \sim \alpha K$ and eventually becoming the diffuse parabola of fig. 9 as α tends to infinity. This latter limit is of course unreasonable since the spreading of the one peak of $c(k)$ which has been considered so far will meet the others to amalgamate into fig. 4, but again of course leading to fig. 9.

Fig. 15

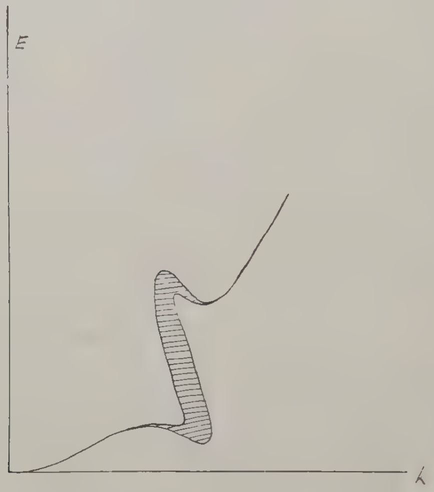

Fig. 16

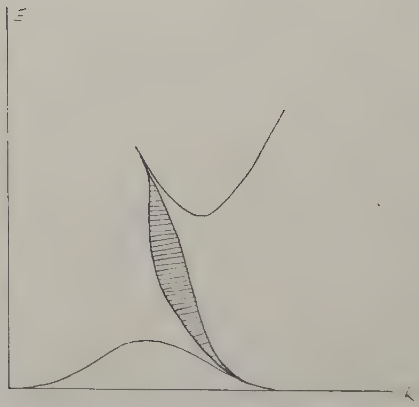

The linking curve is a characteristic of the disorder of fig. 7. An analysis of the disorder represented by fig. 6 will not have this feature. In this case the kernel of (3.2) is like a mixture of the complete disorder kernel weighted with $(1-f(k)f(-k))$ and the completely ordered case weighted with $f(k)f(-k)$. So the behaviour of the (E, k) curves will resemble the completely ordered case (fig. 8) with $\lambda^2 f(k)f(-k)$ replacing the interaction strength λ^2, and the curves will also acquire a width. As f tends to zero the curves E_2 and E_3 tend to E_0 and E_1 and the density of states along E_1 tends to zero, so that finally one reaches fig. 9. In fact the behaviour is just like that of a perfectly ordered system as the interaction tends to zero, with the addition of a steadily increasing width.

Fig. 17

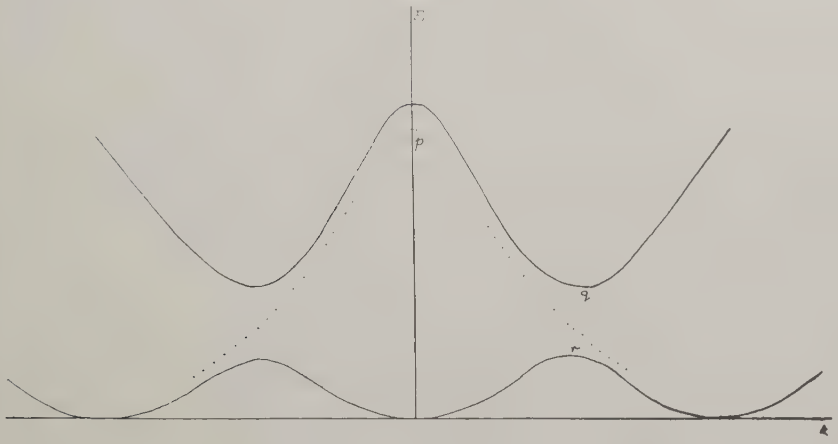

Fig. 18

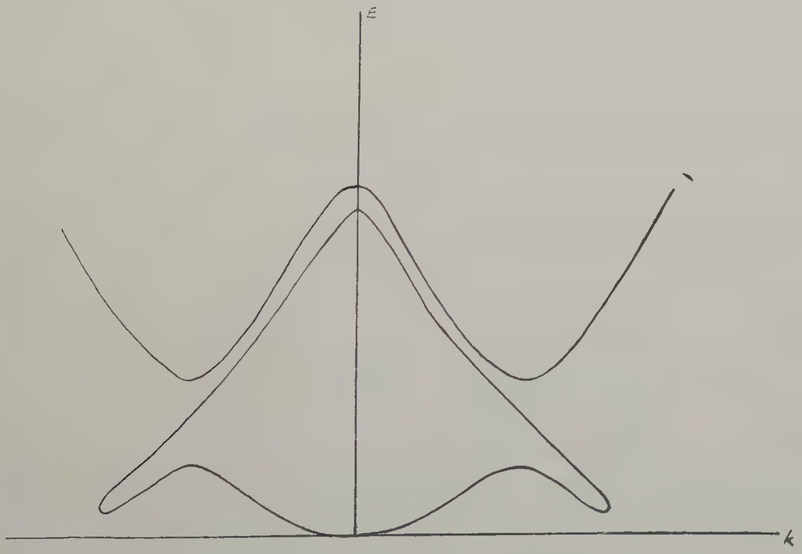

§ 5. The Level Density of the Disordered System

The $\rho(k, E)$ diagram must be symmetric in k and this modifies figs. 8–16 in the states of complete and near complete order in a way which will be important for the final discussion of this section, so the modified $E-k^2+Q=0$ curves are now given. Figure 17 is for complete order.

The limiting linking curve which in this case has zero density, has been dotted in. Figure 18 is for almost complete order, fig. 19 is the intermediate case between fig. 18 and fig. 17 in which the upper and linking branches meet at a cusp. The curve has one branch in fig. 20 in which there is less order, whilst complete disorder returns again to fig. 9.

Fig. 19

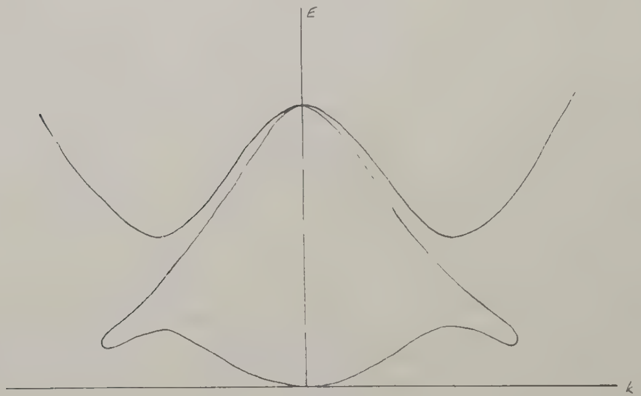

Fig. 20

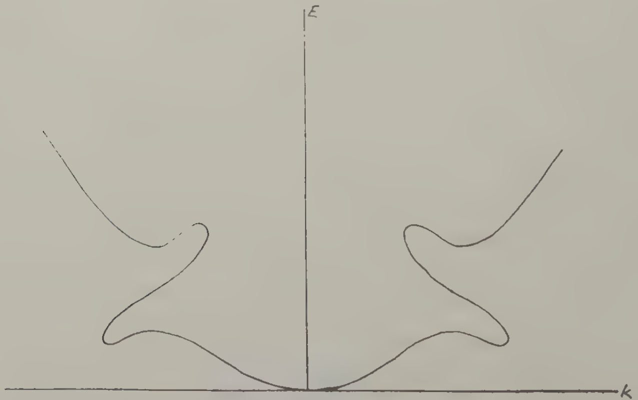

It will be seen that the main effect is that the linking curves link with one another rather than with the upper principal curves which themselves link with one another. These curves result from using both terms in (4.12). Note that there is also a further branch of $E-k^2+Q=0$ lying above the others and touching the higher of the two where it meets the axis. This branch is omitted here as it has no bearing on the analysis and belongs to a discussion of the higher Bloch curves. The linking curve fig. 17 meets the E axis at the point (p) where $E=K^2$. The minimum of the upper (full) curve is at (q) and the maximum of the lower at (r), these points corresponding to the energies E_q, E_r, both of which have $k=K/2$. These gap energies satisfy

$$E-K^2/4 \simeq \lambda^2(E-K^2/4)^{-1}; \qquad (5.1)$$

i.e.

$$\left.\begin{aligned} E_q &= \tfrac{1}{4}k^2+\lambda, \\ E_r &= \tfrac{1}{4}k^2-\lambda. \end{aligned}\right\} \qquad (5.2)$$

Thus in the spirit of the almost free electron model with a small interaction λ, it is clear that $E_p > E_q > E_r$, as has been drawn. Now $n(E)$ is defined by

$$n(E)=\int \rho(k, E)\,dk.$$

To visualize it from the diagrams think of the projection of $\rho=\rho(k, E)$ onto the E, k plane, itself projected onto the E axis. In the completely ordered case, considering only the neighbourhood of $k=K/2$, one gets from (4.10)

$$n(E) \propto (E-\tfrac{1}{4}k^2-\lambda)^{-1/2}$$

and similarly near $E \gtrsim E_r$; so that $n(E)$ behaves as is shown in fig. 1 of the introduction. The peaks are characteristic of one dimension only. By looking at figs. 14 and 16 one sees the effects of the disorder to be firstly to round off the peaks, as the width is not zero at the peaks E_q, E_r; but this rounding is mild since the width at E_q, E_r is small, indeed in fig. 16 the peaks remain infinitely sharp. Secondly, a roughly uniform density of states appears between E_q and E_r, this being the projection of the linking curve on the E axis, and the resulting distribution is that of fig. 3 of the introduction.

The analysis of this paper suggests then, that under the conditions of the almost free electron model the energy gap is immediately destroyed upon the slightest disorder of the system. As the disorder tends to be complete $n(E)$ must tend to be a smooth curve, and the current work suggests this comes about by the 'floor' of the gap rising as the peaks diminish. It does not bear out another way one could think of degrading the gap of fig. 1, by softening the walls as in fig. 2 whilst still having the gap until considerable disorder has set in. This latter picture can only be obtained from a disorder which maintains long range order, i.e. that of fig. 6. The results of this paper do not agree with numerical results given by Makinson and Roberts (1960). Presumably the density of states in the gap predicted here is too small to be unambiguously discernible in the cases they consider.

It must be emphasized that these results all refer to the almost free electron model. It is well known however that the results of the tight-binding approximation for a perfectly periodic lattice are topologically identical with the weak-binding case, so it is worth while considering pushing the above calculations outside their region of strict validity to see if they change qualitatively. Consider again then the case of infinitesimal disorder which leads to a linking curve (fig. 17). One can think of an increasing strength of interaction pushing the point (p) down until it lies below the point (q).

In this case the density of states, being the projection of these curves onto the E axis, will still show a gap when disorder appears, and this gap will close upon increasing the disorder by closing the E_p, E_r gap in fig. 21 and by the increasing width associated with the disorder. In the almost free electron model the width is always large since all N atoms contribute, but in the spirit of the extrapolation to tight binding the width associated with fig. 21 should also be considered small and of finite extension. Under these circumstances the $n(E)$ curve will close in from one side but not from the others as in fig. 22.

Fig. 21

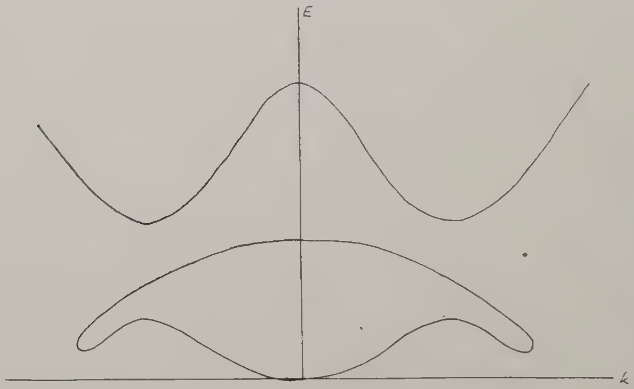

Fig. 22

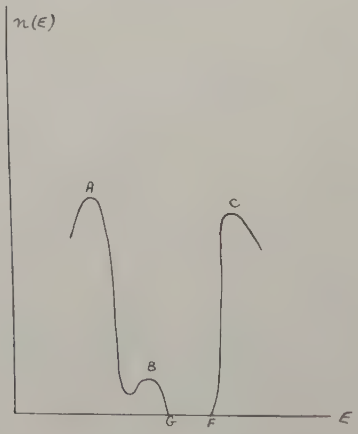

The gap exists between G and F. With increasing disorder, or with a weakening of the interaction constant, the peak at B (which is exaggerated in fig. 22) moves past the peak at C, and the picture of the earlier discussion reappears. The critical interaction comes when $\lambda=0(K^2)$ which clearly corresponds to tight binding. To attempt to make these last considerations rigorous one must treat the problem from the point of view of the tight-binding approximation, and this will be done in a subsequent paper.

§ 6. CONCLUSION

This paper has discussed the problem of disorder within a very limited framework and serves as an introduction to the realistic situations of three dimensions and of taking tight binding into account. However a general result of principle seems to be born out which is that the curves in the (k, E) plane say of $E-k^2+Q=0$, or more generally the surfaces $\rho=\rho(k, E)$, are continuously distorted by the disorder and can be understood much better when considered as a whole. The point can be made even more strongly if one builds in the symmetries which are available in all degrees of order. In the one dimensional model there is only one: $\rho(k, E)$ is even in k, so that $\rho=\rho(k^2, E)$. If one writes $k^2=q$ and studies $\rho=\rho(q, E)$ then by allowing q to be negative the curves figs. 17–20 in the neighbourhood of E_ρ become simpler to understand (fig. 23).

Fig. 23

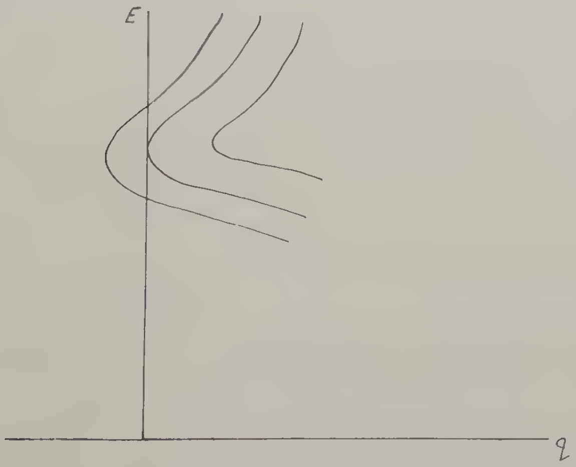

This is also true of ρ itself. Since it is the imaginary part of a function $\langle G\rangle$ which is analytic except for a certain number of poles and branch cuts, it is simpler to consider the complex $\langle G\rangle$, q, E spaces. In three dimensions this geometric thinking will become very difficult, but the advantage of considering the distortion of surfaces which remain topologically invariant except in limiting cases is very great, and it is hoped to bear this point out in subsequent work.

ACKNOWLEDGMENTS

I have to thank many people for discussion of this work especially at the Cambridge conference on liquid metals held at Easter 1960. In particular I have benefited from the comments of Professors Eisenschitz, Frank, Mott and Peierls, and from several discussions with Dr. V. Heine who has also been considering this problem. I should finally like to thank Professor Flowers for his detailed reading of and commenting upon this paper and thank Mr. J. Beeby for checking the calculations and figures and for many discussions.

REFERENCES

ABRAMS, F., and WEISS, P. R., 1958, *Phys. Rev.*, **111,** 722.

ABRIKOSOV, A. A., GORKOV, L. P., and KHALATNIKOV, I. M., 1959, *Soviet Physics, J.E.T.P.* 3518, **182,** 1090.

CHESTER, G. V., and THELLUNG, A., 1959, *Proc. phys. Soc., Lond.*, **73,** 745.

EDWARDS, S. F., 1958, *Phil. Mag.*, **3,** 1020.

EISENSCHITZ, R., and SAH, P., 1960, *Proc. phys. Soc., Lond.*, **75,** 700.

MAKINSON, R. E. B., and ROBERTS, A. P., 1960, *Austr. J. Phys.* (to be published).

LANGER, J. L., 1960, *Phys. Rev.* (to be published).

PEIERLS, R. E., 1955, *Quantum Theory of Solids* (Oxford).

Work-hardening of Hexagonal Close-packed Crystals and in the Easy Glide Region of Face-centred Cubic Crystals†

By A. Seeger, H. Kronmüller, S. Mader and H. Träuble
Max-Planck-Institut für Metallforschung, Stuttgart, and Institut für theoretische und angewandte Physik der Technischen Hochschule Stuttgart, Germany

[Received August 20, 1960]

Abstract

In the present paper we collect the available evidence from work-hardening curves, slip-line observations, and ferromagnetic measurements on the easy glide region of f.c.c. metals and alloys and the low-temperature work-hardening of hexagonal metals. New experimental results are reported on copper single crystals deformed at liquid oxygen temperature. A dislocation theory of work-hardening is given which accounts rather well for the experimental facts. The work-hardening rate can be calculated from slip-line data (distances between and lengths of slip-lines) and is found to agree well with the measurements. The theory is a statistical one and is based on the fact that in the deformation stage considered here the important stress-fields are those of individual dislocations rather than those of piled-up groups. The present paper is another example for the usefulness of slip-line studies in theories of work-hardening.

§ 1. Introduction

In a previous paper (Seeger *et al.* 1957) a general picture was developed of the dislocation processes responsible for the principal features of work-hardening of f.c.c. metal single crystals. A quantitative theory was given for the rate of rapid work-hardening in the so-called stage II of the stress–strain curve. In the meantime this theory was confirmed quantitatively by electron microscope observations of active slip lines (Mader 1957, Kronmüller 1959) and by ferromagnetic measurements (Kronmüller 1959, Seeger and Kronmüller 1960, Kronmüller and Seeger 1961). Furthermore, a quantitative interpretation was given for the onset of the dynamic recovery region in the stress–strain curve of f.c.c. crystals, i.e. the shear stress τ_{III} at the beginning of stage III (Seeger *et al.* 1959, Wolf 1960). This theory was quantitatively confirmed by experiments on copper, gold (Berner 1960), and nickel single crystals (Leitz 1960). Qualitative or semi-quantitative interpretations are available for the work-hardening and work-softening characteristics in stage III, for the transition from the easy glide region (stage I) to stage II, and for the origin of such structural changes as kink bands or bands of secondary slip (Seeger 1958, Mader and Seeger 1960, Seeger and Mader 1960).

---

† Communicated by the Authors.

What is lacking in the present picture of work-hardening of f.c.c. metals is a quantitative understanding of the easy glide region (Andrade and Henderson 1951). It was pointed out some time ago (Mott 1952) that the easy-glide phenomenon in f.c.c. crystals appears to be related to the work-hardening of hexagonal metal crystals such as zinc or cadmium. In our previous paper (Seeger *et al.* 1957) we therefore postponed the detailed discussion of stage I until a more thorough investigation of the work-hardening characteristics of hexagonal metals deforming mainly by basal glide became available. In the meantime the plastic deformation of zinc single crystals was studied experimentally (Träuble 1958, Seeger and Träuble 1960), using the same approach and as far as possible the same experimental techniques as employed in the study of f.c.c. metals. The combination of quantitative slip-line investigations by optical and electron microscopy with measurements of stress-strain curves showed that two principal manifestations of the work-hardening of zinc single crystals deforming by basal glide have to be distinguished: at low temperatures ($\leqslant 250^\circ$K) the deformation process is indeed similar to the easy glide of f.c.c. crystals. The slip-line pattern is essentially that of fine slip (Mader 1957) with slip-line lengths of the order of magnitude of 1 mm, i.e. comparable with the diameter of the specimens. At higher temperatures, the slip-line pattern is rather different, the slip-lines being grouped into rather short bands, showing the phenomenon of 'fanning'. The governing processes in the high-temperature region appeared to be the thermally activated climb of edge dislocations and the condensation of point defects to form obstacles to the gliding motion of the basal dislocations.

The purpose of the present paper is to close the above-mentioned gap in the theory of work-hardening by giving a quantitative explanation of the rate of work-hardening in easy glide and in the low-temperature region of hexagonal metals. In the present paper we shall not consider the high-temperature work-hardening of hexagonal metals, in which recovery processes are important; we shall confine ourselves to those cases in which the hexagonal crystals deform mainly by basal glide. In § 2 we shall mention first some of the experimental difficulties with which quantitative studies of the present topic are beset, and then summarize the main experimental evidence available. In § 3 we shall outline the qualitative features of the theory, stressing in particular the differences to the theory obtaining in stage II. Section 4 contains the quantitative formulation of the theory. It involves a number of statistical calculations, the details of which are deferred to an appendix.

§ 2. SUMMARY OF THE EXPERIMENTAL EVIDENCE

2.1. *Basic Facts*

The outstanding experimental observation on the easy-glide phenomenon is the rather small work-hardening rate. It is an order of magnitude smaller than in stage II of the work-hardening curve of f.c.c. metals.

The work-hardening rate in the easy glide region, which we shall denote by $\theta_{\mathrm{I}}=(d\tau/d\epsilon)_{\mathrm{I}}$, is rather dependent on the orientation of the tensile axis (Diehl 1956 a). We shall fix our attention on crystal orientations in the middle region of the stereographic standard triangle, where θ_{I} is smallest and of the order $2\times10^{-4}G$ (G shear modulus). A brief discussion of the orientation dependence of θ_{I} (Seeger 1957) will be given in § 5.

For hexagonal crystals deforming mainly on one basal glide system the low-temperature work-hardening rate θ/G is of the same magnitude as the lowest values obtained for f.c.c. crystals or even somewhat smaller. Whereas the easy-glide work-hardening curve in f.c.c. crystals is linear within experimental accuracy, this is not so for the low-temperature work-hardening curve of zinc or cadmium crystals. However, even in these cases the slope of the stress–strain curve is practically constant over strain intervals which are considerably larger than the typical extension of the easy-glide region of f.c.c. crystals. Since furthermore the deviation from the idealized behaviour seems to depend on the way the crystals are prepared (see e.g. Lücke *et al.* 1955, and Seeger and Träuble 1960), we shall not discuss here the strain dependence of the low temperature θ (see however § 5).

A similar idealization is necessary for f.c.c. crystals. Diehl (1956 b) for Cu crystals and Meissner (1959) for Ni–Co crystals showed that in easy glide the deformation is not uniform along the specimen. The 'local' work-hardening rate may deviate up to 30% from the average taken over the length of the crystal.

2.2. *Particular Problems*

The experimental investigation of the low work-hardening stage has to face a number of difficulties which are absent in stage II. We list some of them here in order to see the natural limitations to the possible agreement between theory and experiments.

(*a*) In the majority of pure f.c.c. metals deformed at room temperature the easy-glide region extends only over a few per cent shear strain. For some techniques this is not enough to do reliable experiments. We have remedied this by doing experiments also on a hexagonal metal (zinc) and on f.c.c. alloy crystals, in particular nickel–cobalt crystals. It was shown that the rather extended stage of initial low work-hardening of these alloys is indeed closely related to the easy glide of pure metals (Meissner 1959), and is positively distinct from the yield elongation observed e.g. in α-brass single crystals (Piercy *et al.* 1955), which is associated with the propagation of Lüders bands. To some extent it is possible to get longer easy glide regions in pure f.c.c. metals by working at liquid air temperatures.

(*b*) For both f.c.c. crystals and hexagonal crystals the slip-lines observed in the electron microscope are so long that it is rarely possible to measure directly the length of a slip-line. It is therefore difficult to decide whether the active length of slip-lines (i.e. the length of slip-lines active in a small strain interval) varies with strain or not. Furthermore, for f.c.c. metals and also for hexagonal metals at small strains, the height of the slip-lines is rather small, corresponding to $n = 10$–20 dislocations in a glide zone. These small values of n make accurate determinations difficult, particularly if one wishes to decide whether an individual slip-line grows in height with increasing strain or not.

(*c*) Zinc, cadmium, and to a lesser extent also magnesium crystals, recover at room temperature. In our investigations of the low-temperature behaviour it was therefore inadmissible to interrupt the low-temperature tensile tests for an extended period of time in order to obtain a replica or to repolish the surface, since this would have brought in undesirable changes in the dislocated structures of the deformed crystals. We could therefore use neither selected area techniques (' Zielpräparation ') nor determine the active slip-line lengths and slip-line heights as a function of strain. We did use the selected area method, however, in order to study the effect of short recovery intervals on the low-temperature slip-line pattern. Slip-line heights as a function of strain (fig. 1) were obtained by investigating crystals of the same orientation that had been strained (without interruption) by different amounts. For details of these investigations see Seeger and Träuble (1960).

Fig. 1

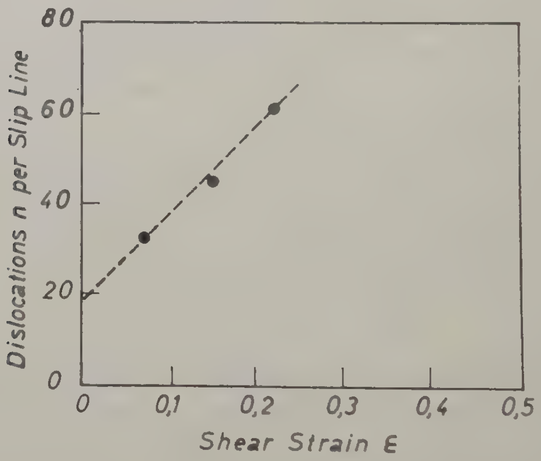

Number n of dislocations per slip-line as a function of shear strain for zinc crystals deformed at 90°K.

(*d*) Whereas the work-hardening rate in stage II is very reproducible and hardly dependent on the impurity content, the perfection of the crystal, or the handling and previous history of the specimen, this is not so in the work-hardening stage with which the present paper is concerned. Examples for this have been given in § 2.1.

The preceding discussion shows that the agreement between theory and experiment, which we can hope to obtain, will be seriously limited by a number of factors. At present it appears that due to these limitations it will not be possible to get agreement better than within a factor of two.

The evidence on the temperature dependence of θ_I/G is not very clear cut. Cu single crystals (Berner 1957, Diehl and Berner 1960) show a decrease by almost a factor of two when going from room temperature to liquid nitrogen temperature, whereas Ni single crystals (Leitz 1960) hardly show any temperature dependence between 90°K and 370°K. A similar situation obtains for hexagonal crystals at low temperatures, where θ/G in some instances is independent of temperature and strain rate, whereas in others there is a slight temperature variation (see e.g. Seeger 1958). Since we do not aim at a better agreement between experiment and theory than within a factor of two, we shall leave the question of the temperature variation of θ/G out of our considerations.

2.3. *The Experimental Approach used in the Present Investigation*

In the following sections we shall summarize our main experimental results. Sections (*a*) to (*d*) are based on slip-line studies by electron microscopy. Sections (*e*) and (*f*) deal with flow stress and creep-rate measurements and with measurements of the approach to ferromagnetic saturation in Ni–Co crystals. The interpretation of the latter group of data requires a certain amount of dislocation theory. They are, however, particularly useful as guides to the type of dislocation model which is appropriate in the easy glide region.

(*a*) Due to the difficulties mentioned in § 2.2 (*c*) it is not possible to follow the history of an individual slip-line on *zinc* as a function of strain without involving recovery. We have therefore determined the slip-line heights after different shear strains ϵ of zinc single crystals at 90°K (Träuble 1958, Seeger and Träuble 1960). Figure 1 shows the average number n of dislocations per line as a function of strain. It will be seen that n varies linearly with ϵ and that it extrapolates to a finite value of $n_0 \approx 18$ at zero strain.

(*b*) On Zn single crystals deformed at 90°K no ending slip-lines could be found within the field of view of the electron microscope. This means that their length was comparable with the diameter of the crystal. On a copper crystal deformed at room temperature, an individual slip-line could be followed over 0·6 mm (Mader 1957). A statistical determination of the slip-line length L by counting the frequency of ending lines was possible on Cu and on NiCo crystals with 20% Co (Kronmüller 1959). In a NiCo crystal deformed at 20°C the easy-glide region extended to $\epsilon = 0{\cdot}25$. In four strain intervals in the easy-glide region we found, independently of the total strain, $L = 1$ mm.

(*c*) The slip plane distance x is defined as the average separation between neighbouring active slip planes (measured perpendicular to the slip planes). In the electron microscope x can be determined by either measuring distances between slip-lines or by counting the number of slip-lines per unit length. On zinc single crystals deformed at 90°K it was found (Träuble 1958, Seeger and Träuble 1960) that the average slip-line distance determined by either one of these two methods was independent of strain for $\epsilon \gtrsim 0{\cdot}1$. Kronmüller (1959) observed that in the easy glide region of a Ni–20% Co crystal deformed at 20°C the slip plane distance x did not depend on the length of the strain interval and hence should be independent of the total strain (for typical slip-line patterns see figs. 2 and 3†).

(*d*) Selected area electron microscopy was carried out on copper single crystals deformed at liquid oxygen temperature as shown in figs. 4 and 5 (crystallographic orientation C/14—see Diehl 1956 a). After a certain amount of strain the average separation x of neighbouring slip-lines was determined by counting the number of slip-lines per unit length. After additional strain increments we determined the number of additional lines by comparing the electron micrographs from the same area, but different strains. In this way we obtained x as a function of strain as reported in the table. The lengths L of the slip-lines were found by counting the number of ending slip-lines on each of the electron micrographs. The values of θ_{I} are calculated from x and $L = L_2$ (eqn. 4.14) for the purpose of checking the theory of § 4. A modified and possibly more accurate method for determining L was used for a second crystal. On an electron micrograph (extending over 250 cm in the direction of the slip-lines, magnification × 10 000) we compared directly individual slip-lines in areas separated by a distance of 0·25 mm parallel to the slip-line direction and counted the number of slip-lines that were visible in only one of the areas. After total strains of $\epsilon_1 = 0{\cdot}048$ and $\epsilon_2 = 0{\cdot}075$ we found $L = 700\,\mu$ and $x = 380$ Å, independent of strain. These observations indicate that L and x are indeed constant, provided the strain ϵ is not too small.

Quantitative data from slip-line pattern of crystal fig. 4

ϵ	x (Å)	$L(\mu)$	θ_{I} (kg/mm^2)
0·0688	386	600	0·88
0·150	330	620	0·77
0·236	322	660	0·72

(*e*) Berner (1957), Diehl and Berner (1960) investigated experimentally, how the temperature independent part τ_G and the temperature dependent part τ_S of the total flow stress τ vary as a function of τ or ϵ in the easy glide region. On copper single crystals it was found by flow-stress measurements involving various temperature changes in the temperature interval between 90°K and 295°K that $\theta_S \equiv d\tau_S/d\epsilon \ll \theta_G \equiv d\tau_G/d\epsilon$ and also that $\theta_S/\theta_G \ll \tau_S/\tau_G$. This means that the density of the dislocation forest threading the principal glide plane does not vary significantly during easy glide. This is in complete agreement with measurements of transient creep of aluminium and copper single crystals, which gave good agreement with a theory based on the assumption that the forest density is constant during easy glide (Seeger 1954, Michelitsch 1959).

---

† Figures 2, 3, 4 and 5 are shown as plates.

(*f*) It was shown elsewhere (Seeger and Kronmüller 1960, Kronmüller and Seeger 1961) that in ferromagnetic crystals measurements of the differential magnetic susceptibility χ in the range of the approach to ferromagnetic saturation provide quantitative information on the density and the arrangement of dislocations. In particular, it can be decided whether the internal stresses in the material are mainly due to piled-up dislocation groups or to isolated dislocations. The separation beyond which dislocations act as individuals rather than members of a group, depends on the magnetic field H and can therefore be varied in the experiments.

In the easy glide region the dislocation density is rather small. In order to obtain quantitative measurements, it is imperative to minimize all the other contributions to χ in the saturation range, in particular that of the crystalline anisotropy. In alloys of 80% Ni and 20% Co the crystalline anisotropy is so small that for field strengths $H \gtrsim 500$ Oe χ is determined mainly by the magnetostrictive action of the dislocation stress fields. We have therefore chosen single crystals of that alloy for a quantitative investigation (Kronmüller 1959). Details are given in Appendix A of the present paper. The result is that the correct relation between χ and τ is obtained, if we assume that the dislocations are distributed in the various glide planes as suggested by the slip-line pictures, and that in the glide planes the dislocations are so far apart that they act as individuals.

§ 3. Outline of the Theory

We shall at first discuss some implications of the experimental evidence reported in § 2.3 (*e*) and § 2.3 (*f*). The flow-stress measurements show that the contribution of the dislocation forest to the work-hardening rate in stage I is negligibly small. θ/G has to be accounted for by the action of the long-range stress fields of the dislocations. The existence of well-defined slip-lines shows that the dislocations are generated from their sources in groups of at least ten to twenty. However, if one calculates the internal stress as produced by such groups, one finds on quite general arguments similar to those outlined by Kronmüller and Seeger (1961) that the work-hardening rate should be approximately that observed in stage II. A similar discrepancy in order of magnitude is obtained for the χ–τ relation. We must conclude, as already indicated by the remarks at the end of § 2.3 (*f*), that in the easy glide region and also in the hexagonal crystals the stress fields of the dislocations must be considered individually and not as that of piled-up groups.

The main task of the present section is to understand how the difference from stage II comes about, where the dislocations piled up towards the end of a slip-line act as a group. The flow stress is determined by certain averages over the stress fields of the dislocations, and they will necessarily be different for stage I and for stage II. In the present section we shall confine ourselves to a qualitative discussion. A quantitative treatment will be given for stage I in the next section, whereas for stage II it may be found elsewhere (Seeger 1958, Kronmüller and Seeger 1961).

In stage II the piled-up groups of n dislocations may be treated as giant dislocations of strength nb. Relaxing this simplifying assumption (Kronmüller and Seeger 1961) has virtually no effect on the final result. The reason for this is that in stage II the extension of a piled-up group is smaller than the distance between groups. In stage I, however, the opposite is true. It is therefore essential to allow for the spacial spread of the piled-up groups. The quantitative results of the present paper show in fact that it is a very good approximation to calculate the stress fields of the dislocations as those of isolated dislocations.

In the subsequent discussion we use explicitly the picture that the dislocation multiplication during plastic deformation occurs by the Frank–Read mechanism. In stage II the theory is based on the following criterion for the flow stress: in the area of the glide plane swept out by the first ring emitted from a Frank–Read source before the next ring is formed the opposing stress (due to internal stresses or other obstacles) must not be greater than the applied stress. This leads to the estimate that the flow stress is approximately equal to the internal stress halfway between piled-up groups of the same sign.

The preceding condition is obviously necessary but may not be sufficient. The generation of one or two dislocation rings from a number of Frank–Read sources would not give a macroscopic strain (implied in any flow-stress definition) if the rings would get held up after having travelled only a short distance from their source. This is in fact likely to occur, since in general the rings will have to pass rather close to other dislocations. However, by that time more dislocations may have been produced by the source and the corresponding stress magnification acting on the leading dislocation may push this dislocation past the obstacle until it gets eventually stuck at an unsurmountable obstacle like the head of a piled-up group or a Lomer–Cottrell barrier. This mechanism works well in stage II, since the slip distances are short anyway, and since a piled-up group can develop in a rather small area behind the leading dislocation of a ring system.

In stage I, however, the preceding consideration leads to an additional necessary condition for the flow stress. If a gliding dislocation gets stuck because it has to pass too close to another dislocation, it has to wait until enough dislocation multiplication at the source with the accompanying stress multiplication has occurred in order to push it over the obstacle. In fact, in stage I this appears to be the determining mechanism. The analysis to be given in § 4 provides an equation relating the flow stress to the number of dislocations generated from a source.

The dislocation model which we shall adopt for the quantitative treatment is the following: dislocations are generated by Frank–Read sources. They get finally held up by obstacles which are grown into the crystals (e.g. sub-boundaries) and—as an idealization—do not increase in number during glide. Behind these obstacles the dislocations are arranged in active glide planes, sometimes called glide zones (Seeger 1955). The dislocations in these glide zones are so far spread out (on account of the rather low applied stress) that they cannot be considered as piled-up groups. Gliding dislocations will have to pass them individually, and to this passing the preceding considerations regarding the effect of stress multiplication will be applied.

§ 4. QUANTITATIVE FORMULATION OF THE THEORY

Any quantitative theory of work-hardening has to proceed in three steps (Seeger 1956): (*a*) choose a dislocation model; (*b*) calculate the flow stress for this model; (*c*) find out how the parameters of the model vary with strain. If step (*b*) has been performed, (*c*) gives the rate of work-hardening and hence by integration the stress–strain curve $\tau=\tau(\epsilon)$.

The dislocation model we wish to adopt is described in § 3. The experimental results suggest that to a reasonable approximation the lengths of the slip-lines and the density N of active dislocation sources remain constant. This means that the strain ϵ and the number n of dislocations coming from a source should be related linearly, namely

$$\frac{d\epsilon}{dn}=\frac{9}{16}bL_1L_2N. \qquad (4.1)$$

Here L_1 and L_2 are the slip-line lengths of edge and screw dislocations. b is the dislocation strength, and the factor $(3/4)^2$ comes in since the average separation between positive and negative dislocations in a slip zone is only three-quarters of its length. Expressing N in terms of the slip plane distance x, defined in § 2.3, according to

$$N=(L_1L_2x)^{-1}, \qquad (4.2)$$

we obtain

$$\frac{d\epsilon}{dn}=\frac{9}{16}\frac{b}{x}. \qquad (4.3)$$

Since x can be measured in the electron microscope, eqn. (4.3) provides the answer to problem (*c*).

We shall now treat problem (*b*). The flow stress may be defined as the minimum shear stress at which large-scale dislocation movements are possible. As discussed in § 3, a necessary condition for large-scale dislocation movement is the following: if a dislocation emitted from a source gets stuck after a glide distance L_0, the back stress exerted on the source must be less than or at best equal to the increase of external stress during the strain interval corresponding to the emission of one dislocation from a source. For screw dislocations this condition can be written

$$\frac{\partial \tau}{\partial n} = \Delta \tau \geqq \frac{Gb}{2\pi} \cdot \frac{1}{L_0}. \qquad (4.4)$$

The next step is the calculation of L_0. A gliding dislocation will be stopped if it passes too close to a parallel dislocation of the same sign. The shear stress necessary to push a screw dislocation past another one at the distance y_0 is equal to $(Gb/2\pi)(1/2y_0)$. The simplest assumption we can make (which might not be too good if the applied stress is almost equal to the critical shear stress) is the following: glide can proceed if the difference between the stress τ acting on the moving dislocation and the critical shear stress τ_0 is at least equal to that 'passing' stress.

We obtain as a second necessary condition for the continuation of glide

$$\tau - \tau_0 \geqq \frac{bG}{2\pi} \cdot \frac{1}{2y_0}. \qquad (4.5)$$

In order to relate y_0 and L_0 to each other we have to calculate the probability $p_{y_0, v}$ that after travelling a distance L_0 a dislocation will meet another dislocation the glide plane of which has a distance y_0 from that of the first dislocation. This probability is determined by two events:

1. The passing of an activated glide plane in a distance y_0.
2. The meeting of a dislocation on this glide plane before having travelled a distance R_0.

When the dislocation has travelled a distance R_0, it will meet another activated glide plane. This changes the internal stresses acting on the dislocation and the whole process is repeated. In a simplified picture we find (for the full calculations see Appendix B) that the probability for the first event is

$$p_{y_0} = \frac{L_0 y_0}{R_0^2} \qquad (4.6)$$

and that for the second event is

$$p_v = \frac{2nR_0}{L_2}. \qquad (4.7)$$

The combined probability $p_{y_0, v}$ is (approximately) given by the product of eqns. (4.6) and (4.7)

$$p_{y_0, v} = \frac{2nL_0 y_0}{R_0 L_2}. \qquad (4.8)$$

The event we are looking for, namely the meeting of a parallel dislocation of opposite sign at a distance y_0, has taken place if $p_{y_0, v} \approx 1$†. We obtain thus as the desired relation between y_0 and L_0

$$y_0 L_0 = \frac{R_0 L_2}{2n}. \qquad (4.9)$$

As the condition for the flow stress we take that in eqns. (4.4) and (4.5) the equality signs should hold. This means that during easy glide $\partial\tau/\partial n$

---

† The possibility that the probabilities considered here may become larger than one is only apparent. Compare the full treatment in Appendix B.

and L_0 adjust themselves in such a way that when a dislocation meets an obstacle which it cannot overcome with the aid of the applied stress, the applied stress will be raised until another dislocation is generated at the source and will now help to push the previous one past the obstacle.

By combining the preceding equations we get (eliminating y_0)

$$L_0 = \frac{2\pi}{n}\frac{R_0 L_2}{b}\frac{\tau-\tau_0}{G} \qquad (4.10)$$

and (eliminating L_0)

$$(\tau-\tau_0)\,d\tau = \left(\frac{bG}{2\pi}\right)^2 \frac{n\,dn}{R_0 L_2}. \qquad (4.11)$$

Integration gives

$$\tau = \tau_0 + \frac{nb}{2\pi} G(R_0 L_2)^{-1/2}. \qquad (4.12)$$

Equation (4.12) completes step (*b*).

We may now obtain the expression for the stress–strain curve by combining eqns. (4.3) and (4.12). Since

$$L_1 N = R_0^{-2}, \qquad (4.13)$$

we eliminate R_0 by using eqn. (4.2) and find as the final result for the rate of work-hardening

$$\theta/G = (8/9\pi).(x/L_2)^{3/4}. \qquad (4.14)$$

Equation (4.14) can be checked experimentally, since θ, x, and L_2 can be measured. On account of the great length of the slip lines, in some cases the experimental determination of L_2 is somewhat uncertain, however.

Let us first compare eqn. (4.14) with the experimental results obtained on copper single crystals deformed at 90°K. In the last column of the table we give the values of θ_{I} as calculated from the measured values of x and L_2. The experimental value for the work-hardening rate of that crystal is $\theta_{\mathrm{I}} = 0{\cdot}70$ kg/mm². For the other copper crystal mentioned in § 2.3 (*d*) we calculate $\theta_{\mathrm{I}} = 0{\cdot}77$ kg/mm², which is exactly the value obtained from the stress–strain curve.

In Ni–20% Co alloy single crystals Kronmüller (1959) finds $x = 500$ Å, $L_2 = 0{\cdot}1$ cm. The numerical values calculated from eqn. (4.14) are at 90°K: $\theta_{\mathrm{I}} = 1{\cdot}4$ kg/mm², at 20°C: $\theta_{\mathrm{I}} = 1{\cdot}3$ kg/mm². Experimentally one finds at 90°K: $\theta_{\mathrm{I}} = 1{\cdot}7$ kg/mm², at 20°C: $\theta_{\mathrm{I}} = 2{\cdot}1$ kg/mm². The agreement is as good as one may expect in view of the inherent difficulties of the problem.

In Appendix A it is shown that the picture of work-hardening used in this section also explains quantitatively the results on the approach to ferromagnetic saturation.

The low-temperature work-hardening of zinc single crystals requires a separate discussion, since ending slip lines are not or only extremely rarely observed. This means that the average slip distance may be larger than the diameter of the crystal. This situation was considered elsewhere (Seeger 1958, § 52) with the following result: if the number of obstacles for the dislocation movement is not increased during deformation (i.e. if in an infinite crystal the slip distance were independent of the strain), the correct formula for the work-hardening coefficient is obtained by using the slip distance L_∞ in an infinite crystal and *not* the diameter L_p of the glide planes within the crystal. This condition is fulfilled for our work-hardening model. The model therefore does not predict a dependence of the work-hardening rate of hexagonal crystals on the crystal thickness, in agreement with the (rather scarce) experimental observations. We should get an upper limit for θ by replacing in eqn. (4.14) L_2 by L_p, which under our experimental conditions was typically of the order 0·5 cm. This gives as an upper limit $\theta = 2 \times 10^{-4} G$. The experimental value is indeed smaller by about a factor of two, namely $\theta = 10^{-4} G$.

§ 5. DISCUSSION

In the present paper we give a quantitative theory for the work-hardening of f.c.c. metal single crystals in the easy-glide region and for basal glide in h.c.p. metals at low temperatures. The basic idea of the theory is that while the dislocations are arranged in slip zones on glide planes, they act through their stress fields as individual dislocations and not as piled-up groups. This fact is particularly strikingly borne out by the measurements of the differential susceptibility in the range of ferromagnetic saturation in NiCo single crystals. The agreement between the calculated and the measured rates of work-hardening is better than one could have expected in view of the limited experimental accuracy and the statistical nature of the theory.

The theory of stage II (Seeger *et al.* 1957) and the present theory appear as limiting cases of a general theory of work-hardening, which postulates that the applied stress must be large enough both to drive dislocations through the internal stresses of the crystal and to generate new dislocations from Frank–Read sources against the back stresses of dislocations generated earlier. The present theory is the limiting case where the distance R_0 between neighbouring groups of dislocations (each of them generated from one source) is smaller than the separation between dislocations in the same glide plane, whereas in stage II the reverse case is realized.

The theory developed in this paper contains two parameters that must be taken from experiments: the length of the slip lines (L_2) and the separation between slip lines (x). The situation differs therefore from that in stage II, where the length and the height of the slip lines can be eliminated from the theory and where an expression for the work-hardening rate valid for all metals can be obtained (Seeger 1958). The parameters x and L_2 are determined by the dislocation structure of the undeformed crystal and depend therefore on the individual metal, the previous history (in particular the conditions of crystal growth), and the impurity content.

This is indeed borne out by the experiments, which show that stage I and the deformation of hexagonal metals are much more sensitive to impurity content and previous history than stage II.

The values of x (essentially the density of active sources) and L_2 (slip distance between the obstacles to the dislocation movement) that should be used in the theory may to some extent depend on external parameters. This has been discussed in relation to the temperature dependence of θ_{I} by Seeger and Träuble (1960). The orientation dependence of θ_{I} in f.c.c. single crystals (Diehl 1956 a—there is no corresponding variation with orientation in the hexagonal metals) may have a similar explanation (Seeger 1957, 1958). The present theory predicts that θ_{I} is independent of the crystal diameter (Seeger 1958), in agreement with the observations on the orientations in the middle of the stereographic triangle considered in this paper (Suzuki *et al.* 1956). Other orientations do show a size effect in the easy-glide region. This can be explained by assuming that during deformation some new obstacles (e.g. Lomer–Cottrell dislocations) are formed. A continual reduction of L_2 during deformation will indeed lead to an increased rate of work-hardening as observed for orientations closer to the boundaries of the orientation triangle.

The present theory cannot hold for very small deformation. Even at the smallest strains investigated, a substantial number of dislocations per slip line ($n=10$–20) is observed. This is incompatible with the notion of constant density and length of slip lines. We must rather expect that during an initial stage extending over a few per cent of shear strain the number of active dislocation sources increases with strain†. For the case of zinc this is discussed by Seeger and Träuble (1960). Mader (1957) observed such an increase in the slip line density in copper single crystals deformed at room temperature, the easy glide region of which may well be too short to display fully the stage covered by our theory. Detailed observations on that initial part of stage I are very difficult to obtain, since the complications discussed in § 2.2 apply *a fortiori*.

We have excluded from our discussion the work-hardening of hexagonal metals at higher temperatures, where recovery can no longer be neglected. The dislocation processes in that range appear to be rather complicated. The reader is referred to a recent paper (Seeger and Träuble 1960), where a detailed qualitative picture of these processes has been given.

ACKNOWLEDGMENTS

We acknowledge gratefully the support of the Deutsche Forschungsgemeinschaft who has made available to us the electron microscope, and the invaluable help of Frl. Marianne Rapp in the electron-microscopy work.

---

† If at very small strains there were slip lines with n less than, say, $n \gtrsim 5$, we could not see them until they had grown larger and we would therefore observe an increase in slip-line density with strain.

APPENDIX A

Approach to Ferromagnetic Saturation

In this appendix we give a more detailed account of our measurements on the approach on ferromagnetic saturation in deformed Ni–20% Co single crystals. As shown in detail elsewhere (Kronmüller 1959, Seeger and Kronmüller 1960, Kronmüller and Seeger 1961) the nature of the long-range stress fields due to dislocations in ferromagnetic materials can be studied by measurements of the differential susceptibility $\chi = dI/dH$ in the saturation range. These are therefore ideally suited to investigate whether in stage I the dislocations act as piled-up groups (as they do in stage II) or whether they act as individual dislocations (as is supposed in the theory of the present paper).

Fig. 6

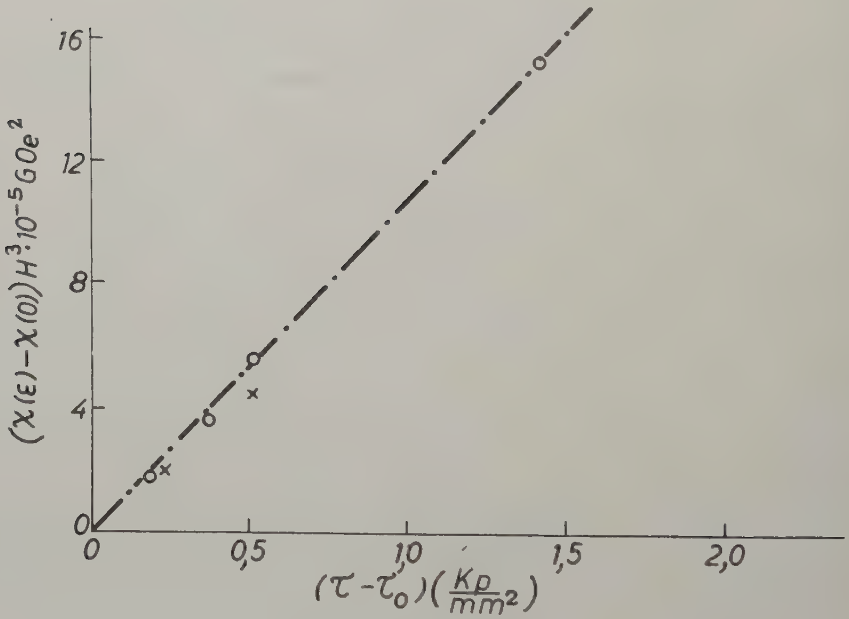

$(\chi(\epsilon)-\chi(0))H^3$ versus resolved shear stress τ for two Ni–20% Co single crystals deformed in stage I and $H=2000$ Oe. Temperature of deformation: × 300°K ; ○ 90°K.

The general quantitative expression to start from is eqn. (6.16) of Kronmüller and Seeger (1961). It was evaluated in that paper for piled-up groups of n dislocations. The result for n individual dislocations can be obtained from eqn. (6.16) by putting the distance R_{ij} between neighbouring dislocations equal to the separation R_0 between dislocation groups of both signs. The physical basis of this is that the stress field of a dislocation is screened within the radius R_0. Assuming for simplicity rectangular dislocation rings, we obtain

$$\chi H^3 = \frac{nG^2NL_1b^2}{4\pi I_s} 6\cdot6 \times 10^{-9} \log (\kappa R_0/2). \qquad \text{(A 1)}$$

In eqn. (A 1) I_s denotes the saturation magnetization, $\kappa = (HI_s/C)^{1/2}$ the reciprocal of the exchange length, and C the exchange stiffness. Equation (A 1) predicts about n^{-1} times the effect of piled-up groups of n dislocations. With the magnitudes of n as deduced from slip-line data, this difference in magnitude should be easily discernible experimentally. Figure 6 gives our experimental results for χH^3 as a function of the flow stress for $H = 2000$ Oe and for two temperatures of deformation†. From fig. 6 we determined $\Delta\chi H^3/\Delta\tau$, i.e. the change of susceptibility during a strain interval divided by the corresponding increase in flow stress (fig. 7). Making use of the relation (see eqn. (4.1))

Fig. 7

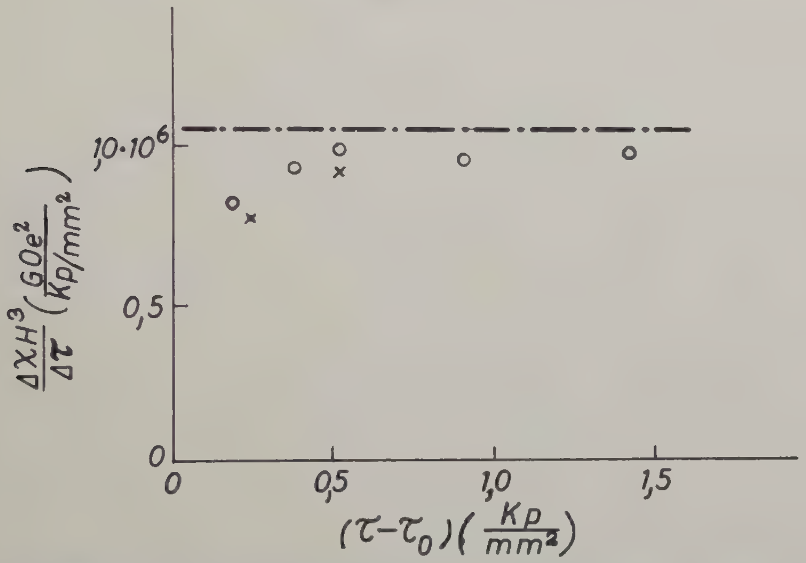

$d(\chi H^3)/d\tau$ versus τ, derived from fig. 6. The straight line is obtained theoretically from eqn. (A 3). Temperature of deformation: × 300°K; ○ 90°K.

$$nbL_1N = \frac{16(\tau_G - \tau_G^0)}{9b\theta_I L_2},$$

we obtain

$$d\chi H^3/d\tau_G = \frac{4}{9\pi} \frac{bG^2}{I_s L_2 \theta_I} 6\cdot6 \times 10^{-9} \log (\kappa R_0/2). \qquad \text{(A 2)}$$

---

† We plot only that portion of χH^3 which is due to plastic deformation (Kronmüller 1959).

Inserting $\kappa^{-1}=130$ Å and the experimental results $L_2=0\cdot1$ cm, $\theta_{\mathrm{I}}=2\cdot1$ kg/mm², and $R_0=1\cdot6\times10^{-4}$ cm, we finally get

$$\left.\frac{d(\chi H^3)}{d\tau_G}\right|_{H=2000\ \mathrm{Oe}}=1\cdot05\times10^6\,\frac{G\,\mathrm{Oe}^2}{\mathrm{kg/mm}^2}. \quad . \quad . \quad . \quad \text{(A 3)}$$

Comparison between experiment and theory in fig. 7 shows that the agreement is rather good. A theory based on pile-ups would have given a much too large effect and a wrong dependence on the applied stress. For this reason Kronmüller (1959) plotted χH^3 against the strain ϵ in the easy glide region rather than the stress. Since he used (apart from a numerical factor) the same formula for the strain as in the present paper, he got satisfactory agreement with experiment.

APPENDIX B

CALCULATION OF SOME PROBABILITIES

Let us first calculate the probabilities p_{y_0} and p_v defined in § 4. It is convenient to divide an area A of the crystal into A/y_0^2 'cells'. If R_0 is the separation between active dislocation sources, we have to consider A/R_0^2 active glide planes. As mentioned in § 4 the first prerequisite in order to stop a dislocation is the meeting of an activated glide plane in a distance y_0. There are A/R_0^2 (the number of activated dislocation sources) possible events which are distributed at random over A/y_0^2 cells. The probability p that a cell is occupied by such a possible event is y_0^2/R_0^2, provided $p\ll1$. We now wish to find out with which probability $p_{y_0}(L_0')$ a dislocation gliding through a distance L_0' passes at least once within the distance y_0 from an active glide plane. This means that we have to consider $m=L_0'/y_0$ specified cells and find the probability that not all of them are empty. The probability that a specific one of these cells is empty is $q=1-p$. The probability that all these m cells are empty is q^m. The desired probability is therefore given by

$$p_{y_0}(L_0')=1-(1-p)^m. \quad . \quad . \quad . \quad \text{(B 1)}$$

By the same kind of limiting process that leads from the binominal distribution to the Poisson distribution we obtain for $p\ll1$ and $m\gg1$

$$p_{y_0}(L_0')=[1-\exp(-mp)]=mp+\ldots. \quad . \quad . \quad . \quad \text{(B 2)}$$

The approximation $p_{y_0}(L_0')=mp=L_0'y_0/R_0^2$, which we will use subsequently, has a simple geometrical meaning and can easily be derived by inspection.

We have now to determine the probability p_v that a gliding dislocation actually meets one of the n dislocations in a neighbouring glide plane before it has passed that glide plane. The calculation is similar to the preceding one and gives as a simplified result under the condition $\dfrac{2nR_0}{L_2}\ll1$

$$p_v=\frac{2nR_0}{L_2}. \quad . \quad . \quad . \quad . \quad . \quad . \quad . \quad . \quad \text{(B 3)}$$

Equation (B 3) can also be obtained by the following simple consideration: the average linear density of dislocations of a given sign in a slip line of length L_2 is $n/(L_2/2)$, where n is the number of dislocation rings given out by the source of the line. The average linear separation between sources and therefore also lines (characterized by their centres, say) is R_0. The probability of meeting a dislocation in such a line before a new event in the trial leading to eqn. (B 1) takes place is therefore given by eqn. (B 3).

Finally, we have to consider the probability $p_{y_0, v}$ that both events considered above take place simultaneously at least once while the dislocation moves a distance $L_0 = kL_0'$. $p_{y_0, v}$ can again be found from the trial leading to eqns. (B 1) and (B 2) with

$$p = p_{y_0}(L_0')p_v \qquad \text{(B 4)}$$

and

$$m = k \equiv L_0/L_0'. \qquad \text{(B 5)}$$

The final result is

$$p_{y_0, v} = 1 - \exp\left(-\frac{2nL_0y_0}{R_0L_2}\right). \qquad \text{(B 6)}$$

We are interested in the value L_0 which makes eqn. (B 6) approximately equal to one. For practical purposes we may take

$$R_0L_2 = 2nL_0y_0, \qquad \text{(B 7)}$$

which is the result used in § 4.

REFERENCES

ANDRADE, DA C., E. N., and HENDERSON, C., 1951, *Phil. Trans.*, **244,** 177.

BERNER, R., 1957, Diplomarbeit, Stuttgart; 1960, *Z. Naturf.*, **15a,** 689.

DIEHL, J., 1956 a, *Z. Metallk.*, **47,** 331; 1956 b, *Ibid.*, **47,** 411.

DIEHL, J., and BERNER, R., 1960, *Z. Metallk.*, **51,** 522.

KRONMÜLLER, H., 1959, *Z. Phys.*, **154,** 574.

KRONMÜLLER, H., and SEEGER, A., 1961, *J. Phys. Chem. Solids*, **18,** 93.

LEITZ, C., 1960, Diplomarbeit, Stuttgart.

LÜCKE, K., MASING, G., and SCHRÖDER, K., 1955, *Z. Metallk.*, **46,** 792.

MADER, S., 1957, *Z. Phys.*, **149,** 73.

MADER, S., and SEEGER, A., 1960, *Acta Met.*, **8,** 513.

MEISSNER, J., 1959, *Z. Metallk.*, **50,** 207.

MICHELITSCH, M., 1959, *Z. Metallk.*, **50,** 548.

MOTT, N. F., 1952, *Phil. Mag.*, **45,** 742.

PIERCY, G. R., CAHN, R. W., and COTTRELL, A. H., 1955, *Acta Met.*, **3,** 331.

SEEGER, A., 1954, *Z. Naturf.*, **9a,** 758; 1955, *Handbuch der Physik*, Bd. VII, 1, S. 383 (Berlin–Göttingen–Heidelberg: Springer); 1956, *Z. Naturf.*, **11a,** 985; 1957, *Report Lake Placid Conference on Dislocations and Mechanical Properties of Crystals*, p. 243 (New York : J. Wiley); 1958, *Handbuch der Physik*, Bd. VII, 2, S. 1 (Berlin–Göttingen–Heidelberg: Springer).

SEEGER, A., DIEHL, J., MADER, S., and REBSTOCK, H., 1957, *Phil. Mag.*, **2,** 323.

SEEGER, A., BERNER, R., and WOLF, H., 1959, *Z. Phys.*, **155,** 247.

SEEGER, A., and MADER, S., 1960, *Trans. Indian Inst. Metals.*, **13,** 249.

SEEGER, A., and KRONMÜLLER, H., 1960, *J. Phys. Chem. Solids*, **12,** 298.

SEEGER, A., and TRÄUBLE, H., 1960, *Z. Metallk.*, **51,** 534.

SUZUKI, H., IKEDA, S., and TAKEUCHI, S., 1956, *J. phys. Soc. Japan*, **11,** 382.

TRÄUBLE, H., 1958, Diplomarbeit, Stuttgart.

WOLF, H., 1960, *Z. Naturf.*, **15a,** 180.

The Development of Cascades Initiated by Nuclear Interaction[†]

By K. Pinkau
H. H. Wills Physics Laboratory, University of Bristol[‡]

[Received October 10, 1960]

Abstract

The distribution function describing the development of electromagnetic cascades has been derived under the assumption that the primary particles are γ-rays with a certain energy spectrum and angular spread. By comparing experimental results on the lateral distribution of electrons in cascades initiated by nuclear interactions with the calculations presented here one may obtain information on some characteristic features of 'jets'. At large distances from the cascade 'core', the electron distribution is identical with that derived from ordinary cascade theory, thus indicating that the angular spread of the primary γ-rays can then be neglected. This result is of interest when measurements in large air showers are compared with theory.

§ 1. Introduction

In recent years, large assemblies of particle detectors and layers of heavy materials have been frequently used to study nuclear interactions of high energy; see, for example, *Proceedings of the Moscow Cosmic Ray Conference*, 1960, Vol. I, the papers by Babayan *et al.*, Duthie *et al.*, Fujimoto *et al.*, and Grigorov *et al.* By measuring the development of the electromagnetic cascade created by these interactions, one can obtain information about the energy liberated in the primary and secondary interactions, and of other parameters characteristic of nuclear interactions.

If one employs counters together with dense materials, it is comparatively easy to study experimentally the longitudinal development of a nuclear cascade. These results can then be compared with theoretical predictions of the development of nucleonic cascades; see, for example, Rozental (1952), Ueda and Ogita (1957, 1958), Fukuda *et al.* (1959), Olbert *et al.* (1957). The disadvantage of counters is their low resolving power and the complicated experimental equipment, which cannot easily be carried to high altitudes.

On the other hand, the use of nuclear emulsions allows a careful study of the 'core' of the cascades; since most of the energy is carried in the core, it is there that most of the information is to be found. The principal difficulty is to relate *closely* the quantities that can be measured accurately and with confidence—such as the lateral distribution of the cascade particles (mainly electrons) and the variation of this distribution with the depth of penetration of the material in which they develop—to the important parameters of the primary nuclear interaction such as the spread in angle and energy characterized by the transverse momentum, or the energy spectrum and total energy of the secondary particles.

[†] Communicated by the Author.

[‡] Now at the Institut für Reine und Angewandte Kernphysik, Kiel, Germany, Olshausenstr. 40–60, Gebäude 32.

The aim of this paper is to take the first steps towards establishing such a close relationship. Since we are not interested in testing any particular theory of meson production, a model of the primary interaction can be employed which displays clearly the parameters to be determined by measurements on the ensuing electromagnetic cascade.

§ 2. THE MODEL OF THE NUCLEAR INTERACTION

Recent experimental results (Edwards *et al.*, 1958, Co-operative Emulsion Group in Japan 1958) suggest that the transverse momentum of a particle created in a nuclear interaction is nearly independent of its direction of emission, and of its energy. Further, the average value, τ, of this quantity appears to vary very slowly, or not at all, with the energy of the primary particle initiating the interaction (Edwards *et al.*, 1958, Aly *et al.*, 1959). We therefore assume that the distribution in transverse momentum, p_{t}, may be represented by the relation

$$N(p_{\mathrm{t}})\,dp_{\mathrm{t}}=\frac{\pi}{2\tau^2}p_{\mathrm{t}}\exp\left(-\frac{p_{\mathrm{t}}^2\pi}{4\tau^2}\right)dp_{\mathrm{t}}. \quad . \quad . \quad . \quad . \quad (1)$$

Figure 1 shows the distribution in p_{t} thus determined together with the corresponding experimental results for pions as measured by Edwards *et al.* (1958). It may be seen that eqn. (1) is in satisfactory accord with experiment.

We have next to consider the energy spectrum of the secondary particles. This may be assumed to be given by a power law

$$N(E)\,dE \propto E^{-\alpha}\,dE$$

in the centre-of-mass system of the interaction. Such an energy distribution is also reflected, however, in the energy spectrum of the secondary particles in the laboratory system, if particles projected forwards are alone considered. Transforming to the laboratory system the energy spectrum of particles that are emitted forwards in the centre-of-mass system, and assuming that for each particle the relation $p_{\mathrm{t}}=\tau$ holds, one finds that their energy spectrum is well approximated by the same power law distribution with a lower cut-off at about $2\tau\gamma_{\mathrm{c}}$, were γ_{c} is the Lorentz factor of the centre-of-mass system. In what follows, it will therefore be convenient to confine attention to particles emitted in the 'forward cone' of the jet. This restriction is justified, because the particles emitted backwards are of very small energy in the laboratory frame of reference. Under these assumptions, the function describing the forward cone in the laboratory system of a nuclear interaction becomes

$$N(E,\theta)\,dE\,d\theta=YE^{2-\alpha}\theta\exp\left(-\frac{E^2\theta^2\pi}{4\tau^2}\right)dE\,d\theta, \quad 1<\alpha<2, \qquad (2)$$

where E and θ are, respectively, the energy and tangent of the angle of emission with respect to the primary direction. Equation (2) has been obtained by substituting $E\theta$ for p_t in eqn. (1), and multiplying it by the energy spectrum. The normalization factor Y is obtained by considering the energy radiated, χ:

$$\chi = Y \frac{2\tau^2}{\pi} \int_{2\tau\gamma_c}^{\rho} E^{1-\alpha}\, dE$$

from which follows:

$$Y(\chi, \rho) = \frac{\pi(2-\alpha)}{2\tau^2} \chi \rho^{\alpha-2}, \quad 1 < \alpha < 2. \qquad (3)$$

Fig. 1

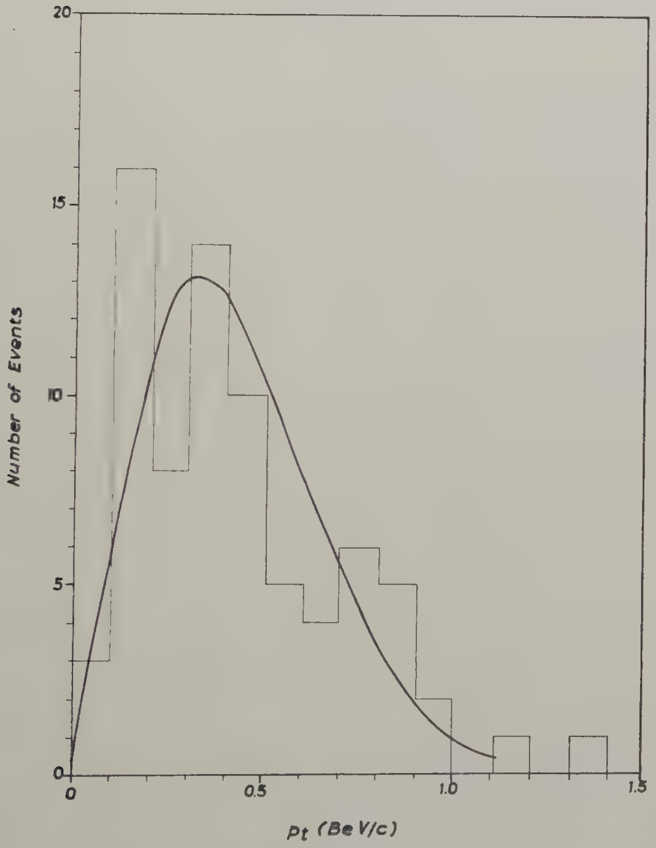

Plot of the number of events vs. the transverse momentum p_t. The experimental results are from Edwards *et al.* (1958) for pions. The curve represents eqn. (1) with a value for τ of 0·4 BeV/c.

Here, the contribution from the lower limit of the integral has been neglected on account of the subsidiary condition of eqn. (3).

The transverse momentum p_t may be expressed by $E\theta$ only if θ, the tangent of the angle of emission, is small. The lower limit of E is $2\tau\gamma_c \gg 2\tau$, however, so that the exponential is practically zero for values of $\theta > 1/\gamma_c$. It is therefore permissible to let θ range from zero to infinity without introducing a great error, provided $E > 2\tau\gamma_c$.

In the energy spectrum, the upper limit, ρ, has not been identified with the primary energy E_0 of the interaction, which appears only in γ_c. This has been done to illustrate the effects of such a cut-off, since doubts have been raised by Duthie *et al.* (1961), as to whether, for primaries of very high energy, the energy radiated in interactions caused by nucleons, χ, is still proportional to the primary energy E_0.

If $\alpha = 2$ (as in Heisenberg's theory), $Y(\chi, \rho)$ becomes

$$Y(\chi, \rho) = \frac{\chi\pi}{2\tau^2}\left(\ln \frac{\rho}{2\tau\gamma_c}\right)^{-1}. \qquad (4)$$

§ 3. DERIVATION OF THE DISTRIBUTION FUNCTION OF ELECTRONS

In this section we derive a formula for the lateral distribution of electrons in a cascade which originated in a nuclear interaction of which the secondary particles are characterized by eqns. (2) and (3). A similar attempt has been made by Hasegawa (1958) who did not, however, give an exact distribution covering all distances from the main axis of the cascade.

The procedure adopted here is to consider projected distributions first and then to transform to the true spatial distribution. This will be done in the following way. Consider the Fourier transform $F(n_1, n_2)$ of a spatial distribution $f(x_1, x_2)$, where x_1 and x_2 are the Cartesian coordinates in the 'target diagram'. The relation between F and f is

$$F(n_1, n_2) = \frac{1}{2\pi}\int\!\!\int_{-\infty}^{+\infty} dx_1\, dx_2\, f(x_1, x_2) \exp(in_1x_1 + in_2x_2). \qquad (5)$$

Let $\mathbf{f}(x_1)$ be the projected distribution

$$\mathbf{f}(x_1) = \int_{-\infty}^{+\infty} dx_2\, f(x_1, x_2), \qquad (6)$$

and $\mathbf{F}(n_1)$ its Fourier transform,

$$\mathbf{F}(n_1) = (2\pi)^{-1/2}\int_{-\infty}^{+\infty} dx_1\, \mathbf{f}(x_1) \exp(in_1x_1), \qquad (7)$$

then we find the relation

$$\mathbf{F}(n_1) = (2\pi)^{1/2} F(n_1, n_2 = 0). \qquad (8)$$

In the course of the calculation with projected distributions we will arrive at an expression for the function $\mathbf{F}(n_1)$. We know that the final solution must be symmetrical with respect to x_1 and x_2, hence $F(n_1, n_2)$ must be symmetrical with respect to n_1 and n_2. Therefore we will, according to eqn. (8) enlarge $\mathbf{F}(n_1)$ in a symmetrical way so as to find a function $F(n_1, n_2)$ which satisfies eqn. (8). This can be done in one way only, and it provides us with the Fourier transform of the final solution.

The projected distribution describing the nuclear interaction is obtained from eqn. (2) as

$$n(E,\delta)dE\,d\delta = Y'(\chi,\rho)E^{1-\alpha}\exp\left(-\frac{E^2\delta^2\pi}{4\tau^2}\right)dE\,d\delta, \qquad . \ . \ . \ (9)$$

with $$Y'(\chi,\rho) = (\tau/\pi)Y(\chi,\rho).$$

In eqn. (9), δ is the tangent of the projected angle of emission.

We need in addition the projected distribution of the electron density in a cascade originated by a single γ-ray of energy W_0. To simplify calculations, we consider Landau's approximation of Kamata and Nishimura's equations (1958). From their functions (3.32) together with (3.42), we find by using an integral representation of the Beta function:

$$\prod\nolimits_2^{\text{proj.}}(W_0,0,y,t) = -\frac{1}{4\pi^3}dy\int\int_{-i\infty}^{+i\infty} ds\,dp\left(\frac{W_0}{\epsilon}\right)^s\frac{\epsilon}{E_s}\left(\frac{\epsilon|y|}{E_s}\right)^{-2p-1}$$
$$\times\,\Gamma(p+1/2)\pi^{1/2}\Gamma(s+2p)\mathfrak{N}_2(p,-s-2p,s,t) \qquad (10)$$

where the notations are as in Kamata and Nishimura's paper, and y is the projected distance from the cascade core. For the purpose of simplifying the notation we introduce

$$\prod\nolimits_2^{\text{proj.}} = \phi(p,s)W_0{}^s|y|^{-2p-1}\,dy, \qquad . \ . \ . \ . \ . \ . \ (11)$$

with the integral operator

$$\phi(p,s) = -\frac{1}{4\pi^3}\int\int_{-i\infty}^{+i\infty} ds\,dp\,\epsilon^{-s}\left(\frac{\epsilon}{E_s}\right)^{-2p}\Gamma(p+1/2)\Gamma(s+2p)\pi^{1/2}$$
$$\times\,\mathfrak{N}_2(p,-s-2p,s,t). \qquad . \ . \ . \ (12)$$

The distribution of electrons is found as follows. In the primary interaction, a number

$$n_{\pi^0}dE\,d\delta = Y'(\chi,\rho)E^{1-\alpha}\exp\left(-\frac{E^2\delta^2\pi}{4\tau^2}\right)dE\,d\delta \qquad . \ . \ . \ (13)$$

of neutral pions are emitted into $dE\ d\delta$ at E and δ. In eqn. (13), and in what follows, the quantity χ describes the energy radiated into the neutral pion component. Each π^0-meson decays into two γ-rays almost immediately. The probability distribution of finding a γ-ray at energy W_0 in dW_0 is well approximated by a rectangular distribution, extending from 0 to E,

$$(2/E)dW_0, \quad 0 < W_0 < E. \qquad . \ . \ . \ . \ . \ . \ . \ (14)$$

The maximum transverse momentum of a γ-ray with respect to the direction of its parent π^0-meson is 70 MeV/c, much smaller than τ. Thus we can neglect the angular divergence of the γ-rays from the direction of motion of their parent pion, and assume them to be collinear with it. Hence the number of γ-rays emitted from the jet into $dW_0\ d\delta$ at W_0 and δ is

$$n_\gamma dW_0\,d\delta = 2dW_0\,d\delta\int_b^\rho dE\,n_{\pi^0}\frac{1}{E}, \qquad . \ . \ . \ . \ . \ (15)$$

where the lower limit b has the value W_0 or $2\tau\gamma_c$, whichever is the larger

Each of the γ-rays creates a cascade. Consider the electron density at a projected distance x from the core, and a distance t from the jet (all distances are measured in units of the radiation length). According to eqn. (11), each γ-ray of energy W_0 contributes a density

$$\phi(p,s)W_0{}^s|\delta t-x|^{-2p-1}\,dx \quad . \; . \; . \; . \; . \; . \; . \quad (16)$$

towards the total electron density $D(x)$ at x. This total electron density is found by integrating over all angles of emission, δ, and all photon energies, W_0:

$$D(x)=d\delta\int_0^\rho dW_0\phi(p,s)W_s{}^0|\delta t-x|^{-2p-1}n_\gamma. \quad . \; . \; . \; . \; . \quad (17)$$

The integral over $d\delta$ can be solved by a Fourier convolution (Sneddon 1951).

$$\int_{-\infty}^{+\infty} d\delta|\delta t-x|^{-2p-1}\exp\left(-\frac{E^2\delta^2\pi}{4\tau^2}\right)=\int_{-\infty}^{+\infty} dn\exp\left[-in(x/t)\right] \times A(n)B(n)t^{-2p-1}, \quad . \quad (18)$$

with

$$A(n)=(2\pi)^{-1/2}\int_{-\infty}^{+\infty} dk\,|k|^{-2p-1}\exp(ink)=(2\pi)^{1/2}\frac{\Gamma(-2p)n^{2p}}{\Gamma(1/2+p)\Gamma(1/2-p)},$$

$$B(n)=(2\pi)^{-1/2}\int_{-\infty}^{+\infty} dk\exp\left(ink-\frac{E^2\delta^2\pi}{4\tau^2}\right)=\left(\frac{2}{\pi}\right)^{1/2}\frac{\tau}{E}\exp\left(-\frac{n^2\tau^2}{E^2\pi}\right). \quad (19)$$

One obtains the following expression for the electron density:

$$D(x)dx=\frac{dx}{t}\int_0^\rho dW_0\phi(p,s)W_0{}^s4\tau Y'(\chi,\rho)\int_b^\rho dE\,E^{-\alpha-1}\int_{-\infty}^{+\infty} dn\exp\left[-in\left(\frac{x}{t}\right)\right] \times\exp\left(-\frac{n^2\tau^2}{E^2\pi}\right)t^{-2p}n^{2p}\frac{\Gamma(-2p)}{\Gamma(1/2+p)\Gamma(1/2-p)}. \quad . \; . \; . \quad (20)$$

At this stage, the transformation to the spatial distribution can be performed. Identifying n with n_1 and x with x_1 in eqn. (20), one realizes that the Fourier transform of the projected distribution, $\mathsf{F}(n_1)$ is

$$\mathsf{F}(n_1)=(2\pi)^{1/2}\int_0^\rho dW_0\,\phi(p,s)W_0{}^s4\tau Y'(\chi,\rho)\int_b^\rho dE\,E^{-\alpha-1}\exp\left(-\frac{n_1{}^2\tau^2}{E^2\pi}\right) \times t^{-2p}n_1{}^{2p}\frac{\Gamma(-2p)}{\Gamma(1/2+p)\Gamma(1/2-p)}. \quad . \; . \; . \; . \; . \quad (21)$$

Therefore, the double Fourier transform of the true spatial distribution, $F(n_1,n_2)$ must be, according to eqn. (8),

$$F(n_1,n_2)=\int_0^\rho dW_0\,\phi(p,s)W_0{}^s4\tau Y'(\chi,\rho)\int_b^\rho dE\,E^{-\alpha-1}\exp\left(-\frac{(n_1{}^2+n_2{}^2)\tau^2}{E^2\pi}\right) \times t^{-2p}(n_1{}^2+n_2{}^2)p\frac{\Gamma(-2p)}{\Gamma(1/2+p)\Gamma(1/2-p)}, \quad . \; . \; . \; . \; . \quad (22)$$

since it yields eqn. (21) for $n_2=0$ and it is symmetrical in n_1 and n_2.

The spatial electron density distribution is therefore

$$D(x_1, x_2)dx_1\,dx_2$$
$$= \frac{dx_1}{t}\frac{dx_2}{t}(2\pi)^{-1}\int\int_{-\infty}^{+\infty} dn_1\,dn_2 F(n_1, n_2)\exp\left(-in_1\frac{x_1}{t} - in_2\frac{x_2}{t}\right). \quad \ldots \quad (23)$$

Introducing $r=(x_1{}^2+x_2{}^2)^{1/2}$, $m=(n_1{}^2+n_2{}^2)^{1/2}$ and ν, the angle between the vectors (x_1, x_2) and (n_1, n_2), we obtain by transforming to polar coordinates:

$$D(r)=\int_0^\rho dW_0\,\phi(p,s)W_0{}^s 4\tau Y'(\chi,\rho)\int_b^\rho dE\,E^{-\alpha-1}(2\pi)^{-1}\int_0^\infty dm\,m\,m^{2p}$$
$$\times\int_0^{2\pi} d\nu\exp\left(-im\frac{r}{t}\cos\nu - \frac{m^2\tau^2}{E^2\pi}\right)t^{-2p-2}\frac{\Gamma(-2p)}{\Gamma(1/2+p)\Gamma(1/2-p)}. \quad (24)$$

This turns into the inverse Hankel transform:

$$D(r)=\int_0^\rho dW_0\,\phi(p,s)W_0{}^s 4\tau Y'(\chi,\rho)\int_b^\rho dE\,E^{-\alpha-1}\int_0^\infty dm\,m\,m^{2p}J_0\left(m\frac{r}{t}\right)$$
$$\times\exp\left(-\frac{m^2\tau^2}{E^2\pi}\right)t^{-2p-2}\frac{\Gamma(-2p)}{\Gamma(1/2+p)\Gamma(1/2-p)}. \quad \ldots \quad (25)$$

For the solution of these integrals we introduce the Mellin transform with respect to E, i.e. we write:

$$\int_b^\rho dE\,E^{-\alpha-1}\exp\left(-\frac{m^2\tau^2}{E^2\pi}\right)=\int_b^\rho dE(2\pi i)^{-1}\int_{-i\infty}^{+i\infty} du\,E^{-u-1}M(u), \quad (26)$$

with

$$M(u)=\int_0^\infty dE\,E^{u-\alpha-1}\exp\left(-\frac{m^2\tau^2}{E^2\pi}\right)=1/2\left(\frac{m\tau}{\pi^{1/2}}\right)^{u-\alpha}\Gamma\left(\frac{\alpha-u}{2}\right). \quad (27)$$

In doing this, the integrals over dW_0 and dE and the inverse Hankel transform can be solved. The final solution is:

$$D(r)=-(16\pi^4 i)^{-1}\int\int\int_{-i\infty}^{+i\infty} ds\,dp\,du\,Y'(\chi,\rho)2\tau\left(\frac{\tau}{\pi^{1/2}}\right)^{u-\alpha}\epsilon^{-s}\left(\frac{\epsilon}{E_s}\right)^{-2p}$$
$$\times\left(\frac{r}{2t}\right)^{\alpha-2p-u-2}t^{-2p-2}\pi^{1/2}\Gamma(s+2p)\Gamma(-2p)\mathfrak{R}_2(p,-s-2p,s,t)$$
$$\times.\frac{\Gamma\left(\frac{2p+u+2-\alpha}{2}\right)\Gamma\left(\frac{\alpha-u}{2}\right)}{\Gamma\left(\frac{1-2p}{2}\right)\Gamma\left(\frac{\alpha-2p-u}{2}\right)}\frac{1}{(s+1)(s-u+1)}(\rho^{s-u+1}-(2\tau\gamma_c)^{s-u+1}).$$
$$\ldots \quad (28)$$

§ 4. DISCUSSION OF THE SOLUTION

If one wants to consider the distribution of electrons for small values of r, one may follow the method employed by Kamata and Nishimura (1958) in a similar situation. This is to consider, in the integral over p, the contribution from the pole at $p=-s/2$ of $\Gamma(s+2p)$ only. Then, eqn. (28) becomes

$$D(r)=-(16\pi^3)^{-1}\int\int_{-i\infty}^{+i\infty} ds\,du\,Y'(\chi,\rho)2\tau\left(\frac{\tau}{\pi^{1/2}}\right)^{u-\alpha} E_s{}^{-s}\left(\frac{r}{2t}\right)^{\alpha+s-u-2}$$

$$\times t^{s-2}\pi^{1/2}\Gamma(s)\mathfrak{N}_2(-s/2,0,s,t)\frac{1}{(s+1)(s+1-u)}(\rho^{s-u+1}-(2\tau\gamma_c)^{s-u+1})$$

$$\times\frac{\Gamma\left(\frac{u+2-\alpha-s}{2}\right)\Gamma\left(\frac{\alpha-u}{2}\right)}{\Gamma\left(\frac{1+s}{2}\right)\Gamma\left(\frac{\alpha+s-u}{2}\right)}. \qquad (29)$$

For very small r, the pole at $u+2-\alpha-s=0$ is leading, so that the distribution is flat in the middle. Furthermore, $s+1-u=3-\alpha>1$, so that the term with ρ is predominant. It should, perhaps, be emphasized that an electromagnetic cascade initiated by a single particle has also a flat distribution in the middle, just like the function of eqn. (29). This is due to the fact that one can write the electron density for small values of r in a cascade produced by a single particle in the form

$$\Pi_2\sim r^{s-2}$$

where s is determined by the equation

$$\lambda_1'(s)t+\ln\frac{E_0 r}{E_s}-1/2\psi\left(\frac{2-s}{2}\right)=0. \qquad (30)$$

Equation (30) is slightly different from the corresponding equation (3.46) of Kamata and Nishimura (1958) where the ψ function has been dropped. Though this is permissible for larger r, this is not the case when r is small, since it is the ψ function which compensates the large negative values of the logarithmic term, so that $s\rightarrow 2$ for $r\rightarrow 0$ according to eqn. (30). Therefore

$$\Pi_2=\text{const.},\ s=2$$

in the centre of a single electromagnetic cascade.

The integral number

$$N(R)=2\pi\int_0^R rD(r)dr$$

of electrons within a circle of radius R has been calculated by a double saddle-point method, and numerical values have been obtained for the special assumptions

$$\rho=E_0 \quad\text{and}\quad 10\chi=E_0.$$

It has to be remembered that these results have been obtained under Landau's approximation of the cascade function. However, the results can be normalized to the cascade function of a single photon in Landau's approximation. This normalized distribution can finally be multiplied

Fig. 2

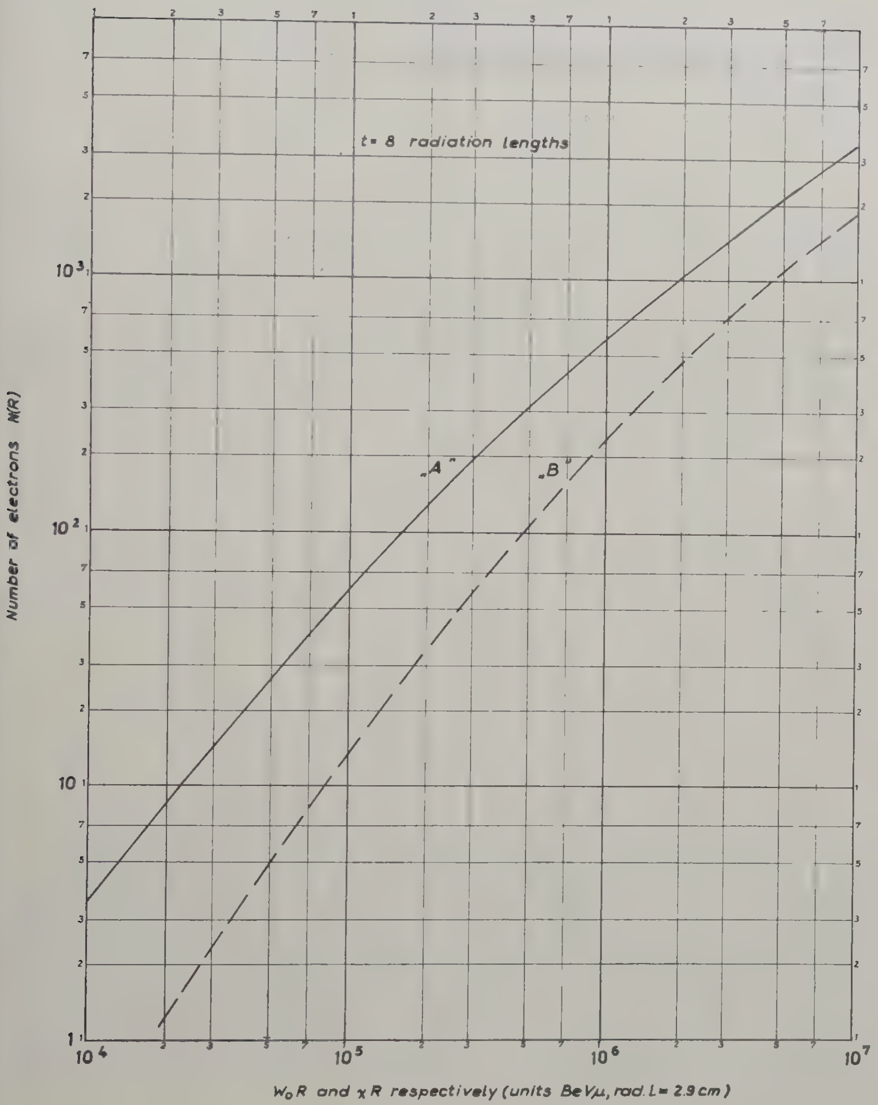

Plot of the integral number of electrons $N(R)$ vs. the quantities W_0 times R and χ times R respectively. Curve A is the distribution of electrons caused by a γ-ray incident at zero radiation lengths, according to Nishimura (1960). Curve B is the distribution due to a jet, when an energy χ was radiated in form of π^0-mesons with an average transverse momentum $\tau = 0{\cdot}4$ BeV/c, and an energy spectrum with an exponent $\alpha = 1{\cdot}5$. The inelasticity χ/E_0 was assumed to be 1/10. The graph is for pure emulsion with a radiation length of 2·9 cm. The distance to the jet or origin of the γ-ray is $t = 8$ radiation lengths.

by the true cascade distribution obtained without using Landau's approximation, and the result is displayed in fig. 2. Curve A represents the number of electrons vs. the quantity W_0R (W_0 is the energy of the primary photon), curve B is the distribution due to a jet with $10\chi = E_0$, and the bottom scale is in units of χR.

The meaning of the term

$$\beta(s, u) = \frac{1}{(s+1)(s-u+1)}(\rho^{s-u+1} - (2\tau\gamma_c)^{s-u+1})$$

in eqn. (28) can be elucidated in the following way. Consider a pencil of γ-rays incident upon an absorber. Their spectrum may be

$$E^{-u}dE,$$

and it may have the upper and lower limits ρ and $2\tau\gamma_c$ respectively. The electromagnetic cascade created by these γ-rays can be described by the well-known formulae for the cascade development (Rossi 1956, Kamata and Nishimura 1958), where the term $W_0{}^s$ containing the primary photon energy has been replaced by $\beta(s, u)$. This quantity therefore represents the energy term of the 'collinear approximation' of all the γ-rays from a jet. Since u varies with r, however, the effective slope of the energy spectrum, u, is not constant with the radius.

For larger values of r, the pole at $\alpha = u$ in eqn. (28) becomes leading. Evaluating eqn. (28) at this pole, one finds:

$$D(r) = -(4\pi^3)^{-1}\int\int_{-i\infty}^{+i\infty} ds\, dp\, 2\tau Y'(\chi, \rho)\beta(s, \alpha)\epsilon^{-s}(\epsilon/E_s)^{-2p}r^{-2p-2}$$
$$\times\,\Gamma(s+2p)\Gamma(p+1)\mathfrak{H}_2(p, -s-2p, s, t). \quad . \quad . \quad . \quad . \quad (31)$$

This is identical with Kamata and Nishimura's (1958) expression (3.28) for the lateral distribution of electrons, apart from the energy term which is now $\beta(s, \alpha)$. This means that, away from the core, the shower becomes identical with one being created by a narrow collinear beam of γ-rays, with energy spectrum and cut-offs according to the jet model. Therefore, one may use the distribution functions of Kamata and Nishimura (1958) for larger values of r, i.e. their expressions of § 3.C, together with their figs. 2 to 5. The shower age s is determined in a slightly different way, like

$$\lambda_1'(s)t + \frac{\partial}{\partial s}\ln\beta(s, \alpha) - \ln\epsilon = 0. \quad . \quad . \quad . \quad . \quad . \quad (32)$$

ACKNOWLEDGMENTS

The author would like to thank Professor C. F. Powell for the facilities of this laboratory, and for reading the manuscript. He is grateful to Dr. D. Bohm and Dr. P. H. Fowler for discussions. Mr. W. Barthold of Kiel University kindly checked the mathematics.

REFERENCES

ALY, H. H., DUTHIE, J. G. M., and FISHER, C. M., 1959, *Phil. Mag.*, **4**, 993.

CO-OPERATIVE EMULSION GROUP IN JAPAN, 1958, *Nuovo Cim.*, Suppl., **8**, 761.

DUTHIE, J. G. M., FISHER, C. M., FOWLER, P. H., KADDOURA, A., PERKINS, D. H., and PINKAU, K., 1961, *Phil. Mag.*, **6**, 81.

EDWARDS, B., LOSTY, J., PERKINS, D. H., PINKAU, K., and REYNOLDS, J., 1958, *Phil. Mag.*, **3**, 237.

FUKUDA, H., OGITA, N., and UEDA, A., 1959, *Progr. theor. Phys.*, **21**, 29.

HASEGAWA, S., 1958, INSJ-Report 13.

KAMATA, K., and NISHIMURA, J., 1958, *Progr. theor. Phys.*, Suppl., **6**, 93.

NISHIMURA, J., 1960, Mimeographed preprint for the I.C.E.F. collaboration.

OLBERT., S., and STORA, R., 1957, *Ann. Phys.*, **1**, 247.

ROSSI, B., 1956, *High Energy Particles* (Englewood Cliffs, N.J. : Prentice-Hall).

ROZENTAL, J. L., 1952, *J. exp. theor. Phys.*, **23**, 440.

SNEDDON, I. N., 1951, *Fourier Transforms* (New York : McGraw-Hill).

UEDA, A., and OGITA, N., 1957, *Progr. theor. Phys.*, **18**, 269 ; 1958, *Ibid.*, **19**, 582.

Lattice Spacing Relationships and the Electronic Structure of H.C.P. ζ Phases Based on Silver†

By H. W. King and T. B. Massalski
Mellon Institute, Pittsburgh 13, Pa., U.S.A.

[Received October 25, 1960]

Abstract

The lattice spacings of h.c.p. ζ phases in the systems Ag–Cd, Ag–Hg, Ag–Ga, Ag–In, Ag–Sn, Ag–As and Ag–Sb have been studied by the x-ray powder method.

The results show consistent trends in the changes of lattice spacings when plotted as functions of electron : atom ratio. These trends may be interpreted in terms of distortions of the Brillouin zone following interactions between the Fermi surface with various zone faces. The results indicate that in Ag-based alloys the overlap of Fermi electrons across the {10·0} faces of the Brillouin zone occurs in the region of e/a between 1·39 and 1·40.

The influence of particular solute elements on the changes in lattice spacings may be interpreted qualitatively by considering that the band gaps in the Brillouin zone of silver are decreased by the addition of the solute element.

§ 1. Introduction

Interest in the theory of the properties of h.c.p. metals and alloys was initiated by Jones (1934) when he applied the Bloch Theory to interpret the lattice spacings of the ϵ and η phases in the Cu–Zn system. However, it was not till some twenty years later that his theory was used to discuss the occurrence and stability of the h.c.p. ζ phases in other noble metal alloys (Raynor and Massalski 1955, Massalski 1956, 1957, 1958), and the lattice spacings of the latter phases were studied in detail. The ζ phases, which occur in alloys of the noble metals with the B-sub-group elements of the Periodic Table have been included in the group of intermediate phases classified as 'electron compounds' (Hume-Rothery and Raynor 1954). These phases usually follow the primary solid solutions in the phase diagrams of the respective alloy systems and often extend over wide ranges of electron concentration‡ within the general range between 1·2–1·8.

In recent studies the ζ phases in two systems based on copper (Massalski and Cockayne 1959) and in four systems based on gold (Massalski and King 1960 a) have been examined in detail. Several consistent trends in the changes in lattice spacings and axial ratios were recognized when these were plotted against the electron concentration.

---

† Communicated by the Authors.

‡ The term electron concentration, or e/a, is used to denote the ratio of all valency electrons to the number of atoms.

Additional interesting information was obtained by comparing the lattice spacings of the ζ phases with those of the respective primary solid solutions. The tentative conclusion reached was that the lattice spacings are influenced by interactions between the Fermi surface and the Brillouin zone. The trends in lattice spacings observed for the ζ phases based on gold differed significantly from those for the copper-based alloys. Therefore, it was proposed (Massalski and King 1960 a) that the Fermi surface at the beginning of the gold-based ζ phases is probably considerably distorted from the spherical shape; whereas in alloys based on copper it is likely that the Fermi surface is nearly spherical. Furthermore, the degree of distortion of the Fermi surface was considered to be somewhat greater in alloys of gold with Hg or In than in gold-based alloys containing Cd or Sn. These conclusions were shown to be in general agreement with the model suggested by Cohen and Heine (1958) to allow for the influence of the solute element on the band structure of a noble metal solvent.

Following the studies of copper and gold-based alloys, and the conclusions reached regarding their band structure, it thus became of interest to investigate in a similar manner the lattice spacings of the seven ζ phases formed when Ag is alloyed with the following B-sub-group elements of the Periodic Table:

—	Ag–Ga	—	Ag–As
Ag–Cd	Ag–In	Ag–Sn	Ag–Sb
Ag–Hg	—	—	—

The materials and methods used in this investigation are described in the Appendix, § 1.

§ 2. RESULTS

The values of the a and c lattice spacings and of axial ratio, together with the composition and other pertinent data, of the alloys studied are listed in the table. In accordance with a preliminary metallographic examination, diffraction lines of a second phase, in addition to the h.c.p. pattern, were observed in alloys Ag–Cd 26, Ag–Hg 1, Ag–Hg 6, Ag–Ga 6, Ag–In 3, Ag–Sn 13 and Ag–As 1. The electron : atom ratio values for these alloys listed in the table were estimated by locating the vol/atom data on the respective plots in fig. 1. A comparison between the present results and those reported previously in the literature is given in the Appendix, § 2.

The lattice spacings and volumes of the unit cell per atom (vol/atom) for the silver-based alloys are plotted in fig. 1 as functions of electron concentration, e/a. This figure has been arranged to follow the plan of the Periodic Table for the B-sub-group elements which have been alloyed with silver. In its own second long period silver forms ζ phases with all the elements from Groups IIB–VB, and with the exception of Ag–Cd these phases extend over wide ranges of electron concentration. The absence of ζ phases when Ag is alloyed with Tl, Pb or Bi from the third long period may be due to the large differences in atomic size between

Composition, heat-treatment, and lattice spacings at 30°c of h.c.p. ζ phases in silver-based alloys

Alloy	At. % silver	At. % solute	Heat-treatment		Structure	a, Å	c, Å	c/a	Vol/atom, $Å^3$	e/a
			Temp. °c	Time, days						
Ag–Cd										
23	49·28	50·72	438	60	ζ	3·9867	4·8253	1·6156	18·638	1·507
24	48·18	51·82			ζ	2·9904	4·8244	1·6133	18·681	1·518
25	46·11	53·89			ζ	2·9976	4·8237	1·6092	18·768	1·540
26	44·87	55·13			$\zeta+\gamma$	2·9983	4·8234	1·6087	18·776	1·542†
Ag–Hg										
1	60·00	40·00	150	100	$\alpha+\zeta$	2·9758	4·8417	1·6270	18·565	1·418†
3	56·50	43·50			ζ	2·9853	4·8413	1·6217	18·683	1·435
4	55·50	44·50			ζ	2·9896	4·8413	1·6194	18·736	1·445
5	54·00	46·00			ζ	2·9990	4·8410	1·6143	18·853	1·460
6	52·50	47·50			ζ+second phase	3·0004	4·8408	1·6134	18·870	1·463†
Ag–Ga										
2	78·30	21·70	462	44	ζ	2·8820	4·6933	1·6285	16·880	1·434
3	77·50	22·50	540	21	ζ	2·8827	4·6896	1·6268	16·875	1·450
4	76·50	23·50	600	14	ζ	2·8840	4·6851	1·6245	16·874	1·470
5	75·00	25·00	575	14	ζ	2·8869	4·6753	1·6195	16·872	1·500
6	73·50	26·50	540	21	ζ+second phase	2·8895	4·6645	1·6143	16·864	1·528†
Ag–In										
3	78·00	22·00	540	21	$\alpha+\zeta$	2·9455	4·7912	1·6266	18·000	1·448†
4	76·50	23·50	655	14	ζ	2·9495	4·7891	1·6237	18·041	1·470
5	75·00	25·00	600	14	ζ	2·9563	4·7857	1·6188	18·111	1·500
6	73·50	26·50	600	14	ζ	2·9642	4·7821	1·6133	18·194	1·530
7	72·00	28·00	600	14	ζ	2·9739	4·7767	1·6062	18·293	1·560
8	70·50	29·50	540	21	ζ	2·9840	4·7690	1·5982	18·388	1·590
9	69·00	31·00	540	21	ζ	2·9950	4·7585	1·5888	18·483	1·620
10	77·50	32·50	462	44	ζ	3·0054	4·7488	1·5801	18·573	1·650
Ag–Sn										
2	87·10	12·90	395	21	ζ	2·9284	4·7844	1·6337	17·766	1·387
3	86·67	13·33			ζ	2·9302	4·7850	1·6330	17·790	1·400
4	86·00	14·00	475		ζ	2·9335	4·7854	1·6312	17·832	1·420
5	85·00	15·00			ζ	2·9386	4·7860	1·6287	17·896	1·450
6	84·00	16·00			ζ	2·9436	4·7845	1·6254	17·951	1·480
7	83·00	17·00			ζ	2·9491	4·7840	1·6222	18·017	1·510
8	82·00	18·00			ζ	2·9548	4·7835	1·6189	18·084	1·540
9	81·00	19·00			ζ	2·9598	4·7822	1·6157	18·141	1·570
10	79·99	20·01			ζ	2·9658	4·7824	1·6125	18·215	1·603
11	79·60	21·40			ζ	2·9730	4·7818	1·6084	18·301	1·642
12	78·00	22·00			ζ	2·9760	4·7824	1·6070	18·342	1·660
13	77·50	22·50			ζ+second phase	2·9783	4·7819	1·6056	18·367	1·672†
Ag–As										
1	90·50	9·50	540	21	$\alpha+\zeta$	2·8985	4·7347	1·6335	17·224	1·400†
2	89·50	10·50			ζ	2·8993	4·7346	1·6330	17·233	1·420
3	88·50	11·50			ζ	2·9008	4·7347	1·6322	17·252	1·460
4	87·50	12·50			ζ	2·9025	4·7339	1·6310	17·269	1·500
Ag–Sb										
2	90·80	9·20	550	21	ζ	2·9276	4·7831	1·6338	17·751	1·368
4	89·75	10·25			ζ	2·9327	4·7894	1·6331	17·837	1·410
5	89·00	11·00			ζ	2·9368	4·7920	1·6317	17·896	1·440
6	87·80	12·20			ζ	2·9439	4·7950	1·6288	17·994	1·488
7	86·00	14·00			ζ	2·9553	4·7973	1·6233	18·143	1·560
8	85·00	15·00			ζ	2·9616	4·7990	1·6204	18·226	1·600
9	84·50	15·50			ζ	2·9646	4·7997	1·6190	18·266	1·620
10	84·00	16·00			ζ	2·9681	4·8003	1·6173	18·312	1·640

† e/a estimated by locating the vol/atom on the respective plots given in fig. 1.

the solvent and solute in these systems, a measure of which is provided by the size factors (Hume-Rothery, Reynolds and Raynor 1940) listed at the bottom of fig. 1. This is consistent with the observation that the ranges of homogeneity of the primary solid solutions of Ag with Tl, Pb and Bi are more restricted (fig. 1) compared to those for the remaining Ag-based systems. The size factors for the systems Ag–Ge and Ag–As are on the borderline for the formation of h.c.p. ζ phases (Hume-Rothery, Reynolds and Raynor 1940). Attempts to discover intermediate electron-phases under equilibrium conditions in Ag–Ge have so far proved

Fig. 1

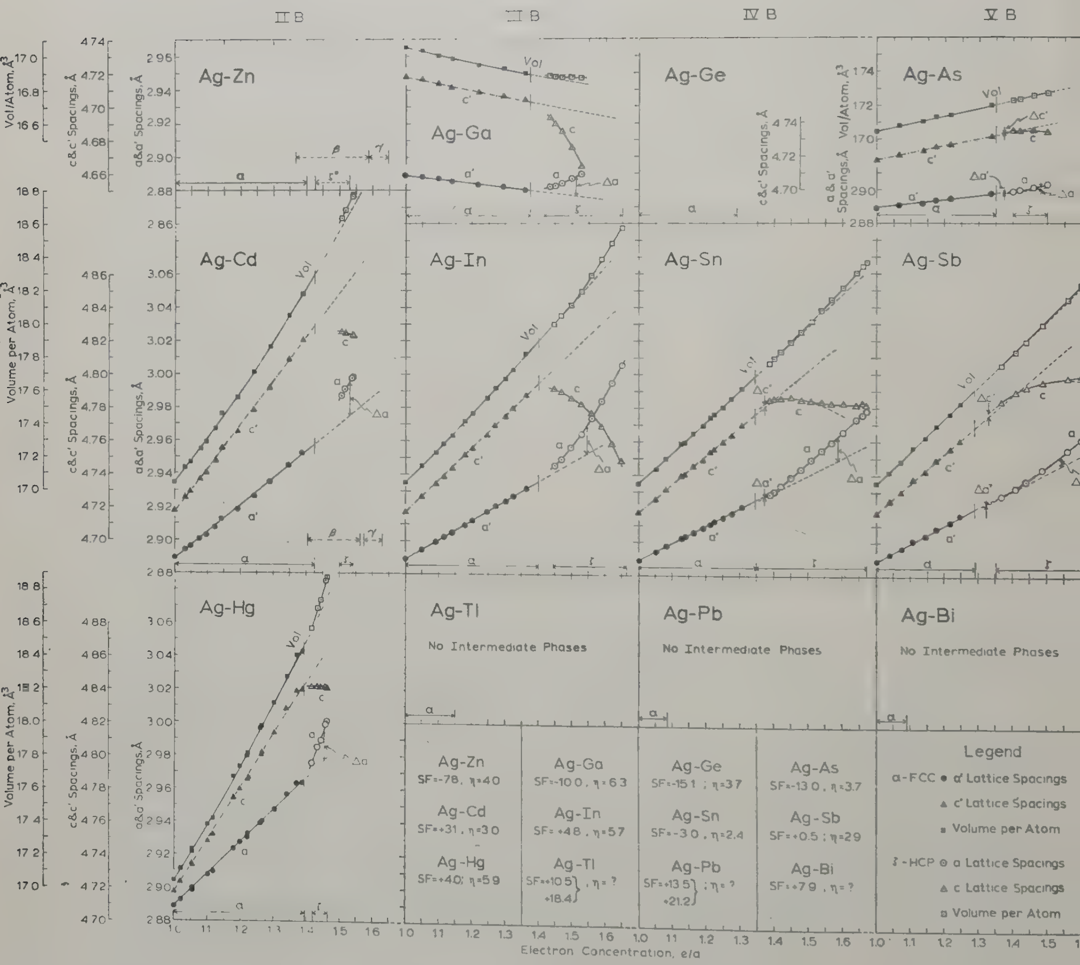

Variation of lattice spacings with electron concentration in α and ζ alloys of silver with the B-sub-group elements.

unsuccessful (Hume-Rothery, Raynor, Reynolds and Packer 1940). However, Duwez *et al.* (1960) have recently reported that metastable h.c.p. phases may be induced in this system by very rapid quenching from the melt. It is also possible that electrochemical effects (Hume-Rothery, Reynolds and Raynor 1940) play a role in limiting the range of homogeneity of the ζ phase in the Ag–As system and possibly also in Ag-Hg. The tendency towards ordering at low temperatures stabilizes the b.c.c. β phases in the systems Ag–Cd and Ag–Zn at the expense of the disordered h.c.p. ζ phases, even though the size factors appear to be favourable for the latter phases. In Ag–Cd the onset of the ζ phase is displaced towards higher contents of cadmium, and its range of homogeneity is further limited by the presence of the more stable γ phase in the region of e/a from 1·55–1·63. In Ag–Zn the tendency towards order is such that a pseudo hexagonal phase, ζ^0, is formed in place of the usual ζ phase, but a h.c.p. structure may be induced by cold-working the ordered β' phase (obtained by quenching β) (King and Massalski 1961) at room temperature. It is of interest to note that at values of e/a beyond the γ-phase range (i.e. for $e/a > 1{\cdot}7$) extensive h.c.p. ϵ phases are observed in both Ag–Zn and Ag–Cd.

As in the previous study of gold alloys (Massalski and King 1960 a) values of a' and hypothetical c' spacings and of vol/atom for the α primary solid solutions have been included in fig. 1 for comparison with the present results. The values for the α-phase alloys were calculated† from the data of Owen and Roberts (1939) for Ag–Cd, Ag–In, Ag–Sn and Ag–Sb; the data of Owen and Rowlands (1940) for Ag–Ga and Ag–As; and that of Day and Mathewson (1938) and Rayson and Calvert (1958) for Ag–Hg.

On passing from the primary solid solution to the ζ phases in the systems Ag–Sn, Ag–As and Ag–Sb there is a small but measurable decrease, $\Delta a'$ (fig. 1) in the a lattice spacings, and a complementary increase, $\Delta c'$, in the c spacings. These deviations are similar in form, but very much smaller in magnitude, to those observed previously in gold-based alloys (Massalski and King 1960 a). As a result of such deviations the axial ratios at the onset of a number of ζ phases lie above the ideal value for the close-packing of hard spheres, as shown in fig. 2.

Immediately following the onset of the ζ phases in Ag–Sn, Ag–As and Ag–Sb the curves of the a lattice spacings appear to lie parallel to the a' spacings curves for the respective primary solid solutions. However, at values of e/a in the region 1·39–1·40 the a spacings show an expansion Δa which is increased with increasing electron concentration as shown in fig. 1. Although the ζ phases in the remaining silver-based systems are not stable until values of e/a greater than 1·4, they also show Δa deviations in the a spacings with respect to the a' spacings extrapolated from the respective primary solid solutions. In the Ag–Ga system the Δa deviation is such as to cause the a spacings to increase with increasing e/a whereas the addition of Ga to silver causes the lattice spacings of the primary solid solution to be diminished. This behaviour is similar to that observed earlier in the system Ag–Al (Massalski and Cockayne 1959).

---

† $a' = 1/\sqrt{2} \, . \, a_{\text{f.c.c.}}$; $c' = 2/\sqrt{3} \, . \, a_{\text{f.c.c.}}$. The $a_{\text{f.c.c.}}$ data were corrected to 30°c using the thermal coefficients of expansion reported by Owen and Roberts (1939) and interpolating for the systems Ag–Hg, Ag–As and Ag–Ga.

Fig. 2

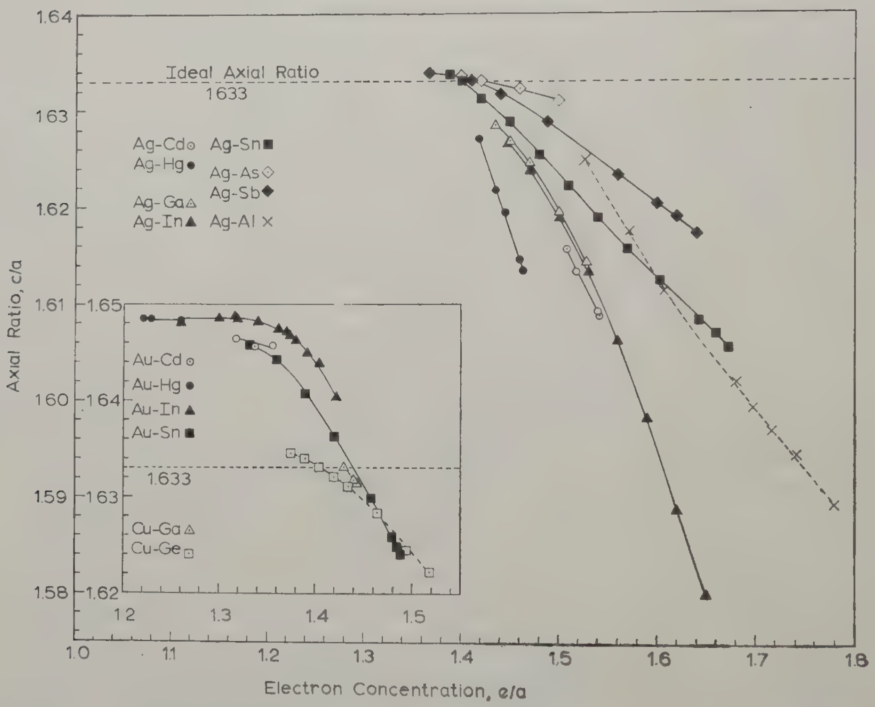

Axial ratio changes with electron concentration in h.c.p. ζ phases based on silver compared with data for alloys based on copper and on gold.

The c lattice spacings also show a decrease in slope with respect to the hypothetical c' curves in the region of e/a near 1·39–1·40. The form of this deviation is also dependent on the trend in lattice spacings in the α primary solid solutions. In the Ag–Ga system for which the latter trend is a decrease in a', and hence also a decrease in c', the c lattice spacings decrease at an accelerated rate. In Ag–Sb and Ag–As, however, the rate of increase of the c spacings is merely diminished, whereas in Ag–Sn the c spacings pass through a shallow maximum. The deviation is more marked in the remaining systems since, even though the c' spacings increase rapidly, the trend is for the c spacings to be decreased. In general the degree of the change in slope of the c spacings follows the magnitude of the Δa deviations for the respective systems, both effects being greatest in Ag–In and least in Ag–As.

The accelerated increase in the a spacings and the simultaneous decrease in the c spacings at $e/a = 1{\cdot}39$-$1{\cdot}40$ causes a rapid fall in axial ratio to values below the ideal. The axial ratios of ζ phases in alloy systems based on copper (Massalski and Cockayne 1959) and on gold (Massalski and King 1960 a) also show this rapid fall in axial ratio (fig. 2), which is one of the distinctive characteristics of the ζ phases (Massalski 1956, 1957, 1958). However, the present results for the silver-based ζ phases reveal that the rate of the decrease in axial ratio with increasing electron concentration is not constant but varies markedly with the particular solute alloyed with silver, as shown in fig. 2. Nevertheless, the axial ratios in all systems, with the possible exception of Ag–Al (Massalski and Cockayne 1959), may be extrapolated to a common value $\simeq 1{\cdot}6337$ (i.e. slightly greater than the ideal) in the region of e/a between 1·39 and 1·40.

The vol/atom at the onset of the silver-based ζ phases appears to fall almost exactly on the respective curves extrapolated from the α primary solid solutions. With increasing e/a, however, the volume shows a departure towards higher values, and the vol/atom curves rise above the curves extrapolated from the primary solid solutions. At the onset of the ζ phases in the gold-based systems the vol/atom curves were also found to superimpose upon those extrapolated from the α phase.

§ 3. DISCUSSION

The significance of the lattice spacings results will be considered in general in terms of their changes with electron concentration (e/a). For this purpose we shall assume that both the f.c.c. and h.c.p. phases are not defect structures and that all lattice sites are occupied in each unit cell. Similarly we shall assume that the conventional valencies usually associated with the noble metals and the B-sub-group elements are applicable; i.e. Cu, Ag, Au = 1; Zn, Cd, Hg = 2, etc.

Since the Brillouin zone of the h.c.p. structure does not possess cubic symmetry, interactions between the Fermi surface and various zone faces may result in distortions of the zone without altering its basic symmetry. Such zone distortions should in turn cause changes in lattice spacings along the related directions in the real lattice. Conversely, deviations observed in the trends in lattice spacings as functions of electron concentration may be used to provide information concerning possible changes both in the shape of the Fermi surface and in the nature of the band structure, which occur on alloying.

A section through the Brillouin zone proposed by Jones (1934) is shown in fig. 3 for an h.c.p. alloy of ideal axial ratio. This zone is bounded by 20 faces: six of the $\{10{\cdot}0\}$ type, two of the $\{00{\cdot}2\}$ type, and twelve of the $\{10{\cdot}1\}$ type. According to the original model of Jones (1934) overlap of electrons across a zone face may cause that face to be moved closer to the origin of k space and hence may result in an expansion of the corresponding lattice spacings in real space. The accelerated expansions in the a spacings of the h.c.p. alloys, marked Δa in fig. 1, are most likely associated with such a mechanism; i.e. in this case the overlap of Fermi electrons across the {10·0} faces of the Brillouin zone which are nearest to the origin (fig. 3). The simultaneous contraction of the c spacings is very likely a compensating effect for the Δa expansion, and hence the detailed form of the c spacings curve (e.g. slope, presence of maximum, etc.) is of no special significance as discussed previously for Au-based alloys (Massalski and King 1960 a). However, this compensation appears to be only partial, since an increase in the vol/atom is observed (fig. 1) as the electron concentration is increased beyond about 1·4.

A measure of the relative expansion of the a spacings for the various silver-based ζ phases may be obtained from the plots of the fractional distortions $\Delta a/(a-\Delta a)$ plotted as functions of e/a in fig. 4. On the basis of similar plots for the systems Cu–Ge, Cu–Ga and Ag–Al it was suggested that the rates of distortion were nearly identical for these three systems (Massalski and Cockayne 1959). However, the present results reveal that any such agreement between the rates of distortion in the copper-based alloys and in Ag–Al must be regarded as coincidental, since the rates of distortion vary over wide limits depending on which particular solute element is alloyed with Ag. Nevertheless, all the plots $\Delta a/(a-\Delta a)$ for the B-sub-group Ag-based alloys extrapolate to zero at values of electron concentration which lie in a narrow region of e/a between 1·39–1·40. If the above interpretation of the Δa expansion is accepted, these values of e/a may be taken as the points at which overlap occurs across the {10·0} faces in the various alloys. The equivalent ranges of e/a associated with overlap across the {10·0} zone faces in ζ phases of the other noble metals were reported to be 1·415–1·43 in Cu-based alloys (Massalski and Cockayne 1959) and 1·35–1·36 in Au-based alloys (Massalski and King 1960 a). Hence, the value of electron concentration associated with overlap varies considerably from one noble metal solvent to another, but only slightly when various solutes are alloyed with any one of the noble metals. An exception is the value of 1·47 extrapolated for Ag–Al (Massalski and Cockayne 1959) indicating that the A-sub-group element Al when alloyed with silver has an effect which is different from that of the B-sub-group elements.

Studies of the anomalous skin effect (Pippard 1957), the de Haas-van Alphen effect (Shoenberg 1960) and of ultra-sonic attenuation (Morse *et al.* 1960) indicate that the Fermi surface in all three noble metals, Cu, Ag and Au, may be considered to a first approximation as a sphere with small cylinders (referred to as 'necks', Shoenberg 1960) which make contact with the {111} faces of the f.c.c. Brillouin zone. The cross-sectional area of these necks is considered to be greatest in copper and least in silver. For the case of a hypothetical ideally close-packed h.c.p. noble metal it is thus reasonable to assume that the Fermi surface would contain analogous cylinders making contact with the {00·2} faces of the zone, since these faces lie the same distance from the origin as the {111} faces of the f.c.c. zone and are related to similarly close-packed planes

Fig. 3

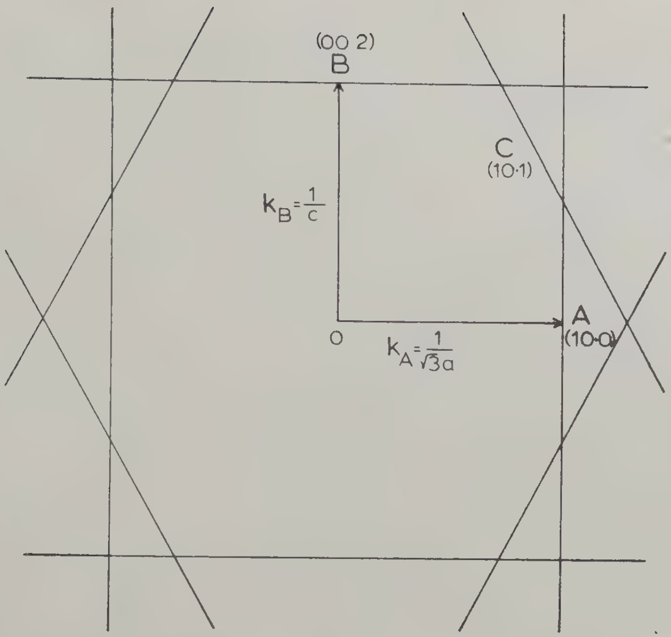

Vertical section through the Brillouin zone of h.c.p. structure of ideal axial ratio (after Jones 1934).

Fig. 4

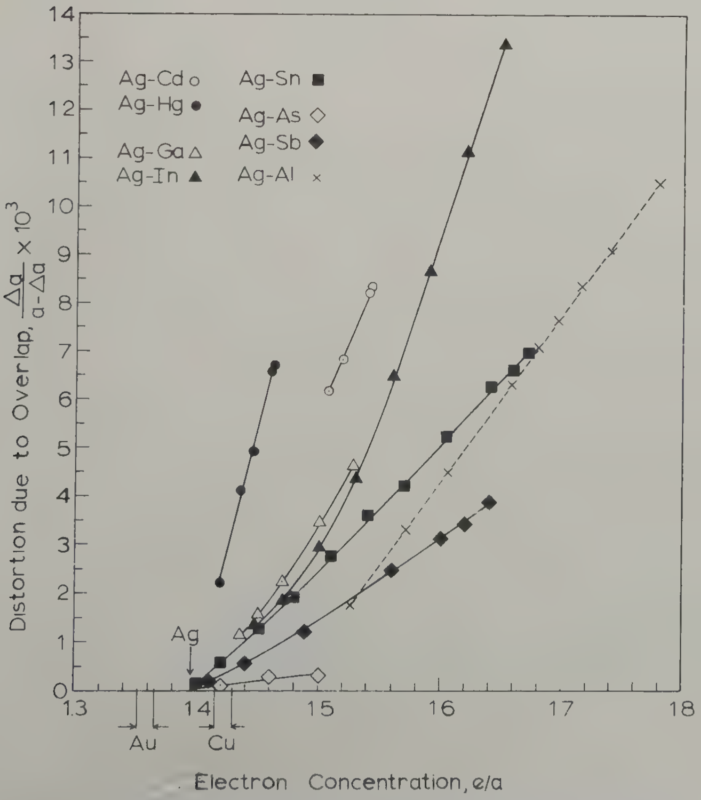

Plot of the distortion due to overlap $[\Delta a/(a-\Delta a)]$ against electron concentration for h.c.p. ζ phases based on silver.

in the real lattice. Considerable contact would probably also take place between the Fermi surface and the {10·0} faces which are nearest the origin (see fig. 3), but in directions perpendicular to the {10·1} faces, which are furthest away, it is likely that the Fermi surface would remain approximately spherical as in directions perpendicular to the {200} faces of the f.c.c. zone.

If it is considered that the degree of contact, i.e. the size of the necks, is indicative of the band gaps across the zone faces, and that these band gaps are modified by alloying as suggested by Cohen and Heine (1958), changes in the Fermi surface due to alloying may be predicted in a qualitative manner. In Cu, for which $E_{\mathrm{p}} < E_{\mathrm{s}}$, the band gaps are considered to be decreased by alloying. Hence, the diameter of the necks should be decreased while at the same time the volume enclosed by the main body of the Fermi surface should become increased due to the change in e/a. Conversely, in Au, for which it is considered that $E_{\mathrm{p}} > E_{\mathrm{s}}$, the band gaps should increase on alloying, and the size of the necks should become even greater, at the expense of the volume of the main Fermi surface. The main body of the Fermi surface, being approximately spherical, will make direct contact (i.e. without the need of additional cylinders) with the {10·0} faces of the h.c.p. zone at e/a near 1·14. However, in order to enable the contours of constant energy to intersect the zone face at right angles, the Fermi surface will tend to spread along the zone faces resulting in a short, wide neck. An increase in electron concentration due to further alloying will in general cause the Fermi surface to spread further, and hence to a first approximation it may be considered that the area of contact will be independent of any changes in the band gaps across the {10·0} faces. Any application of the Cohen and Heine (1958) model to the h.c.p. ζ phases should thus be limited to the {00·2} and perhaps the {10·1} zone faces. Interpreting the lattice spacings results in terms of these predictions, the much higher-than-ideal values of e/a observed in Au-based alloys (fig. 2) appear to be in some way associated with a large degree of contact between the Fermi surface and the {00·2} faces of the h.c.p. zone. For Cu-based alloys the axial ratios are only slightly greater than the ideal and this, in comparison, would be consistent with a relatively smaller amount of contact between the Fermi surface and the {00·2} faces.

If the magnitude of the departure of the axial ratio above the ideal value may be taken as a qualitative measure of the degree of distortion of the Fermi surface from a spherical shape, the Fermi surface in Ag-based alloys may be considered to be almost spherical in the ⟨00·2⟩ directions since the axial ratio is only just greater than the ideal, being 1·6335–1·6338 (fig. 2). In this respect it is of interest to note that the Ag-based ζ phases of almost ideal axial ratio occur in the region of electron concentration near 1·36, which is the value at which a spherical Fermi surface would just touch the {00·2} faces of the Brillouin zone, assuming any distortion due to interaction with the {10·0} faces to be quite local. Hence, it may be inferred that the necks, which form part of the Fermi surface in pure Ag, are reduced in size by alloying until they tend to almost disappear. This indicates that, according to the model of Cohen and Heine (1958), $E_{\mathrm{P}} < E_{\mathrm{S}}$ in pure Ag, i.e. that the band structure of silver is similar to that of Cu.

Since it appears probable that in h.c.p. alloys of the noble metals the Fermi surface would remain in contact with the $\{00{\cdot}2\}$ faces over the range of e/a from 1·0 up to the onset of these phases at $e/a = 1{\cdot}2$–$1{\cdot}36$, earlier interpretations (Massalski and King 1960 a) of the $\Delta c'$ deviation, and the higher-than-ideal axial ratios, in terms of an electron stress effect (Goodenough 1953) as the Fermi surface *approaches* the $\{00{\cdot}2\}$ faces, must be reconsidered. It might be supposed that the electrons in the necks of the Fermi surface adjacent to the intersection with the $\{00{\cdot}2\}$ exert an attractive force on the zone boundary, and that the total electron energy may be lowered if the boundary moves closer to the main body of Fermi surface thus reducing the length of the cylinders. The number of electrons in these positions would be proportional to the circumference of the necks and hence be increased with the diameter of the area of contact. It is of interest to note that the zone distortion which causes the higher-than-ideal axial ratios has no effect on the trend in vol/atom as a function of e/a; whereas, as discussed earlier, the overlap of electrons across the $\{10{\cdot}0\}$ faces apparently causes an overall increase in the vol/atom (fig. 1).

The axial ratio results in fig. 2 and the $\Delta a/(a-\Delta a)$ plots in fig. 4 indicate that, in addition to increasing the number of electrons per atom, the solute elements also have an effect on the band structure of the alloys. It is possible to correlate these results with the parameter η defined by Cohen and Heine (1958) as a measure of the change in band structure caused by the addition of the solute element. The η parameters, in units of ev, for the B-sub-group elements which form ζ phases with Ag are listed at the bottom of fig. 1. It is to be expected that similar trends in lattice spacings will be observed in those ζ phases for which the η parameters are nearly the same. Consider, for example, the alloys containing In, Sn and Sb from the second long Period and for which the size factors (fig. 1) are all favourable. The rate of change of the a' spacings for the primary solid solutions in these systems are almost identical, whereas in the ζ phases the rate of change of a (as shown by the plots of $\Delta a/(a-\Delta a)$ in fig. 4) and of the decrease in c (fig. 1) and c/a (fig. 2) is much greater in Ag–In for which $\eta = 5{\cdot}7$ than in Ag–Sn or Ag–Sb for which $\eta = 2{\cdot}4$ and 2·9 respectively. If, on the other hand, alloys with solutes in the same B-sub-group are compared, it is found that Ag–Ga and Ag–In, which have similar η parameters, show similar rates of change of axial ratio and fractional distortion $\Delta a/(a-\Delta a)$ as shown by the plots in figs. 2 and 4 respectively. Again comparing solutes from the same B-sub-group. the changes in c/a and $\Delta a/(a-\Delta a)$ with electron concentration are more rapid in Ag–Hg ($\eta = 5{\cdot}9$) than those in Ag–Cd ($\eta = 3{\cdot}0$). Ag–As ($\eta = 3{\cdot}7$) forms the only exception to a consistent correlation between η parameters and lattice spacing changes, since the changes in c/a and $\Delta a/(a-\Delta a)$ in this system are more gradual than those in Ag–Sb ($\eta = 2{\cdot}9$), even though the η parameter of the former is slightly greater than that of the latter. However, this discrepancy may not be too serious since the s–p excitation energies used to calculate η for the polyvalent solutes are known to be open to considerable error (Cohen and Heine 1958).

Using the relationship for the energy of free electrons, $E = h^2k^2/2m$, and that relating the electron concentration z with the radius k of the Fermi sphere, $z = 2\Omega\,.\,\frac{4}{3}\pi k^3$ where Ω is the atomic volume, an order of magnitude estimate of the band gap across a zone face can be made from a knowledge of the lattice parameters and the value of z at overlap. Assuming that the Fermi surface is very nearly spherical in Ag-based alloys and that z at overlap is given by the plots of $\Delta a/(a-\Delta a)$ in fig. 4, sufficient information is available to evaluate the band gaps, $\Delta E_{\{10{\cdot}0\}}$, across the $\{10{\cdot}0\}$ zone faces. A typical calculation for the Ag–Sn system for which z at overlap $\simeq 1{\cdot}395$ yields $\Delta E_{\{10{\cdot}0\}} \simeq 0{\cdot}73$ ev. Further, since it has been shown that the band gaps divided by the energy of the electrons at the $\{10{\cdot}0\}$ and $\{00{\cdot}2\}$ zone faces are in the ratio $1:1{\cdot}6$ (Goodenough 1953), the band gap across the $\{00{\cdot}2\}$ faces, $\Delta E_{\{00{\cdot}2\}}$, may also be obtained. Thus, for Ag–Sn $\Delta E_{\{00{\cdot}2\}} \simeq 1{\cdot}32$. Comparing this value with that for the band gap across the equivalent zone faces in the f.c.c. zone, for which Tibbs (1938) has calculated $\Delta E_{\{111\}} \simeq 2{\cdot}43$ ev, it may once again be concluded that the addition of Sn (or any other B-sub-group solute) to Ag results in a decrease in the band gaps.

ACKNOWLEDGMENTS

We are grateful to Professor M. H. Cohen and to Dr. L. F. Vassamillet for many stimulating and informative discussions. We also wish to thank Mr. C. L. Ruffner for his valuable assistance with the experimental work. Following the submission of the paper, we have received several helpful suggestions from Professor Hume-Rothery, for which we should like to thank him.

APPENDIX

1. MATERIALS AND METHODS

All alloys were prepared from spectroscopically standardized materials (supplied by Messrs. Johnson, Matthey and Co., Ltd.). Weighed quantities of the pure metals were melted with frequent vigorous shaking under reduced pressure of helium in small, sealed, thin-walled tubes of fused quartz or 'Vycor'; details of this technique have been published earlier (Raynor and Massalski 1955). Following previous experiences, the synthesized compositions of the alloys were accepted without chemical analyses provided that no significant change in weight had occurred during casting. After casting all ingots were given a homogenizing treatment (see table) in sealed pyrex tubes under a reduced atmosphere of helium, and later examined metallographically under polarized light for the presence of impurities and additional phases. X-ray powder specimens of the alloys were requenched from the respective homogenizing temperatures.

A 2 radian film camera with 0·5 mm pin holes was used for the x-ray work, and the powder specimens of less than 325 mesh were held in 0·3 mm diameter capillaries. The film was used in the asymetrical position and measured with a vernier device (Klug 1940) which enabled line positions to be located to 0·02 mm. The last ten high-angle lines in the diffraction patterns were used to calculate the lattice spacings by an extrapolation procedure involving successive approximations of the axial ratio (Massalski and King 1960 b). All lattice spacings are reported in Angstrom units, based upon the following values assumed for CuKα radiation:

$$\mathrm{CuK}\alpha_1 = 1{\cdot}5405006\,\text{Å}$$

$$\mathrm{CuK}\alpha_2 = 1{\cdot}5443412\,\text{Å}.$$

The temperature of the specimens during the exposure was 30° ± 1°c. The accuracy of the reported results is ±0·0002 Å for the a spacings, and ±0·0003 Å for the c spacings. This accuracy of one part in 15 000 is not absolute, but is indicative of the degree of reproducibility obtained in the authors' laboratory. The significance of absolute and relative accuracy in the measurement of lattice parameters has been discussed recently by Parrish (1960).

2. PRESENT RESULTS COMPARED WITH PREVIOUS DATA

A close comparison between the present results and the previous data available in the literature for silver-based ζ phases is not possible, since most of the latter were obtained as a by-product of phase identification studies and are often reported only to the third decimal place. The data reported by Pearson (1958) for several alloys in the systems Ag–Cd, Ag–In, Ag–Sn and Ag–Sb, and by Eade and Hume-Rothery (1959) for Ag-As, are in general agreement with the present trends in lattice spacings, even though individual values may differ from those of the present work. Similar general agreement is found between the present results and Stenbeck's data for Ag–Hg (Pearson 1958) even though only two values were reported. A single value reported by Rayson and Calvert (1958) for a Ag–Hg alloy is in complete disagreement both with the earlier work of Stenbeck and with the present results. A similar discrepancy between the results of Rayson and Calvert (1958) and those of other investigators has been reported previously for the lattice spacings of the ζ phase in Au–Hg (Massalski and King 1960 a). The values of both a and c lattice spacings for a single Ag–Ga alloy reported by Hellner (Pearson 1958) are considerably greater than the present results for this system. Although it has been reported (Hume-Rothery and

Andrews 1959) from the results of high-temperature x-ray studies that the ζ phase in Ag–Ga extends up to about 32 at. %, in the present work it was found that this phase could not be retained, by quenching to room temperature, in alloys containing more than 26·5 at. % Ga.

REFERENCES

COHEN, M. H., and HEINE, V., 1958, *Advanc. Phys.*, **7,** 395.
DAY, H. M., and MATHEWSON, C. H., 1938, *Trans. Amer. Inst. min.* (*metall.*) *Engrs*, **128,** 261.
DUWEZ, P., WILLENS, R. H., and KLEMENT, W., 1960, *J. appl. Phys.*, **31,** 1137.
EADE, G. A., and HUME-ROTHERY, W., 1959, *Z. Metallk.*, **50,** 123.
GOODENOUGH, J. B., 1953, *Phys. Rev.*, **89,** 282.
HUME-ROTHERY, W., and ANDREWS, K. W., 1959, *Z. Metallk.*, **50,** 661.
HUME-ROTHERY, W., and RAYNOR, G. V., 1954, *The Structure of Metals and Alloys*, Institute of Metals Monograph and Report Series No. 1, revised edition.
HUME-ROTHERY, W., RAYNOR, G. V., REYNOLDS, P. W., and PACKER, H. K., 1940, *J. Inst. Met.*, **66,** 209.
HUME-ROTHERY, W., REYNOLDS, P. W., and RAYNOR, G. V., 1940, *J. Inst. Met.*, **66,** 191.
JONES, H., 1934, *Proc. roy. Soc.* A, **147,** 396.
KING, H. W., and MASSALSKI, T. B., 1961 (to be published).
KLUG, H. P., 1940, *Ind. Eng. Chem.*, Anal. Ed., **12,** 753.
MASSALSKI, T. B., 1956, *Theory of Alloy Phases* (Cleveland, Ohio : A.S.M.), p. 63 ; 1957, *Acta Met.*, **5,** 541 ; 1958, *Met. Rev.*, **3,** 45.
MASSALSKI, T. B., and COCKAYNE, B., 1959, *Acta Met.*, **7,** 762.
MASSALSKI, T. B., and KING, H. W., 1960 a, *Acta Met.*, **8,** 677 and 684; 1960 b, *J. Inst. Met.*, **89,** 169.
MORSE, R. W., MEYERS, A., and WALKER, C. T., 1960, *Phys. Rev. Letters*, **4,** 605.
OWEN, E. A., and ROBERTS, E. W., 1939, *Phil. Mag.*, **27,** 294.
OWEN, E. A., and ROWLANDS, V. W., 1940, *J. Inst. Met.*, **66,** 361.
PARRISH, W., 1960, *Acta cryst., Camb.*, **13,** 838.
PEARSON, W. B., 1958, *Handbook of Lattice Spacings and Structures of Metals and Alloys* (London and New York : Pergamon Press).
PIPPARD, A. B., 1957, *Phil. Trans.* A., **250,** 325.
RAYNOR, G. V., and MASSALSKI, T. B., 1955, *Acta Met.*, **3,** 480.
RAYSON, H. W., and CALVERT, L. D., 1958, *J. Inst. Met.*, **87,** 88.
SHOENBERG, D., 1960, *Phil. Mag.*, **5,** 105.
TIBBS, S. R., 1938, *Proc. Camb. phil. Soc.*, **34,** 89.

A Search for Anisotropy of Inertial Mass using a Free Precession Technique

By R. W. P. Drever
Department of Natural Philosophy, University of Glasgow

[Received February 8, 1961]

The idea that the inertial mass of a body may arise from a gravitational coupling with distant matter has led to suggestions that the concentration of matter near the centre of our galaxy may result in an anisotropy of inertia at the earth which could be detected experimentally. In particular, Cocconi and Salpeter (1958, 1960) have pointed out that such an anisotropy might cause shifts in energy levels of atoms and nuclei in magnetic fields. They suggest, for example, that in a nucleus which can be regarded as a single $p_{3/2}$ nucleon moving in an isotropic central potential the energies of the states with magnetic quantum numbers $m_I = \pm 3/2$ would be increased slightly if the magnetic field were parallel to the direction of the centre of the Galaxy, and the energies of the states with $m_I = \pm 1/2$ would be decreased by an equal amount; while if the magnetic field were perpendicular to the direction of the centre of the Galaxy the energies would be shifted in the opposite directions. From models of inertia like those discussed by Cocconi and Salpeter, as well as those referred to by Dicke (1959), one could expect that the ratio of the anisotropic part of the inertial mass of a body to the isotropic part might lie in the range from 10^{-7} to 10^{-13}; and in this case the suggested energy shifts would be large compared with the shifts which can be measured by nuclear resonance methods, being about 30 Mc/sec even for the smaller anisotropy. In fact data from nuclear resonance experiments with crystals indicate that no energy shifts as large as this take place (Drever 1960). However, in view of the cosmological interest of the question, and the speculative nature of the calculations, it seems worth while to make the search for effects of this kind as sensitive as possible. Some relevant observations on lithium 7, a nucleus of spin $I = 3/2$ with an unpaired $p_{3/2}$ proton, are described here.

Since this work was begun Hughes *et al.* (1960) have reported a rather similar experiment done by nuclear magnetic resonance, which gave an upper limit to anisotropy of inertia of 10^{-20}; while Sherwin *et al.* (1960) have obtained an upper limit of 5×10^{-16} from studies of resonance scattering of gamma rays from ^{57}Fe. The present experiment, which is more sensitive, has also given a negative result.

The four energy levels of a nucleus of spin 3/2 in a magnetic field are normally taken to be equally spaced, and any modification of the spacing by shifts like those suggested by Cocconi and Salpeter would split the single resonance obtained in a magnetic resonance experiment into a triplet. The minimum splitting detectable with simple resonance technique is usually limited by inhomogeneities in the magnetic field; but in the present case the splitting, if small compared with the separation of the levels, is independent of the magnitude of the field and this restriction may be eased by working in a weak field. The magnetic field of the earth itself is very suitable, and this was the field used here.

Fig. 1

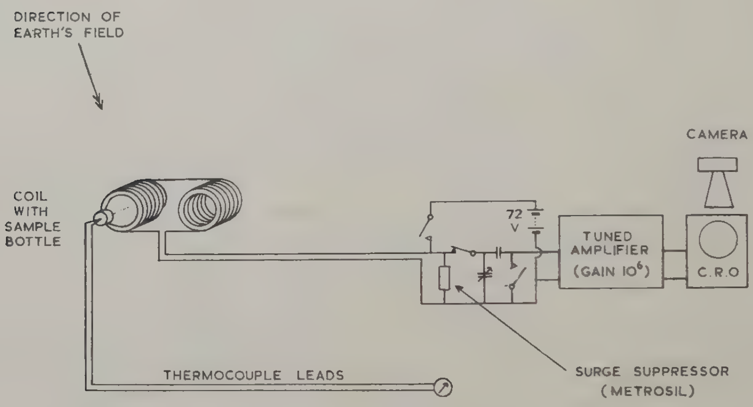
DIRECTION OF EARTH'S FIELD
CAMERA
COIL WITH SAMPLE BOTTLE
72 V
TUNED AMPLIFIER (GAIN 10^6)
C.R.O
THERMOCOUPLE LEADS
SURGE SUPPRESSOR (METROSIL)

Schematic diagram of apparatus. The switches, operated by relays, disconnect and short-circuit the amplifier while current is passed through the sample coil; and the Metrosil non-linear resistor limits the peak voltage generated during switch-off without affecting the nuclear signals.

The experimental technique was based on that employed by Packard and Varian (1954) and Waters and Francis (1958) to observe free precession of protons in the earth's field, and the arrangement is shown schematically in fig. 1. The lithium, in the form of a solution, is contained in a polythene bottle surrounded by a coil placed with its axis perpendicular to the direction of the earth's field. Initially a direct current is passed through the coil to produce a field of about 200 gauss at right angles to the earth's field. When this is switched off rapidly the resultant nuclear magnetic moment precesses about the earth's field and an alternating e.m.f. is generated in the coil. Under suitable conditions with a single resonance, this signal decays exponentially with a time constant equal to the transverse relaxation time T_2 of the spin system. If, however, the resonance were split into a close triplet one would expect the signal to exhibit beats, corresponding to interference between oscillations at the three resonance frequencies which would be detected in a steady-state experiment. The results of a detailed analysis by Das and Saha (1955) of the analogous situation of free precession in the presence of a weak electric quadrupole interaction indicate in fact that when the earth's field is parallel to the direction of the centre of the Galaxy, and the splitting is at its maximum, the amplitude of the signal would vary as

$$\{2+3\cos(2\pi t\Delta f)\}\exp(-t/T_2),$$

where Δf is the frequency separation between each satellite and the central component of the triplet, and t is the time from the beginning of the free precession. As the earth rotates the splitting, and hence the modulation of the precession signal, would alter; and a maximum splitting too small to give rise to obvious beats might show as an apparent change in the decay rate with sidereal time. At the place where the experiment was performed, latitude 55° 54′ N, longitude 4° 30′ W, the declination and inclination of the earth's field are 71° N and 9° W respectively, and the direction of the field passes within 10° of the centre of the Galaxy at about 5 h sidereal time, when almost the maximum splitting would be expected.

The frequency of precession of ^{7}Li in the earth's field is only about 800 cycles/sec, and in practice the signal was weak and it was necessary to use a large sample (2·5 l.) to obtain an adequate signal-to-noise ratio. The sample coil was situated in the open air in a position remote from steel-framed buildings and power cables; and to minimize pick-up of electromagnetic interference a second similar coil was mounted near the sample coil and connected in opposition with it. It was necessary to control the temperature of the lithium solution to maintain a constant relaxation time, and this was done by passing a suitable current through the coil in the intervals between measurements. A stirring device of flexible polythene was incorporated in the bottle, and the temperature was kept at (37 ± 1)°c. Data on relaxation times (Bloembergen *et al.* 1948) suggested that a solution of lithium nitrate would be a particularly suitable material to use as sample, and after preliminary tests with other compounds this was employed throughout. Nitrogen was bubbled through the solution before use to reduce the amount of dissolved oxygen, and the polythene bottle was hermetically sealed to prevent changes in oxygen content during the experiment. When care was taken to eliminate magnetic material from the vicinity of the sample (and some borosilicate glass proved appreciably ferromagnetic) the decay constant of the observed ^{7}Li signal was 3·7 sec.

Two continuous 24-hour runs and numerous shorter ones were made (during May and July 1960), the precession signals being examined on an oscilloscope and recorded on film at intervals of 20 or 30 min. A typical photograph is shown in fig. 2†. No beats of the type expected were seen, and no significant changes in the decay rate of the signal or its initial amplitude were detected. Some small changes in the shape of the envelope were in fact noticed but these were comparable with fluctuations due to noise, were not reproduced from one run to another, and appeared to be correlated with slight changes in the temperature of the solution. The examination of the photographs was made by projecting them onto a drawing of the envelope expected for a pure exponential decay in the presence of noise. Comparision with a theoretical envelope for the case of a splitting for which $\Delta f = 0{\cdot}04$ cycles/sec (in which the first minimum occurs at $t = 10$ sec) indicates that a slowly-varying splitting of this magnitude, which would arise from individual level shifts of 0·02 cycles/sec, would have been readily detectable.

---

† Figure 2 is shown as a plate.

These results themselves do not completely rule out energy shifts of such a magnitude that the outer components of the triplet remained outside the pass-band of the amplifier for most of the sidereal day, and only came within it for short periods which happened to coincide with intervals between observations. A separate experiment was therefore performed in which the initial amplitudes of the precession signals due to the ^{7}Li nuclei and to the protons in the same lithium nitrate solution were compared. In doing this it was necessary to ensure that the decay of the magnetizing field was sufficiently rapid to give maximum signals from both types of nucleus, and to take into account the difference in the sensitivity of the apparatus at the two frequencies concerned (803 cycles/sec for ^{7}Li and 2068 cycles/sec for protons). The experimental results agreed to within 5% with the ratio of the amplitudes calculated assuming detection of the whole ^{7}Li signal; and in disagreement with the ratio which would be expected if only the central component of a triplet were observed, which is smaller by a factor of 2/5.

It may be remarked that if there were energy shifts large compared with the spacing of the levels in the earth's field there would, in general, be no signal which remained at the expected ^{7}Li precession frequency throughout the sidereal day.

It may be concluded that any shifts of the ^{7}Li energy levels of the type suggested by Cocconi and Salpeter do not alter the spacing of the levels by more than 0·04 cycles/sec. If one applies the calculation of Cocconi and Salpeter directly to ^{7}Li, taking the mean kinetic energy of the $p_{3/2}$ proton to be 10 MeV, this result would correspond to an upper limit for the ratio of the anisotropic part of the inertial mass of a proton to the isotropic part of the order of 5×10^{-23}.

It should be noted, however, that a negative result obtained in an experiment of this kind does not rule out the possibility of a much larger anisotropy in inertial mass which is masked by some other anisotropy. Epstein (1960) has recently suggested that an anisotropy in the potential energy of a nucleon might accompany an anisotropy in its mass and counteract it, and such a situation might well exist without being detected in an experiment like the present one. The experiment does, nevertheless, provide a check of the specific model proposed by Cocconi and Salpeter; and in fact it is difficult to reconcile the shifts in energy levels suggested by this model with the very low upper limit for such shifts found experimentally.

ACKNOWLEDGMENTS

The author would like to thank Mr. T. D. S. Hamilton for doing some preliminary experiments with his nuclear resonance equipment, and for loans of apparatus. He would also like to thank Drs. G. A. P. Wyllie and G. M. Lewis for helpful discussions, and Professor P. I. Dee for his encouragement.

REFERENCES

BLOEMBERGEN, N., PURCELL, E. M., and POUND, R. V., 1948, *Phys. Rev.*, **73,** 679.
COCCONI, G., and SALPETER, E., 1958, *Nuovo Cim.*, **10,** 646; 1960, *Phys. Rev. Letters*, **4,** 176.
DAS, T. P., and SAHA, A. K., 1955, *Phys. Rev.*, **98,** 516.
DICKE, R. H., 1959, *Science*, **129,** 621.
DREVER, R. W. P., 1960, *Phil. Mag.*, **5,** 409.
EPSTEIN, S. T., 1960, *Nuovo Cim.*, **16,** 587.
HUGHES, V. W., ROBINSON, H. G., and BELTRAN-LOPEZ, V., 1960, *Phys. Rev. Letters*, **4,** 342.
PACKARD, M., and VARIAN, R., 1954, *Phys. Rev.*, **93,** 941.
SHERWIN, C. W., FRAUNFELDER, H., GARWIN, E. L., LUSCHER, E., MARGULIES, S., and PEACOCK, R. N., 1960. *Phys. Rev. Letters*, **4,** 399.
WATERS, G. S., and FRANCIS, P. D., 1958, *J. sci. Instrum.*, **35,** 88.

The Magnetic Properties of Three Carboniferous Sills

By C. W. F. Everitt
Physics Department, Imperial College, London

[Received September 15, 1960]

ABSTRACT

An account is given of palaeomagnetic measurements on borehole specimens from three dolerite sills of Carboniferous age. The magnetic directions were closely grouped for one sill but widely scattered for the other two, showing that contrary to the experience of previous workers, specimens from underground do not always yield satisfactory palaeomagnetic results.

The intensities of magnetization were very low at the margin of each sill. In one instance this phenomenon was studied in detail. It seems to be due to the fact that at the margins, the iron occurred mainly in the form of a non-magnetic carbonate, produced when the sill was intruded into limestones Some wider implications of the work are discussed.

---

§ 1. INTRODUCTION

THE present paper describes a series of magnetic measurements on material from deep borings through three dolerite sills in the Carboniferous system of Great Britain. The first boring was through a 400 foot sill at Rashiehill, Stirling, lying between depths 1353 feet and 1742 feet in beds of the Limestone Coal group; the second was through a 140 foot sill at Outmains, Ayrshire, between depths 1774 feet and 1915 feet in Upper Coal Measures; and the third through a 40 foot sill at Plungar, near Nottingham, between 3165 feet and 3205 feet, also in Upper Coal Measures. From the 40 foot sill complete fitting sections of $4\frac{1}{2}$ in. diameter were available over most of the length. From the 140 foot sill, seven short sections 2 in. diameter and from the 400 foot sill, 42 sections $4\frac{1}{2}$ in. diameter were available. The depths of these pieces were known and the tops had been marked by the drillers. These markings will be referred to hereafter as the nominal tops. For the 400 foot sill some of the overlying baked rocks were also available; and in addition oriented samples were collected at Torpichen, near Bathgate, where the sill crops out.

The original object of the work was to obtain an independent test of the palaeomagnetic directions obtained from other work on the Carboniferous system (Everitt and Belshé 1960). Measurements by Gough (1959) on the Pilansberg dykes of South Africa and by Jaeger and Joplin (1955) on Tasmanian sills had shown that the scatter of magnetic directions could be greatly reduced by taking material from underground rather than the surface, presumably because it eliminated the effects of recent weathering and lightning. The orientations of the borehole specimens were not known; but for the present purpose this was not important, since the main point at doubt in the Carboniferous system was the magnetic inclination.

Fig. 1

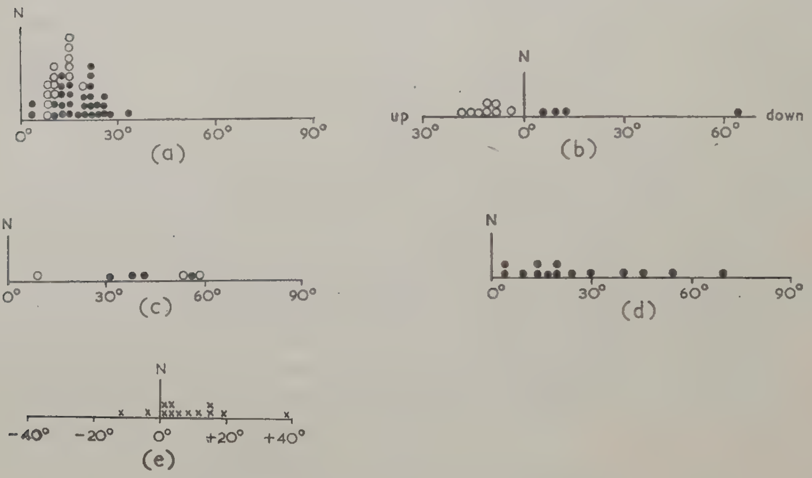

Magnetic directions in the three sills.
○ upward inclination.
● downward inclination.
× declination relative to arbitrary arrow.

(*a*) 400 foot sill, inclination; (*b*) shale baked by 400 foot sill, inclination; (*c*) 140 foot sill, inclination; (*d*) 40 foot sill, inclination; (*e*) 40 foot sill, declination relative to arbitrary arrow.

Each sill was found to have very low magnetic intensities at the margins. Similar low intensities have been observed at the margins of the sills by Jaeger (private communication) and Hatherton (1954), and at the margins of dykes by Leng (1955) and myself (unpublished). Although Bruckshaw and Robertson (1949) and others have found examples of the opposite effect, that is an increase of intensity towards the margins of igneous bodies, the present phenomenon seems sufficiently widespread to be worth investigating.

The palaeomagnetic directions are discussed in § 2 and the measurements on magnetic properties in § 3.

§ 2. Directions of Magnetization

The directions of magnetization of the original pieces of core, measured on an astatic magnetometer are presented in fig. 1. For the 40 foot sill, there were complete fitting lengths extending over most of the core, so histograms are given for inclination and for azimuth relative to an arbitrary line on the core. For the other sills, with broken lengths, only the inclinations could be measured. There is some uncertainty whether these inclinations are up or down, owing to possible mis-marking of the specimens, so they have been plotted without regard to sign, the measured upward and downward values being distinguished only by different symbols. Also included in fig. 1 are the results from a group of strongly magnetized baked pyritous shales from a depth 80 feet above the 400 foot sill; for these there was no possibility of mis-marking since the pieces fitted together. The numerical data from the histograms and measurements on surface specimens from the 400 foot sill are set out in Table 1.

Table 1

Sill	Site	Type of material	Number of specimens	Mean dip	Standard deviation of single readings	Deviation of mean
feet 40	Plungar	Borehole	14	24° down	12°	4°
140	Outmains	Borehole	7	42° down	16°	6°
400	Rashiehill	Borehole igneous	42	16° down	5°	0·8°
		Borehole baked	12	0°	22°	6°
		Surface igneous	6	4° down	30°	12°

The only specimens that show really close grouping are those from the boring through the 400 foot sill; the results from the other two sills are widely scattered and must be discounted for palaeomagnetic purposes. Of the specimens from the 400 foot sill, the inclinations of 30 were nominally downwards and 12 were nominally upwards. One conceivable explanation of this grouping is that some specimens had undergone self-reversal; but in view of the well-known difficulty of marking broken lengths of cores reliably, I am inclined to think that the effect arises from mis-marking. The downward dip, being more frequent, is presumably the true one. The mean value is 16° down.

The specimens from the outcrop of the 400 foot sill were very widely scattered, with a mean direction 216° east of the true north and 4° down. Taking 16° down as the best value for the magnetic inclination, and 216° east as the azimuth, these results fit in well with the mean value for the Carboniferous period as a whole of 200° east and 27° down (Everitt and Belshé 1960).

We see therefore that for the 400 foot sill the scatter was greatly reduced by taking borehole specimens. For the other two sills, however, the scatter in the cores was large. Therefore sampling from underground does not always yield satisfactory palaeomagnetic results. On the other hand, these results serve to emphasize that the existence of magnetic scatter is an interesting problem in itself, and that simple explanations of it in terms of recent weathering or lightning are inadequate.

§ 3. INTENSITIES OF MAGNETIZATION

The intensities of natural magnetization for the three sills are plotted against depth in fig. 2 (*a*), (*b*) and fig. 3 (*a*). At the centres of the sills the intensities fell within the range 200–2000 × 10^{-6} e.m.u./g, which is typical of dolerites; but at the margins, they were much lower. The greatest variation occurred in the 400 foot sill, where the least intensity was 1·8 × 10^{-6} e.m.u./g at the upper margin and the greatest was 5600 × 10^{-6} at 32 feet below the top. Most of the investigations were made on this sill; the main results being set out in fig. 3 (*a*)–(*f*).

Fig. 2

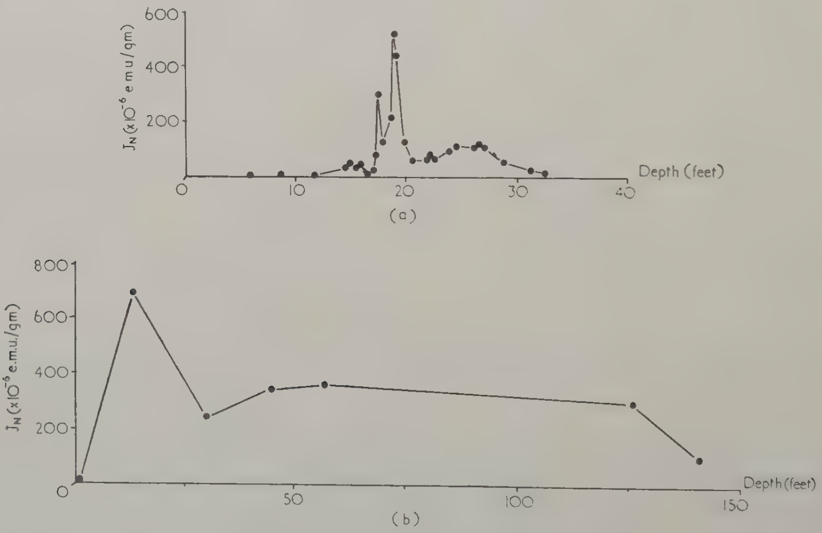

Intensities of natural remanence.
(*a*) 40 foot sill; (*b*) 140 foot sill.

In principle there seem to be four general classes of explanation for the differences of intensity between the margins and centre of the sill:

(1) A variation in the total iron content.

(2) A variation in the proportion of iron existing in a ferromagnetic form.

(3) A variation in the magnetic material giving rise to differences in its saturation intensity.

(4) A variation in the degree of natural remanent magnetization of a single magnetic material.

These possibilities will be discussed in § 3.1.

3.1. *Physical Cause of the Variations in Natural Remanence*

The total iron content for the 400 foot sill is plotted in fig. 3 (*b*) was practically uniform throughout. These measurements, which are due to Dr. A. J. E. Welch, were obtained by x-ray fluorescence counts on flat discs 2·3 cm in diameter (Parrish 1956). Similar results were obtained for the other two sills. Thus possibility (1) above is eliminated.

Fig. 3

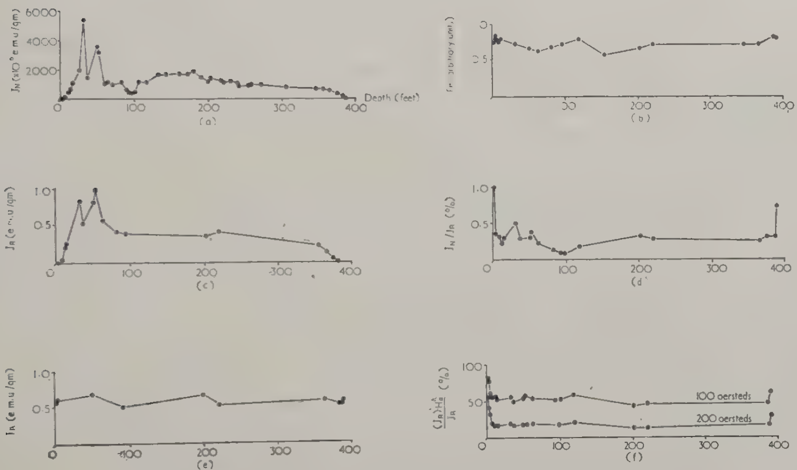

Measurements on 400 foot sill.

(*a*) natural remanence; (*b*) total iron content; (*c*) saturation remanence; (*d*) ration of natural to saturation remanence; (*e*) saturation remanence after heating to 1000°c; (*f*) demagnetization by alternating fields.

In fig. 3 (*c*), the magnetic remanence (J_R) after saturation in a field of 3000 oersteds is plotted against depth for the 400 foot sill; while the ratio of the natural remanence (J_N) to this saturation remanence is plotted in fig. 3 (*d*). Each point on these diagrams represents the mean value for several small pieces cut from the original lengths of core. The ratio of J_N/J_R is approximately uniform, showing that the main variation in J_N does not arise from differences in the degree of magnetization. Thus possibility (4) above is eliminated. There are however one or two small variations in J_N/J_R which will be discussed in § 3.3. Once again, similar results were obtained for the other two sills.

To decide between the two remaining possible explanations of the low intensities, specimens from near the upper margin and the centre of the sill were powdered, and the magnetic fractions extracted. Since the material at the extreme margin was too fine grained to separate successfully, the upper specimen was taken at a depth of 6 feet, where the natural intensity was 30×10^{-6}, or about 3% of the mean value across the centre of the sill. The proportion of magnetic material proved to be obviously much lower at the margin than at the centre. In table 2 measurements of the intensity of saturation remanence for the native rock and the magnetic fraction are set out; together with estimates of the percentage magnetic fractions by weight, obtained from the ratios of the two intensities.

Table 2

Depth	Remanence of native rock (e.m.u./g)	Remanence of magnetic fraction (e.m.u./g)	Proportion by weight of magnetic material (%)
6 feet	0·018	1·6	1·1
95 feet	0·45	7·8	5·8
220 feet	0·39	7·9	5·0

The saturation remanence in the magnetic fraction from a depth of 6 feet, is about 8% of the values at the centres of the sill. However, it was clear under a microscope that the fine-grained material from the margin was very heavily contaminated with quartz; so the estimate of its saturation remanence is merely a lower limit, and the estimate for the proportion of magnetic material is, similarly, an upper limit.

The material has been examined petrologically by Dr. P. H. S. Stubbs. Measurements on thin sections gave the proportion of opaque minerals as 5–10% at the top margin and 10% in the centre of the sill. The main opaque mineral at the margin has been identified by Dr. A. P. Millman, using reflection microscopy, as ilmenite: which is, if pure, non-ferromagnetic.

Some of the ilmenite was separated by centrifuging the powdered rock in tetrabromoethane (density 2·96). A close examination of the finely powdered fraction showed once again that it contained a very small proportion of highly magnetic material. On heating, this gave exactly the same thermal demagnetization curve as the rock in bulk (see § 3.3). Thus the ilmenite did not contribute to the original magnetization.

I conclude, therefore, that the intensity variation across the sill was mainly caused by differences in the proportion of iron existing in a magnetic form. Further measurements to investigate whether there were any differences in the magnetic material will be described in § 3.3.

3.2. *Geological Origin of the Variations in Intensity*

When the rock from the margins of the 400 foot sill was heated to a few hundred degrees centigrade, there was a very marked increase in intensity. Figure 3 (*e*) shows that after treatment for half an hour at 1000°c the increase was so great that the saturation remanence became practically uniform throughout the sill. On the other hand, when the magnetic fraction from the margins was heated separately, the intensity was 1·4 e.m.u./g before heating and 1·1 e.m.u./g afterwards. Therefore the increase must have been due to the breakdown of an initially non-magnetic compound.

Two plausible possibilities are a hydroxide (or hydrated oxide such as chlorophaeite) and a carbonate. Microscopic examination by Dr. P. H. S. Stubbs disclosed the presence at the margins of an abundance of interstitial carbonate, which he considers to be derived from the overlying limestone, probably by replacement of the original pyroxene.

A sample from the margin was powdered and divided into two parts, of which one was treated with dilute HCl to dissolve the carbonate. The two samples were heated at 900°c for a quarter of an hour in evacuated quartz tubes. On cooling, the untreated powder became highly magnetic, while the other was unaffected.

A specimen from the margin was heated to 1000°c for several hours, powdered and separated with a small bar magnet. X-ray diffraction photographs of the magnetic fraction revealed the presence of magnetite and two materials, each with ilmenite structure but slightly different lattice spacings. The simplest explanation is that the newly produced magnetic material consists of intergrowths of magnetite and ilmenite, modified in lattice spacing by solid solution; and that this material co-exists with the original ilmenite phase. This observation rules out the only likely alternative explanation of the intensity increase, that is, that the original ilmenite was reduced to magnetite during the breakdown of the carbonate.

I conclude that the proportion of magnetic material at the margins of the 400 foot sill is low because the iron mainly occurs in the form of a non-magnetic carbonate. This was probably produced when the sill was intruded into limestones.

3.3. *Properties of the Magnetic Material in the* 400 *foot Sill*

In fig. 4 heating curves are given for the saturation remanences at various depths in the 400 foot sill. Across most of the sill the curves were identical giving a single Curie temperature of 550°c. In the top 6 feet there was a change in the shape of the curves, probably indicating the presence of a second magnetic material with a Curie temperature of 300°c. The magnetic material has not been studied in detail, since it was too fine-grained to separate easily.

The opaque minerals were examined under the reflection microscope by Dr. P. H. S. Stubbs. As mentioned in § 3.1 there was a high proportion of ilmenite at the margins, which was in the form of clusters of particles $5\,\mu$ to $20\,\mu$ in diameter. In the rest of the sill there were large skeletal grains of magnetite, 0·3–0·8 mm across, containing ilmenite intergrowths, with some patches of secondary alteration to maghemite. The Curie temperature of 550°c is consistent with the presence of magnetite.

The magnetic moments of the virgin rock and magnetic fractions were measured in fields up to 10 000 oersteds on a vibration magnetometer designed by Blackett and Sutton (1956). Figure 5 shows that at the margins of the sill, there is some material with strong paramagnetic susceptibility (25×10^{-6} e.m.u./g in the rock as a whole) in addition to the ferromagnetic material. This may well be the ferriferous carbonate at the margins, since ferrous carbonate (siderite) has a paramagnetic susceptibility of about $40\text{–}120 \times 10^{-6}$ e.m.u./g (Chapman and Bartels 1940).

Fig. 4

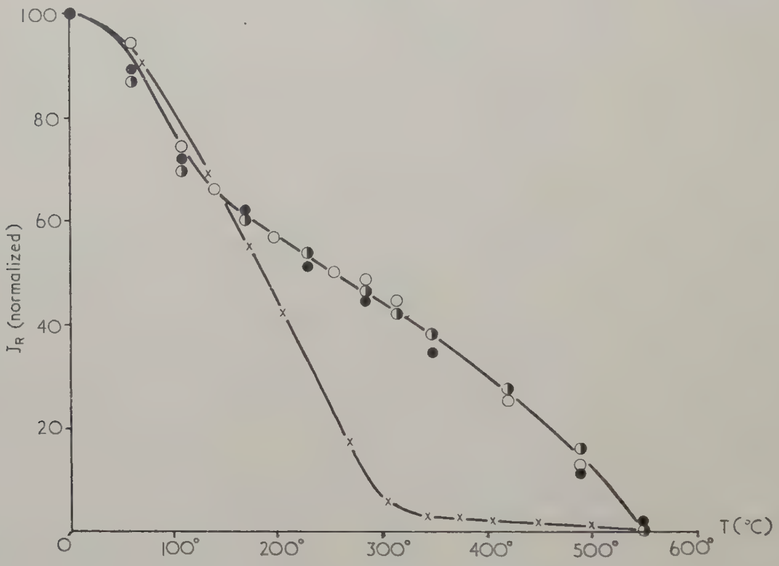

Heating of saturation remanences, 400 foot sill.

× depth 0–5 feet.

◑ depth 50 feet.

● depth 95 feet.

○ depth 201 feet.

There were systematic variations of the coercive properties across the sill. Figure 3 (*f*) shows the effect of alternating field demagnetization on the saturation remanence, giving contours of the percentage reduction produced by peak fields of 100 and 200 oersteds. These curves were used rather than straightforward measurements of coercive force to eliminate the effect of the large background of paramagnetic material. They indicate a great increase of hardness (that is to say coercive force) towards the margins of the sill. This effect may be related to the decrease in grain size at the margins, since it is well known (Néel 1955, p. 220) that coercive force increases with decreasing grain size.

The ratio of natural to saturation remanence (fig. 3 (*d*)) has already been mentioned. There is a sharp increase at the extreme margins, which may, like the increase in coercive force, be related to the small grain size. At the region of low natural intensity 90 feet below the top of the sill, the ratio of natural to saturation remanence was much lower. This probably arises from a secondary change in the natural magnetization: for there was no corresponding effect in the laboratory thermoremanence or saturation remanence, and heating experiments on three separate specimens revealed the existence of two components in the natural magnetization, each in the horizontal plane, differing in azimuth by about 120°. The origin of this effect is unknown. It occurs in the region of largest crystals, which was probably the last part of the sill to cool.

Fig. 5

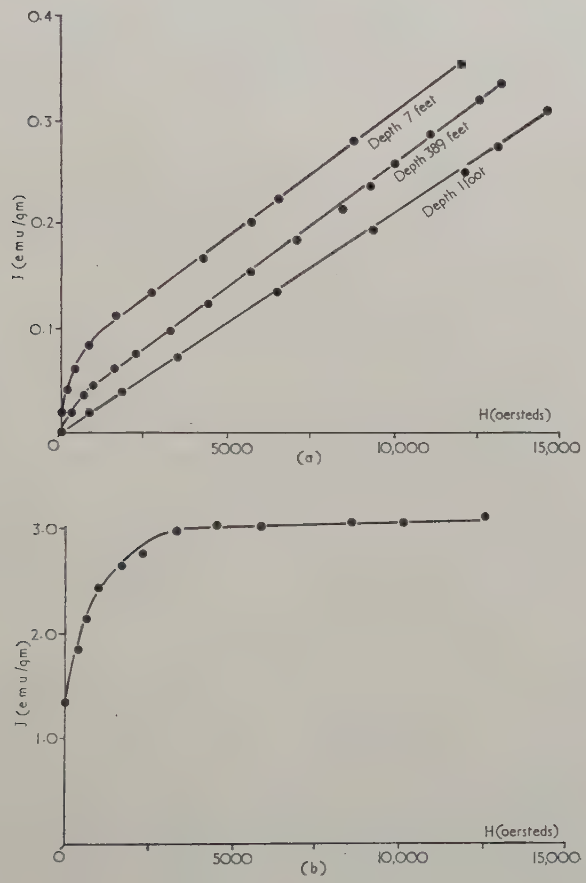

Intensity versus field; specimens from margins of 400 foot sill. (*a*) curves for native rock; (*b*) curve for magnetic fraction.

These measurements therefore show that there were only minor variations in the magnetic properties of the material in the 400 foot sill; but major variations in the amount. Such variations as do occur in the magnetic properties are probably related to the grain size. No detailed study was made of the material from the other sills.

§ 4. CONCLUSION

The conclusions to this work may be summarized as follows:

(1) The measurements on magnetic directions showed that contrary to previous experience, sampling from underground does not always yield satisfactory palaeomagnetic results. The only closely grouped directions were those from the boring through the 400 foot sill, which yielded a mean magnetic inclination of 16° down. Since the mean azimuth from the surface rocks was about 216° east, this result fits well with the figure of 200° east, 27° down already obtained for the Carboniferous system (Everitt and Belshé 1960).

(2) The intensity of natural remanence was very low at the margins of each sill. A detailed study of the effect was made for the 400 foot sill. It appeared to be due to the fact that at the margins the iron was mainly in the form of a non-magnetic carbonate, produced when the sill was intruded into limestones.

(3) The magnetic material was very uniform throughout the sill except within a few feet of the top. This effect is interesting primarily by contrast with other work, especially on lavas, in which major differences in Curie point have frequently been found between specimens only a few centimetres apart. Such differences may be due to weathering, or alternatively to the difference between the conditions of formation of sills and lavas. It would be of great interest to examine sections from borings through unweathered lavas. Any further measurements on the magnetic materials in sills would probably best be concentrated on ones which had suffered extensive differentiation.

ACKNOWLEDGMENTS

I wish to thank Professor P. M. S. Blackett for suggesting this study and for his continued and stimulating interest in it.

The borehole specimens from the 400 foot sill were lent to me by the Geological Survey of Great Britain throguh the courtesy of Dr. A. G. MacGregor, formerly Director of the Scottish Division, and Dr. F. W. Anderson of the English Division: the specimens from the 140 foot sill were lent by Dr. M. Macgregor of the Production Department, National Coal Board, Edinburgh; and those from the 40 foot sill by Professor W. D. Evans, Geology Department, Nottingham University.

I am very grateful to Dr. A. P. Millman, Dr. P. H. S. Stubbs and Dr. A. J. E. Welch for various measurements mentioned in the text. I also wish especially to thank Mr. G. W. Massé, who carried out many of the measurements and has been of great help in a number of other ways.

I am indebted to D.S.I.R. for a Research Studentship.

REFERENCES

BLACKETT, P. M. S., and SUTTON, D. J., 1956, Appendix to P. M. S. Blackett, *Lectures on Rock Magnetism*, p. 97.

BRUCKSHAW, J. McG., and ROBERTSON, E. I., 1949, *Mon. Not. R. astr. Soc. geophys. Suppl.*, **5**, 308.

CHAPMAN, S., and BARTELS, J., 1940, *Geomagnetism*, p. 144.

EVERITT, C. W. F., and BELSHÉ, J. C., 1960, *Phil. Mag.*, **5**, 675.

GOUGH, D. I., 1959, *Phil. Mag.*, **4**, 126.

HATHERTON, T., 1954, *J. geophys. Res.*, **59**, 223.

JAEGER, J. C., and JOPLIN, G., 1955, *J. geol. Soc. Aust.*, **2**, 1.

LENG, J. H., 1955, Thesis, University of London.

NÉEL, L., 1955, *Advanc. Phys.*, **4**, 191.

PARRISH, W., 1956, *Philips tech. Rev.*, **17**, 269.

The Relative Hardness of the Hard Directions in Diamond†

By Eileen M. Wilks
Clarendon Laboratory, Oxford

[Received December 20, 1960]

Abstract

A method is described of determining the relative hardness of the hard directions in diamond, using a micro-abrasion tester and diamond impregnated cutting wheels. Cube, dodecahedron and octahedron planes have been studied and an order of hardness established between the various directions on these planes. This order of hardness should also apply for ordinary diamond polishing when loose diamond powder is used on a flat scaife, although in this case the differences in hardness are very much greater.

§ 1. Introduction

The anisotropy of the hardness of diamond is very relevant to the shaping of diamond tools and to their use for working other hard materials. Diamond polishers have known for a long time that the dodecahedron and cube planes can only be polished in certain directions, and that the octahedron plane is extremely resistant to abrasion in all directions. Quantitative measurements of the resistance of diamond to abrasion by a cast-iron wheel charged with diamond powder, as is used in conventional polishing techniques (see for example, Grodzinski, 1953) have been made by Tolkowsky (1920), Kraus and Slawson (1939), Denning (1953, 1955, 1957), Wilks and Wilks (1954, 1959), and Hukao (1955). As a result a considerable amount of information is now available regarding the variations in the hardness in different directions and on different planes. Although there is general agreement as to which directions are most easily polished, there has been some confusion as to which are the hard directions, and it is this problem that we now discuss.

The cube plane of diamond is very resistant to abrasion in the four directions at 45° to the crystal axes, the dodecahedron plane in the two directions at 90° to the axis, and the octahedron plane in all directions. On the latter plane, all the directions are not equally hard, and there has been some discussion as to which are the hardest (Denning 1953). Using conventional polishing techniques it is very difficult to abrade diamond at all in these hard directions, and there has hitherto been little information as to their relative hardness. Although there seems little prospect of making such measurements using the technique of a cast-iron scaife and loose diamond powder, it is now possible to compare the hard and soft directions on a cube face of diamond by using diamond impregnated grinding wheels (Wilks and Wilks 1959). The variations in hardness so observed are much less than those observed using conventional loose powder techniques, but as we discuss later the same order of hardness should be observed in both measurements. We have therefore applied this technique to compare the hardness in the hard directions of the three principal planes : cube, dodecahedron and octahedron.

---

† Communicated by the Author.

§ 2. Experimental Method

As with the earlier measurements (Wilks and Wilks 1959) a Grodzinski micro-abrasion tester was used with specially prepared diamond impregnated wheels of approximately 1 in. diameter mounted on accurately centred spindles. The wheels rotated at a speed of 10 000 r.p.m. and were brought into contact with the diamond under test under a load of 200 g for 20 secs ; olive oil being used as a lubricant. Smooth cuts were produced whose depths were subsequently determined by multiple beam interferometry ; the inverse of the depth being taken as a measure of the abrasion hardness.

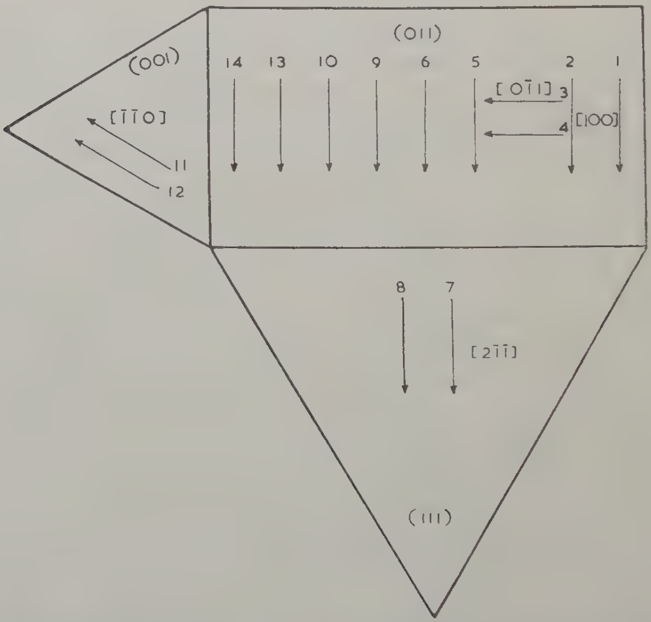

Two octahedron diamonds of fair quality and of size about 2 carats were chosen for the tests. On each stone we were able to select octahedron planes with very few surface markings. Cube and dodecahedron faces were cut and polished on the stones, and checked that they were aligned to within 30 min of the lattice plane (when it was necessary to repolish these planes between two series of tests, this alignment was maintained).

In order to compare the depths of the cuts made in the hard directions on these three planes, it is necessary to allow for any wear of the wheel.

Cuts were therefore also made in the soft direction on the dodecahedron plane. The figure shows the layout of a typical set of 14 consecutive abrasions, cuts 1, 2, 5, 6, 9, 10, 13 and 14 serving as calibration cuts. Finally for completeness cuts were also made in the principal directions of the three main planes.

§ 3. RESULTS

Table 1 shows the average of the depths of each pair of cuts made in the various directions in units of $\lambda/2$. The two cuts of a pair had equal depths to within 10%, which as before (Wilks and Wilks 1954) sets the limit of accuracy of the experiment. Each line in the table represents a series of cuts made with the same impregnated wheel on the same diamond.

Table 1. Average depth of cut in units of $\lambda/2$

Plane		Dodecahedron (011)		Cube (001)		Octahedron (111)	
Direction of abrasion		[100]	$[0\bar{1}1]$	[100]	$[\bar{1}\bar{1}0]$	$[\bar{2}11]$	$[2\bar{1}\bar{1}]$
Diamond	Wheel						
1	A				1·7	7·2	3·5
1	A	17·1	3·3	14·7	2·0		
1	B					6·7	3·5
1	B	9·9				3·9	
2	C	20·5	4·5		3·5		4·9
2	C	15·7	2·1		1·5		3·5

If the depth of cut on the dodecahedron plane in the soft direction is now taken as 10·0 $\lambda/2$, the depths of the other cuts can be normalized to this value, and the average of these results is shown in table 2.

Table 2

	Plane and direction					
Plane	Dodecahedron (011)		Cube (001)		Octahedron (111)	
Direction	[100]	$[0\bar{1}1]$	[100]	$[\bar{1}\bar{1}0]$	$[\bar{2}11]$	$[2\bar{1}\bar{1}]$
Depth of cut $\lambda/2$	10·0	1·8	8·5	1·1	3·9	2·1

The resistance to abrasion is the inverse of the depth of cut made by the abrading wheel. If therefore we take the resistance to abrasion of the soft direction on the dodedcahedron plane as 1·00 the results in table 2 can be presented in order of increasing hardness, as shown in table 3.

Table 3. The resistance to abrasion of various planes and directions presented in order of increasing hardness

Plane	(011)	(001)	(111)	(111)	(011)	(001)
Direction	[100]	[100]	$[\bar{2}11]$	$[2\bar{1}\bar{1}]$	$[0\bar{1}1]$	$[\bar{1}\bar{1}0]$
Hardness value	1·0	1·2	2·5	4·5	5·5	8·5

§ 4. Discussion

The present experiments indicate the relative hardness between the various directions in diamond as measured with diamond impregnated wheels; now we wish to relate these results to the resistance of diamond to abrasion determined by conventional polishing techniques. It has previously been shown that comparable results are obtained from experiments made either with a flat scaife charged with loose diamond powder or with the cast-iron wheel of a micro-abrasion tester also charged with loose diamond powder, e.g. the variation of the rate of abrasion with speed and load, and the effects of orientation (Wilks and Wilks 1954, 1959). In the present experiments the abrading diamond dust was bonded into the wheel, not as in normal polishing where the wheel is charged with loose powder in olive oil. Previous experiments have indicated that the use of loose powder magnifies the basic hardness differences which in themselves are quite small (Wilks and Wilks 1959). This view is confirmed by the results in table 1 which show that the relative hardness between the soft directions in the cube and dodecahedron planes is in agreement with what we have previously observed using loose powder. Thus although the hardness differences when loose powder are used are very much greater, the order of hardness for the various directions is the same in both cases. Thus the order of hardness shown in table 3 for impregnated wheels should also apply for ordinary diamond polishing when loose powder is used on a flat grinding scaife. In particular the hardest directions are those on the cube plane at 45° to the axes.

As we mentioned above, there has been some discussion as to which are the relative hard and soft directions on the octahedron plane. Tolkowsky was unable to grind this plane at all, but by working on planes close to it, he deduced that the hardest direction was that away from the dodecahedron plane. Similar results were later obtained by Slawson and Kohn (1950), but Denning (1953) by actually grinding a plane parallel to the octahedron deduced this direction to be the easiest, and the opposite direction the hardest. Our results confirm that the hardest direction is away from the dodecahedron plane, in agreement with Tolkowsky, and with Slawson and Kohn. It may be noted that both directions on the octahedron plane are less hard than the hard directions on the cube and dodecahedron planes.

ACKNOWLEDGMENTS

I would like to thank Messrs. Triefus Ltd. for the accurate cutting of the diamonds used in this investigation, and Messrs. Impregnated Diamond Products Ltd. for their help in supplying the diamond impregnated wheels.

My thanks are also due to Industrial Distributors (Sales) Ltd. for the loan of the diamonds and for a research grant.

REFERENCES

DENNING, R. M., 1953, *Amer. Min.*, **38**, 108; 1955, *Ibid.*, **40**, 186; 1957, *Ibid.*, **42**, 362.

GRODZINSKY, P., 1953, *Diamond Technology* (London).

HUKAO, Y., 1955, *Industr. Diam. Rev.*, **15**, 45.

KRAUS, E. H., and SLAWSON, C. B., 1939, *Amer. Min.*, **24**, 661.

SLAWSON, C. B., and KOHN, J. A., 1950, *Industr. Diam. Rev.*, **10**, 168.

TOLKOWSKY, M., 1920, D.Sc. Thesis, London.

WILKS, E. M., and WILKS, J., 1954, *Phil. Mag.*, **45**, 844; 1959, *Ibid.*, **4**, 158.

CORRESPONDENCE

The Low Energy Ion Bombardment of Gold

By D. G. Brandon and Piers Bowden
Department of Metallurgy, University of Cambridge

[Received January 30, 1961]

Direct electron microscope examination of thin foils prepared from neutron bombarded copper has revealed the presence of large numbers of small defects and dislocation loops (Silcox and Hirsch 1959). Similar effects have been observed in copper bombarded with α-particles, and in the latter case the occluded helium was found to modify the annealing behaviour (Barnes and Mazey 1960). While current theories of radiation damage require that primary knock-ons should be responsible for most of the damage remaining in a metal after bombardment, much interest has also been shown in focusing collisions which it is thought can transmit interstitial damage over quite large distances at energies less than 1 kev. Neutron bombardment experiments are difficult to analyse because of uncertainties in the neutron energy spectrum and specimen temperature, while the use of high energy ions or α-particles does not permit one to distinguish between damage occurring at high energies and that occurring after energy degradation. It seems desirable, therefore, to have information on the damage produced by particles of much lower energies. However, most of the published work on low-energy ion bombardment is concerned with sputtering yield measurements and little attention has been paid to sub-surface damage produced in the crystal lattice. This note is a preliminary report on the nature of this sub-surface damage and its relation to radiation damage produced by more conventional techniques.

Thin films of annealed gold 99·998% pure, prepared by electro-polishing in a chromic acid–acetic acid bath, were mounted for electron microscope examination. The mounted foils were then bombarded in a specially designed ion gun.

The argon ions (A^+) used in these experiments had an energy distribution with a sharp high energy cut-off at 75 ev and a half peak width of 5 ev. (The maximum energy a 75 ev argon ion can transfer to a gold atom is 42 ev in a held-on collision.) The angular spread of the beam was estimated to be less than 8°. The measured total current flowing to the specimen is due to the ions striking the surface and also to the secondary electrons leaving it. Assuming a secondary electron coefficient of 1 electron per incident ion, the total dose delivered to each specimen was $3{\cdot}5 \times 10^{17}$ ions cm^{-2} in two hours. The background pressure of argon was 4×10^{-5} mm Hg, and of contamination 1×10^{-6} mm Hg. The temperature of the specimen could be controlled during the experiment.

Figure 1† shows an area that was shielded from the beam on a specimen bombarded at +22°C. The structure is typical of a fully annealed foil. There are no dislocation loops or other defects, but there is a fine polishing structure on the surface.

Figure 2 shows a bombarded area from the same foil. The contrast may be interpreted as being due to small planar defects, probably dislocation loops, which show up as short straight lines, sharp if the defect is looked at edge on. These are surrounded by their strain fields, a pair of dark or light crescents one on either side of the line (fig. 3). Similar contrast has been observed around quenched in dislocation loops in aluminium (Silcox 1960, private communication), and also around G.P.II platelets in an aluminium copper age-hardening alloy (Nicholson and Nutting 1958), although in neither case was the strain field as marked.

Fig. 3

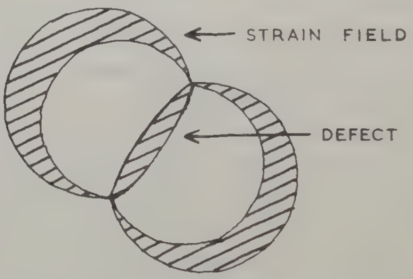

Proposed interpretation of the contrast in fig. 2.

The crystallographic orientation of the foil was found from a same area electron diffraction photograph, and where the defects line up head to tail to form a string, they do so along ⟨111⟩ directions. There is only one such direction near the plane of the foil in fig. 2. As well as the larger defects of 100 Å diameter there are also smaller defects randomly distributed going down to the limit of resolution, less than 20 Å.

Figure 4 shows another grain with a different orientation in the same foil. Here the general defect size is smaller, and the distribution more random. The detailed effects produced by a particular bombardment were found to be very dependent on orientation.

Figure 5 shows a grain from a second gold foil bombarded to the same dose at a lower temperature (−32°C) and subsequently examined at room temperature. The concentration of defects is much higher and many of the larger ones can be identified as dislocation loops. Also present in this grain are irregular strings of loops and short heavily jogged lengths of dislocation. The background of very small defects is more pronounced than in the first specimen.

---

† Figures 1, 2, 4 and 5 are shown as plates.

In interpreting the second specimen it is well to remember that it does not represent the structure as it existed at the temperature of bombardment, but only the structure after it has subsequently been allowed to anneal at room temperature. Consequently defects frozen in at the lower temperature will be able to move subsequently, and this may well account for the dislocations present being heavily jogged.

There is a marked decrease in defect density towards the thinner outside edge of all foils examined, and this can also be seen in fig. 5. The thickest gold film in which detail is visible is about 1500 Å; the foils shown here are all less than this and tapering. Although there were marked differences in the sizes and density of defects in different grains, in no specimen was any grain boundary effect detectable, either preferred growth or denudation in the boundary region.

The efficiency of point-defect production was estimated by comparing a figure for the integrated planar defect area per unit area of specimen with an estimated value for the incident ion current. For a grain in the foil bombarded at +22°c, the efficiency was of the order of 5×10^{-4} point defects retained per incident ion.

The penetration of 75 ev argon ions into gold can be estimated from the effective collision radius as used by Silsbee (1957). He derives an expression for the effective atom radius in an inter-atomic collision as a function of the energy transferred to the struck atom. For gold for 40 ev transferred the effective atom radius is about 0·55 r, for 5 ev transferred 0·7 r, where 2 r is the equilibrium distances of closest approach in the gold lattice. These contractions are not sufficient to allow the argon ions to penetrate beyond the second layer of atoms.

It is possible that there might be some diffusion-assisted penetration of argon. The observed efficiency of point defect production is low and does not necessarily rule out this possibility. However, Tucker and Norton (1960) observed appreciable diffusion rates only above 100°c whereas the effects observed here are in the −30°c to +20°c range where diffusion rates will be very much slower. In no case has anything been seen resembling the small bubbles of helium gas reported in copper after α-particle irradiation (Barnes and Mazey 1960).

If not due to argon atoms, the damage must be due to interstitials or vacancies, or possibly both. The temperatures considered lie above the recovery range for interstitial atom damage as determined from resistivity measurements and at the bottom end of the temperature range for vacancy migration (e.g. Seeger 1958, Seitz 1959). Interstitial atoms would be expected to diffuse very rapidly at all temperatures in the range investigated, while vacancies could diffuse only slowly at the lower temperature but considerably faster at the higher.

The marked difference in the scale of the damage seen at these two temperatures suggests that vacancies are primarily responsible. However, vacancy migration could be merely serving to modify a structure produced initially by interstitial atoms.

If interstitial atoms are the cause of the damage, they may have either diffused in from the surface or they may have been injected to a depth of many atomic planes by a focused collision sequence of the type proposed originally by Silsbee (Silsbee 1957, Nelson and Thompson 1961, Vineyard *et al.* 1959 and 1960). Interstitials created by this second process are less likely to be lost to the surface before being captured by a sink inside the material, and therefore will be more effective in producing sub-surface damage. Further work will be needed to clarify the situation.

Whatever the detailed processes involved, the results show that even in this low-energy range damage may be produced in gold in appreciable quantity by ion bombardment.

ACKNOWLEDGMENTS

This work is being supported by the U.K.A.E.A. The authors are indebted to Professor A. H. Cottrell, F.R.S. for many helpful discussions and to the U.K.A.E.A. for permission to publish.

REFERENCES

BARNES, R. S., and MAZEY, D. J., 1960, *Phil. Mag.*, **5,** 1247.
NELSON, R. S., and THOMPSON, M. W., 1961, *Proc. Roy. Soc.* A, **259,** 458.
NICHOLSON, R. B., and NUTTING, J., 1958, *Phil. Mag.*, **3,** 531.
SEEGER, A. K., 1958, *U.N. Conference on Peaceful Uses of Atomic Energy* (Geneva), **6,** 250.
SEITZ, F., 1959, *Trans. Amer. Inst. min. (metall.) Engrs*, **215,** 354.
SILCOX, J., and HIRSCH, P. B., 1959, *Phil. Mag.*, **4,** 1356.
SILSBEE, R. H., 1957, *J. appl. Phys.*, **28,** 1246.
TUCKER, C. W., Jr., and NORTON, F. J., 1960, *J. nucl. Materials*, **2,** 329.
VINEYARD, G. H., GIBSON, J. B., GOLAND, A. N., and MILGRAM, M., 1959, *J. appl. Phys.*, **30,** 1322 : 1960, *Bull. Amer. phys. Soc.*, **5,** 26.

REVIEWS OF BOOKS

Radio Astronomy. By F. Graham Smith. (Penguin Books, 1960.) [Pp. 265.] Price 7*s.* 6*d.*

Dr. Graham Smith's book is an easily readable account of radio astronomy which can be understood without any specialized radio or technical knowledge. Details of radio receivers and radio telescopes are in fact left to closing chapters. The book covers the whole field of this rapidly advancing subject. Although Dr. Smith initially defines radio astronomy as " the study of heavenly bodies by the reception of the radio waves they emit " he does include descriptions of radio echo investigations or radar astronomy. A more inclusive definition of radio astronomy as " the study of heavenly bodies by radio methods " would seem preferable. Dr. Smith also discusses briefly the contribution to information about the ionosphere which has been derived through radio astronomy and by observations of earth-satellites. A final chapter outlines the main radio-astronomical observatories throughout the world. The book is well illustrated with diagrams and Plates.

Dr. Smith enlightens the discussion with interesting commentary which helps one to view the development of the subject in proper perspective. Anyone with general scientific interests will appreciate the availability at such a reasonable price of a comprehensive, non-technical, and up-to-date picture of radio astronomy.

J. S. H.

Advances in Electronics and Electron Physics, Vol. XII : Photo-Electronic Image Devices. Editor : L. Marton. Volume editors : J. D. McGee and W. L. Wilcock. (Academic Press, 1960.) [Pp. 397.] Price $12.00.

This volume contains the papers contributed at a Symposium on Image Tubes and Related Devices organized by Professor J. D. McGee and held at Imperial College, London University, in September 1958. This publication is a most welcome inclusion of conference proceedings as part of a continuing series of volumes that usually are purchased as a series by scientific libraries. In this way the records of meetings on specialized topics are available for reference later when the field suddenly expands due to universal application of the original subject matter. This may happen in the present case when image conversion tubes have been improved beyond the technical limits discussed in these proceedings and are manufactured in quantity. The principles involved may be described as applied electron physics and the content is connected directly with the general theme of this series. Astronomical applications are discussed in the first three and two subsequent papers, out of the 30 contributions and x-ray uses in the last four. In between, various physical topics are presented in relation to image tubes such as signal-to-noise ratio, secondary electron emission, field emission and contrast perception. Intensification of the tracks of particles traversing a scintillation chamber is discussed as a possible application in nuclear physics. The only major omission is the area of solid state image intensifiers where a photocathode and phosphor are in contact and the applied field is across these two layers alone without a vacuum path for the emitted photo-electrons. No Russian papers are included despite extensive work in this general field reported previously. Each paper is followed by the discussion from the floor which in many cases clarifies ambiguities or omissions in the contribution. The experiment of publishing a symposium proceedings in this series has been successful and we hope will be repeated with other appropriate topics in electronics and electron physics.

W. C. N.

Stochastic Processes: Problems and Solutions. By LAJOS TAKÁCS. (Methuen & Co. Ltd., 1960.) [Pp. 137.] Price 18*s*. net.

THIS unusual little volume is built around a collection of ninety-four problems, but it is rather more than a problem book. Each of the first three chapters (Markov chains, Markov processes, Non-Markovian processes) begins with a rapid but comprehensive sketch of basic theory, the problems then follow in well-graded sequence, and solutions are outlined in a fourth chapter.

As a result of this arrangement, the book is self-contained to the extent that " all probems can be solved by using the listed theorems only ". However, one would certainly be well advised to read a certain amount in stochastic processes beforehand, or to be prepared to do so concurrently, using Takács' book as a guide. The problems themselves are of a very reasonable standard: all worth while, some of them challenging, but, thanks in part to the systematic ordering of the examples, only a few seem really difficult.

Topics covered in the theory include some spectral theory of transition matrices, the classification of Markov chains; diffusion, stationary, recurrent and renewal processes. The initial problems of each chapter are fairly direct illustrations of theory; then follow applications to queueing, telephone traffic, cascade processes, counter theory, statistical prediction, and some of the simpler statistical models of physics and astronomy.

A little effort spent on Professor Takács' book will yield virtually nothing, but the result of a moderate effort should be quite unusually satisfying and rewarding.

P. W.

Paramagnetic Resonance in Solids. By WILLIAM LOW. Solid State Physics, Supplement 2. (New York and London : Academic Press, 1960.) [Pp. 212.] Price $7.50.

PARAMAGNETIC resonance spectroscopy has become an important branch of Solid State Physics. The present book concentrates on a particular part of this field which has been intensively investigated during the past ten years, namely, paramagnetic resonance from transition group ions in magnetically dilute non-conducting crystals. The author has made many contributions in this area and he treats the subject clearly and extensively. After a short introduction, there is a useful chapter (67 pages) on the theory of crystal fields in these substances, in which are collected together tables of matrix elements, group representations and operator equivalents together with some examples of how they are applied. This is followed by a chapter on the experimental results for these crystals (73 pages) which are extensively described with many references. There is some discussion of covalent bonding and also of optical absorption spectra in these compounds. The remaining three chapters (45 pages) deal, rather briefly, with some of the many other aspects of paramagnetic resonance in non-conducting solids, including colour centres, relaxation times, masers and experimental techniques. Although these topics are given short treatment, and some others are omitted altogether, e.g. conductors, the book can be recommended as a good survey of work on transistion group ions.

J. O.

[*The Editors do not hold themselves responsible for the views expressed by their correspondents.*]

Fig. 1

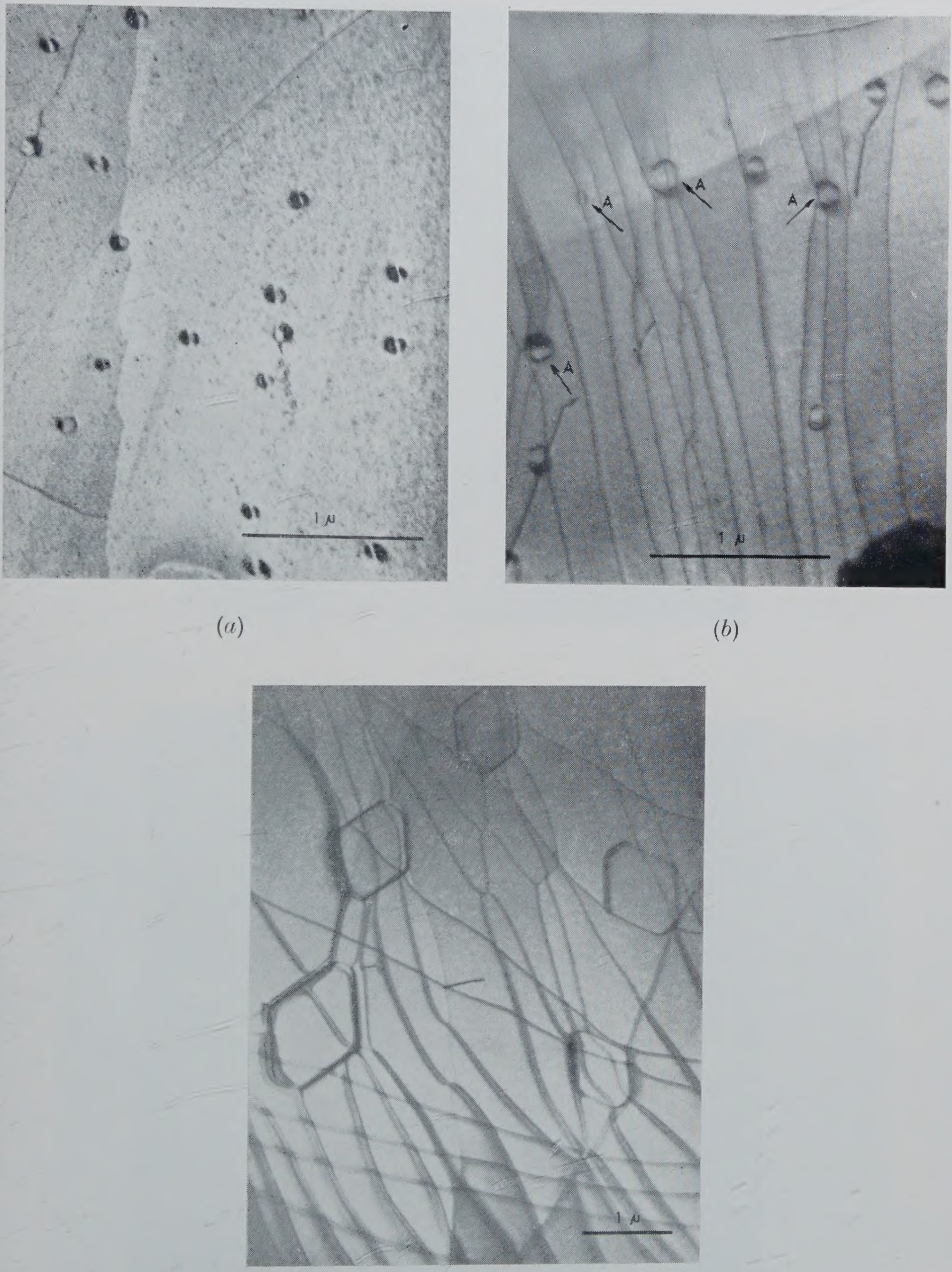

(*a*) (*b*)

(*c*)

Hexagonal prismatic loops in antimony telluride. (*a*) Very rapidly cooled (air quenched); the loops are rounded; (*b*) moderately slowly cooled: the loops are hexagonal; (*c*) slowly cooled (~600°c/4 h) the loops form elongated hexagons. Notice the interaction between loops and glissile dislocations in the *c*-plane at the points marked A.

Fig. 2

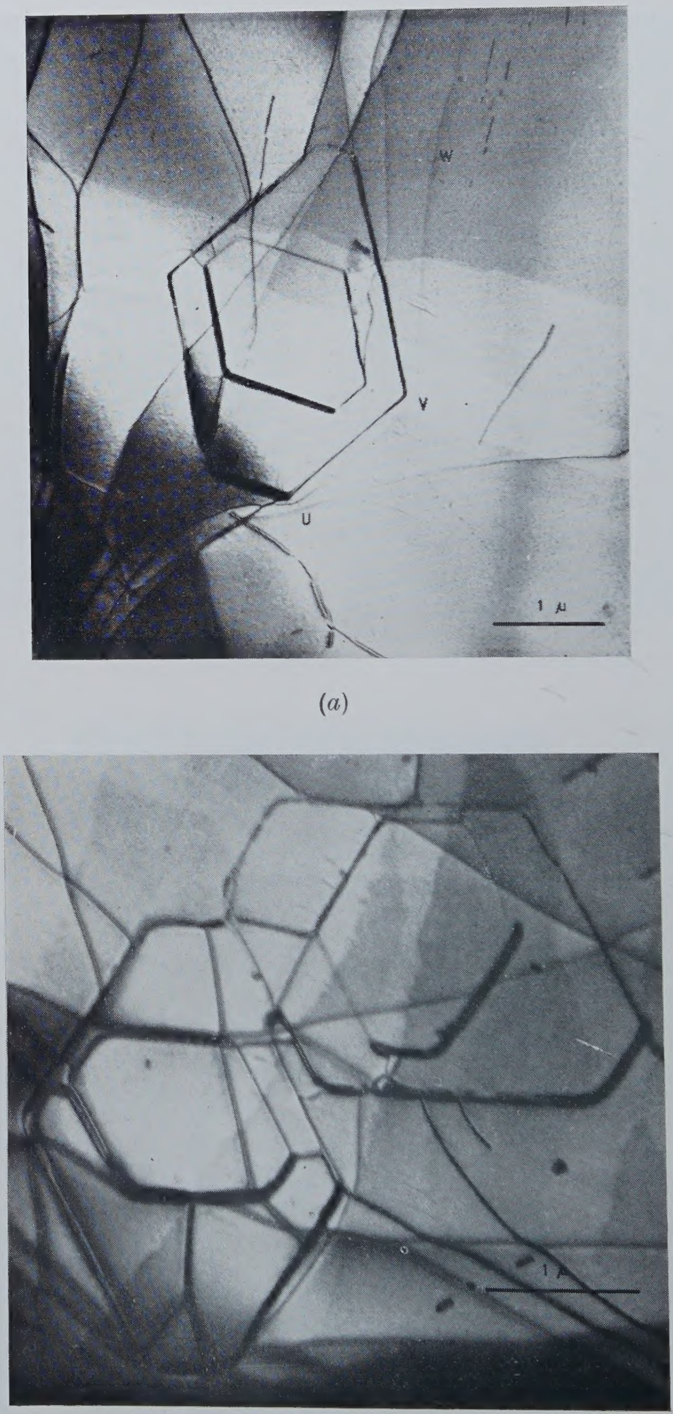

(*a*)

(*b*)

Concentric pairs of elongated large loops in very slowly cooled specimens (~600°c/24 h). The two loops systematically differ 60° in orientations.

Fig. 2

Electron micrograph of a Ni–20% Co single crystal deformed at 300°K in stage I.
Shear–strain interval $\Delta\epsilon$: 0–0·0612.

Fig. 3

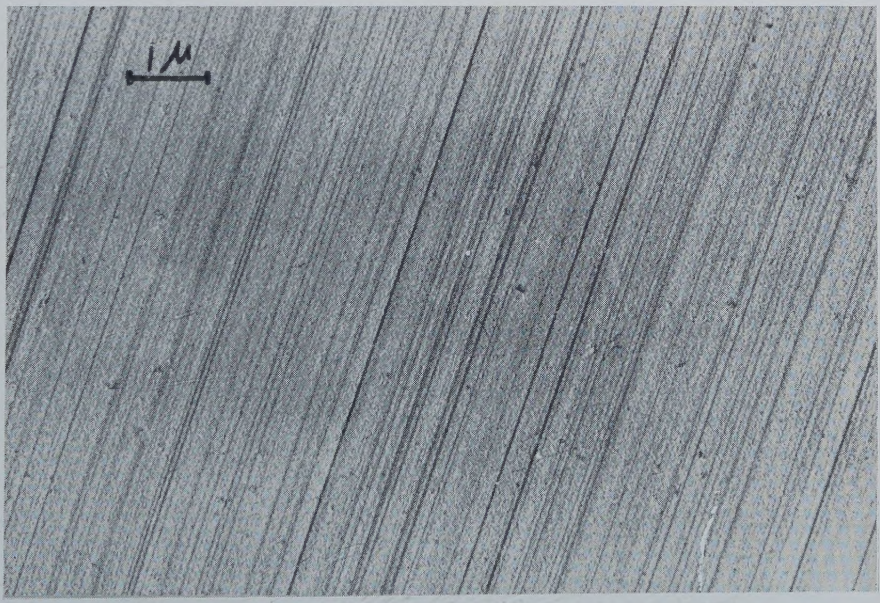

Electron micrograph of a Ni–20% Co single crystal deformed at 90°K in stage I.
Shear–strain interval $\Delta\epsilon$: 0–0·0724.

Fig. 1

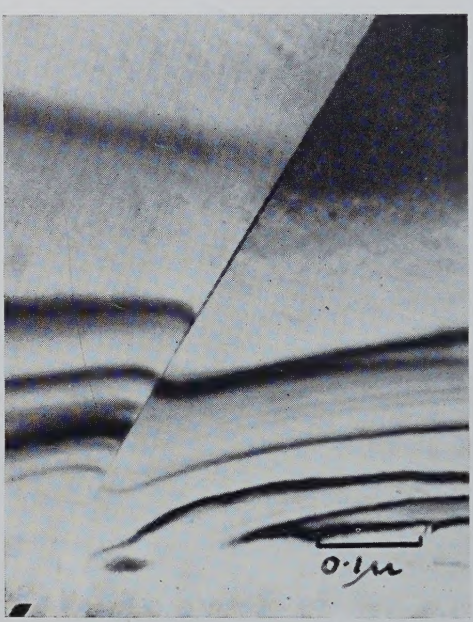

Fully annealed gold containing a grain boundary. The diffuse black lines are Bragg extinction contours.

Fig. 2

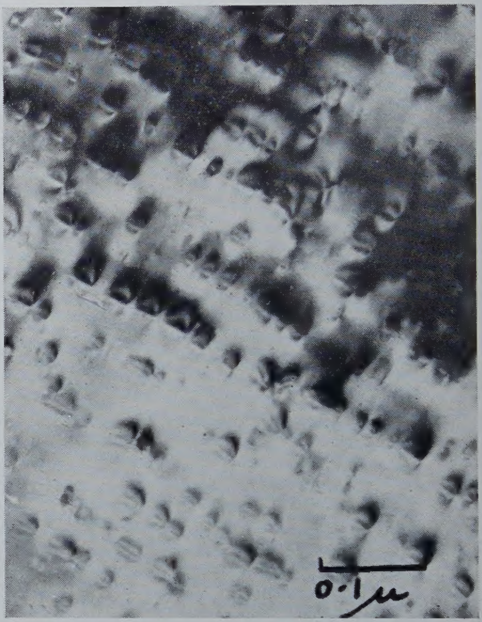

Gold foil bombarded at 22°c. Dislocation loops lined up along the [111] direction.

Fig. 4

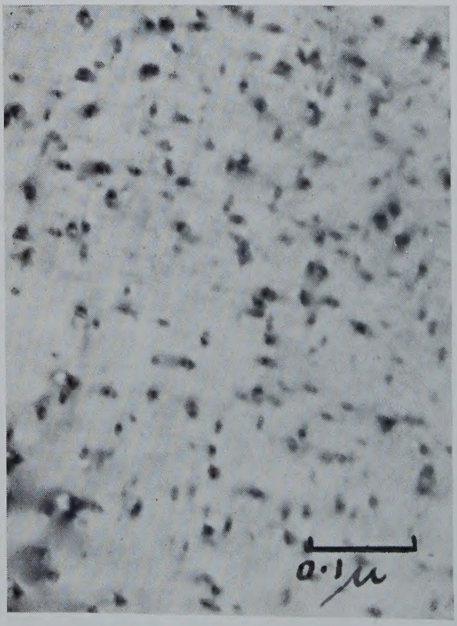

Another grain in the same foil as figs. 1 and 2, showing a different arrangement of defects.

Fig. 5

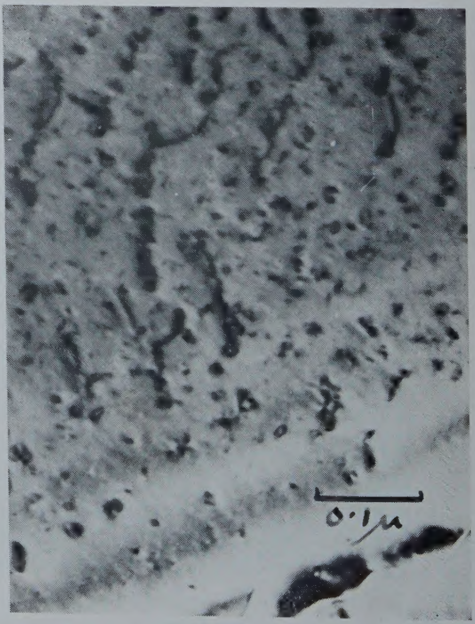

Gold foil bombarded at −32°c. Dislocation loops and jogged dislocations as well as fine scale damage.